NASA Technical Memorandum 110384

An Experimental Study of a Separated/Reattached Flow Behind a Backward-Facing Step. $Re_h = 37,000$

Srba Jovic, Eloret Institute, Ames Research Center, Moffett Field, California

April 1996

National Aeronautics and
Space Administration

Ames Research Center
Moffett Field, California 94035-1000

An Experimental Study of a Separated/Reattached Flow Behind a Backward-Facing Step. Re_h = 37,000

Srba Jovic*
Eloret Institute
Ames Research Center

Summary

An experimental study was conducted to analyze the response and evolution of a two-dimensional incompressible turbulent boundary layer after being strongly perturbed by a one-sided sudden expansion. The hot-wire measurement technique was used to measure three Reynolds stresses and higher-order mean products of velocity fluctuations. The Reynolds number, Re_h, based on the step height, h, and the reference velocity, U_o, was 37,200. The upstream flow was a fully developed turbulent boundary layer with momentum-thickness Reynolds number $Re_\theta = 3600$ and $\delta_{99}/h = 0.82$.

The results show that an internal shear layer, imbedded in the inner part of the original boundary layer, emanates immediately from the step edge. This shear layer has many similarities with a plane mixing layer, but does not resemble it exactly.

The new no-slip and impermeability boundary conditions imposed on the flow in the reattachment region limit further growth of the mixing-layer-like flow, promoting a new internal boundary layer developing on the wall downstream of reattachment. The data show that the structure of the internal layer attains quasi-equilibrium, with production and dissipation of turbulent kinetic energy approximately equal, by about $20h$ from the step. The skin friction coefficient has nearly reached its maximum value at this location. In the external layer, the Reynolds stresses, normalized by the local u_τ^2, initially decrease at about the same rate as those in the internal boundary layer. However, the rate of recovery reduces sharply beyond $x \approx 20h$ so that even at the last measuring station, $x = 51h$, the external layer still has a memory of the upstream disturbance.

*Senior research scientist. Currently with MCAT, Inc.

Nomenclature

$C_{f,0}$	skin friction coefficient, $2\,\tau_w/\rho U^2_o$
C_{fe}	local skin friction coefficient, $2\,\tau_w/\rho U^2_e$
C_p	pressure coefficient, $2(p-p_0)/\rho U^2_o$
h	step height
X_r	mean reattachment length
p	static pressure
Re_h	step height Reynolds number, $U_0\,h/\nu$
Re_θ	momentum thickness Reynolds number, $U_0\,\theta/\nu$
U_0	upstream freestream reference velocity
U	mean velocity in streamwise direction
u_τ	friction velocity

u, v	fluctuating velocity components in x and y directions respectively
u_{rms}, v_{rms}	root mean-square of u and v fluctuations
$\overline{u^2}, \overline{v^2}$	normal Reynolds stresses
$-\overline{uv}$	Reynolds shear stress
$\overline{u^2v}, \overline{uv^2}$	triple-product correlations of fluctuating
$\overline{u^3}, \overline{v^3}$	velocity components
x, y	coordinate system representing stream-wise and wall-perpendicular directions measured from the step and the wall respectively
y^+	normalized distance from the wall, yu_τ/ν
ν	molecular kinematic viscosity of air, nominally $1.5*10^{-5} m^2/s$ at T = 20°C
ρ	air density, 1.2 kg/m^3 at T = 20°C
δ	boundary layer thickness where $U = 0.99U_e$
δ_0	boundary layer thickness upstream of the step
δ^*	displacement thickness, $\int_0^\delta (1 - U/U_e)\, dy$
θ	momentum thickness, $\int_0^\delta (U/U_e)\,(1 - U/U_e)\, dy$
τ_w	wall shear stress

Introduction

Separating/reattaching flows occur in a wide variety of practical engineering applications such as airfoils at angle of attack, re-entry vehicles, diffusers, turbomachines, combustors, sudden area changes in pipes or ducts and atmospheric flows over fences and hills. Separation generally has a negative impact on the performance of these systems, such as reduced maneuverability of aircraft and increased drag, increased local wall heat transfer, increase of dynamic structural loads and noise, etc. There have been many studies on separating/reattaching flows during the past four decades. The research has been conducted for different geometric configurations, mainly two-dimensional. Fundamental features of this class of flows have been addressed most frequently for the backward-facing step, the normal flat plate with a splitter plate, and the blunt flat plate; in all these cases the separation line is straight and fixed by the geometry.

A separating/reattaching flow can be divided into four interacting zones (see fig. 1). The zones are: the separated free shear layer, the recirculating region under the shear layer, the reattachment region and the attached/recovery region. Each flow region bears some similarities to well-studied flow cases such as mixing layers and boundary layers, while the reattachment and recirculating regions are unique to separated flows.

Different researchers have addressed various issues of this class of flows.

The objective of this report is to present a set of detailed measurements of the separated flow behind a backward-facing step, and to perform a detailed analysis of the data. The analysis is confined to the separated free shear layer and the reattachment and attached/recovery regions: the hot-wire measurement technique does not give useful results in or near reversed-flow regions. The controversial issue of the similarity of the separated shear layer to a plane mixing layer is assessed in some detail with particular reference to the presence of a developing internal mixing layer. A thorough analysis of this possible similarity has not been carried out in other back-step flow experiments: it is more likely to occur here than in the highly-disturbed

flow downstream of a normal plate. Secondly, the issue of the readjustment of such perturbed flow to the wall boundary conditions and its recovery to an equilibrium turbulent boundary layer is analyzed. This is just one case from a series of five experiments on the backward-facing step designed to investigate physics of the recovery of a separated flow for $6800 < Re_h < 37{,}000$ and $0.8 < \delta_{99}/h < 2.0$ (Jovic (1995), to be published as a NASA TM).

Unsteadiness

Kim, Kline, and Johnston (1980) observed that the flow was highly unsteady in the reattachment region of the backward-facing step flow, suggesting violent interactions of large structures from the upstream separated shear layer with the wall. Two basic modes of char-acteristic frequencies are found in all the abovementioned flow configurations. The higher-frequency mode is associated with the usual large scale motions in the shear layer while the lower-frequency mode reflects overall separation-bubble growth/decay dynamics or shear layer "flapping" as it is frequently called in the literature. In the case of a blunt plate, Cherry, Hillier, and Latour (1984), using pressure and pressure-velocity cross-correlation measurements, observed low-frequency unsteadiness in the separation bubble. Eaton and Johnston (1982) argued that the observed low-frequency motion in the backward-facing step flow is likely to be a consequence of an instantaneous imbalance between the entrainment rate from the recirculation zone and its resupply near the reattachment line. The nature and physics of this imbalance were further assessed by Pronchick and Kline (1983). They suggested a qualitative model of the reattachment process based on flow visualization studies. They observed two groups of structures in the reattachment region: "overriding" and "interacting" eddies, which will be discussed later. In light of the flow visualization and the proposed qualitative model by Pronchick and Kline (1983), it can be concluded that the separation bubble dynamics depends on very complex interactions of large eddy structures, formed in the upstream free shear layer, with the wall in the reattachment region.

Kiya and Sasaki (1983), using a similar experimental technique to that of Cherry et al. (1984), found that the low-frequency unsteadiness has fX_r/U_o less than about 0.2 while the wide-band mode with frequency of 0.6 to 0.8 corresponds to the frequencies of vortical structures seen in plane mixing layers. Castro and Haque (1987) detected the same two modes of unsteadiness in the separated flow behind a normal flat plate with a long central splitter plate. However, Ruderich, and Fernholz (1986) observed no dominant frequencies in their power spectra for the same flow configuration, which led them to believe that there was no flapping of the reattaching shear layer. In the case of a backward-facing step, Eaton and Johnston (1981); and Driver, Seegmiller, and Marvin (1983) also detected the two characteristic frequencies with approximately the same values obtained by Kiya and Sasaki (1983). Importantly, Driver et al. (1983) found that the contribution of low-frequency unsteadiness to the total turbulent kinetic energy is negligibly small. This suggests that turbulence quantities in a backward-facing step flow are not likely to be contaminated by low-frequency unsteadiness.

Similarity to a Plane Mixing Layer

Cherry et al. (1984) found that the (nearly linear) rate of growth of vorticity thickness, the characteristic frequencies and the spanwise correlation scales for the blunt plate flow are all similar to values found for the fully-developed plane mixing layer. Castro and Haque (1987) strongly argued that the separated shear layer downstream of a normal plate is not closely similar to that of a plane mixing layer. They found that the normal stresses are consistently higher than in the plane layer. In addition, they concluded that the effect of the stabilizing curvature of the shear layer on the flow is weak, and that the re-entrainment of the recirculated fluid (back into the shear layer) represents the dominant mechanism for maintenance of the high normal stresses.

Three-Dimensionality

Cherry et al. (1984) concluded that reattachment affects small and large scale flow structures in different ways. Their spanwise surface-pressure cross-correlation measurements at several streamwise locations indicate progressive reduction of length scales near the wall which is interpreted as a "three-dimensionalizing of the smaller scales." Spanwise velocity correlations (near the shear layer edge where local turbulence intensity was 2.5 percent) reveal that a three-dimensional state has been established well before reattachment and that it is not significantly affected by the reattachment. Troutt, Scheelke, and Norman (1984) looked at the spanwise structure of the flow behind the backward-facing step and arrived at the same conclusion, that the small scales are subjected to a reduction in size near the wall while the large-scale spanwise structure persists far downstream of reatta-chment, only to be gradually affected by the new boundary condition imposed by the bounding wall. In a wall bounded mixing layer experiment, Wood and Bradshaw (1982) observed changes in turbulence structure before the mixing layer "reattached." They observed significant increases of all spanwise scales as the flow became affected by the wall, probably because the irrotational "backflow" around erupting eddies in the intermittent region, required by the continuity equation, tends to be constrained to z-wise motion by the $v = 0$ condition at the solid surface. This effect can take place without significant changes in the (rotational) turbulence itself.

Near-Wall Region within the Bubble

A number of researchers such as Westphal, Johnston, and Eaton (1984); Adams, Johnston, and Eaton (1984); Driver and Seegmiller (1985); Castro and Haque (1987); Ruderich and Fernholz (1986); and Devenport and Sutton (1991) have measured skin friction in the reversed-flow regions of different separated-flow configurations. Studies by Adams et al. (1984); and Devenport and Sutton (1991) showed that the near-wall behavior of the boundary layer within the recirculating zone is very different from that of a standard turbulent boundary layer. Devenport and Sutton showed that mean velocity profiles follow a modified version of Simpson's (1983) model. They also argued that streamwise turbulence intensity profiles appear to be scaleable on the *rms* friction-velocity fluctuations and not on the mean u_τ. Using a simple analytic model, they showed that the extra streamwise velocity fluctuations are driven by pressure-gradient fluctuations imposed by the shear layer above. Jovic and Driver (1994), using laser-oil-film interferometry, investigated the effect of Reynolds number, Re_h, on the skin-friction coefficient in the recirculating region. They found that in the attached part of the flow $C_f = 2\tau_w/\rho U_o^2$ generally decreased slowly with increasing Re, as usual, while the maximum negative C_f in the recirculating region varies as rapidly as $Re_h^{-1/2}$, suggesting predominantly viscous behavior of the thin layer under the recirculating region. The same behavior was observed by Adams et al. (1984); and Devenport and Sutton (1991).

The abundance of experimental data obtained for the abovementioned flow configurations was restricted mostly to the separation bubble and the early part of the reattachment region. The results lead to a consensus on two aspects of the physics of the separated/recirculating region. One is the existence of the two characteristic frequencies in the separation bubble and the second is the structure of the thin layer near the wall in the recirculating region. It appears that none of the experiments studied the very important physics of the flow recovery in detail. Cutler and Johnston (1989) conducted an extensive study of the separated turbulent boundary layer recovery downstream of a fence, in an adverse pressure gradient tailored to achieve boundary layer equilibrium. The length of the recovery region was $83h$ (h is the fence height). They indicated that an equilibrium boundary layer structure is reached only after several hundred fence heights, which is even longer than the value of $100h$ suggested by Bradshaw and Wong (1972) for a backstep flow in zero pressure gradient.

This research was supported by NASA Grant NCC2-465 while the author was with Eloret Institute, and is gratefully acknowledged.

I wish to thank Professor L. W. B. Browne of the University of Newcastle, Australia, who joined the experiment while on the sabbatical leave with the Center for Turbulence Research at NASA Ames. This experiment would have not been possible without his help.

I also wish to thank Dr. Steve Robinson, originally with NASA Ames, who made this project possible.

I am grateful to Professor Peter Bradshaw for his thorough review of the manuscript and valuable suggestions. Throughout the course of this work, I had valuable discussions with Drs. David Driver, Rabi Mehta, and Promode Bandhyopadhyay. I hope that some of the wisdom born from the interactions is imbedded in this report.

I am grateful to Joe Marvin, a former branch chief of Turbulence Modeling and Physics Branch NASA Ames, for his persistent support during the course of this project. I wish to thank Dr. Sanford Davis (FML Branch Chief) and his staff, for hosting me and the wind tunnel used in this experiment, and for offering all the technical and logistic support necessary for the successful running and execution of the test.

Apparatus, Techniques, and Conditions

The measurements were performed in a tunnel with a symmetric three-dimensional 9:1 contraction, a 169*cm* long flow development section with dimensions 20*cm* × 42*cm*, a backward-facing step of the height, *h*, of 3.8cm and a 205*cm* long recovery section. The flow was tripped at the inlet of the development section using 1.6*mm* diameter wire followed by a 110*mm* width of 40 grit emery paper. In order to compensate for blockage effects of the flow due to the side wall boundary layers, the side walls were diverged according to the estimated displacement thickness of the side-wall boundary layers. All the measurements were made at a reference flow speed, U_0, of 14.7*m/s* measured at a station 40*mm* upstream of the step. The free-stream turbulence intensity as determined by the hot-wire measurements in the free stream was 0.4 percent. The boundary layer was fully turbulent at a reference station 1.05*h* upstream of the step, having a Reynolds number based on a momentum thickness, Re_θ, of 3600 and a shape factor, H, of 1.4. The boundary layer thickness, $\delta_o \equiv \delta_{99}$, at the reference station was 31*mm* so that $\delta_o/h = 0.8$. The aspect ratio (tunnel width/step height) of 11 is just above the value of 10 recommended by de Brederode and Bradshaw (1972) as the minimum to assure two-dimensionality of the flow (in the mean) in the central region of a tunnel. The expansion ratio was 1.19 and the Reynolds number based on step height was 37,000.

Surface static pressures were measured on the upper and the lower (step-side) walls using a standard pressure transducer. The skin friction coefficient distribution downstream of the step was measured using a laser-oil interferometer. This technique allowed unambiguous direct measurements of the shear stress, both in the recirculating and the reattached regions of the flow. A more detailed description of the method and the results obtained is presented in Jovic and Driver (1994).

Mean velocity and turbulence measurements were made with normal and X-wire probes driven by constant-temperature anemometers (Miller, Shah, and Antonia (1987)) made in-house. The sensor filaments were made of 10 percent Rhodium-Platinum wire 2.5μm in diameter and 0.5*mm* (or 18 wall units in the upstream boundary layer) in length for the X-wire probe, and 1.25μm in diameter and 0.3*mm* (or 11 wall units) in length for the normal-wire probe. The spacing between the crossed wires was 0.4*mm* or 15 wall units. The aspect ratio, *l/d*, of the sensor filaments was 240 for both probes. To improve accuracy of the measurements in the regions with higher levels of local turbulence intensity, the included angle of the crossed wires, customarily 90°, was increased to 110°. The anemometers were operated at overheat ratios of 1.3 with a

frequency response of 25kHz as determined by the square-wave test. The normal-wire signal was low-pass filtered at 10kHz and digitized at 20,000 samples/*sec* for 30 *sec*. The X-wire signals were low-pass filtered at 6kHz and sampled at 12,000 samples/*sec* for 30 *sec*. Analog signals were digitized using a Tustin A/D converter with 14 bit (plus sign) resolution. The probes were calibrated using a static calibration procedure and calibration data of each hot-wire channel were fitted with a fourth order polynomial. The calibration was checked before and after each profile measurement. If the hot-wire drift was more than ±1 percent of the free stream velocity the profile was repeated. In this manner, an error due to mean ambient temperature variations was minimized.

Accuracy of the Hot-Wire Measurements

It is very important to have a good estimate of the accuracy of the data obtained with hot-wires, particularly in flows with high turbulence intensity (exceeding 20 percent, say) when the turbulence measurements obtained with the standard hot-wire technique using "cosine law" begin to deteriorate. Accuracy of hot-wire measurements are generally affected by uncertainties in all components of a chain of instruments used in an experiment: pressure-transducer calibration, ambient temperature, hot-wire calibration, hot-wire probe alignment, sensor angles, sensor length (l/d), sensor separation, heat loss to supports, hot-wire drift, and other second-order uncertainties. Using a method of Moffat (1988), and Yavuzkurt (1984), the uncertainties in the normal stresses $\overline{u^2}$ and $\overline{v^2}$, and shear stress $-\overline{uv}$ due to the first five listed causes was calculated using response equations. The maximum uncertainties for each Reynolds stress component was found to be not larger than ±5 percent.

The sensor length and the sensor separation are primarily responsible for the X-wire probe spatial resolution. In regions with high turbulence levels and small turbulence scales (near wall regions) X-wire may incur large errors (Nagano and Tsuji (1994)). The sensor length, $l = 0.5mm$ of the present X-wires probe is sufficiently long in terms of the wire diameter ($l/d = 200$) to minimize the end conduction effects resulting in an approximately uniform temperature distribution along the wire (Champagne, Sleicher, and Wehrmann (1967)). On the other hand, the sensor length should be sufficiently small, of the order of Kolmogorov length scale, to avoid spatial averaging of small scales along the wire. The length $l \leq 5L_k$ (L_k is the Kolmogorov length scales which is about $0.1mm$ in the near wall region) minimizes undesirable spatial averaging (Ligrani and Bradshaw (1987); and Browne, Antonia, and Shah (1988)). Ligrani and Bradshaw found that the maximum error in $\overline{u^2}$ due to *l/d* and diameter, *d*, in the near wall region could be as high as 7 percent. Sensor separation $\Delta z \leq 4L_k$ may introduce an error of 5 percent according to Browne et al., Nagano and Tsuji showed that the most sensitive component to the sensor separation is $\overline{v^2}$ and that error in Reynolds stress components is the function of the turbulence intensity. In the separated shear layer region where local turbulence intensity exceeds 30 percent, the total uncertainty in $\overline{u^2}$ is estimated to be ±10 percent, ±15 percent in $\overline{v^2}$, and ±18 percent in $-\overline{uv}$, while the uncertainties reduce to less than ±8 percent respectively in the recovery region where turbulence intensity is still high but gradually decreases.

High levels of turbulence, exceeding nominally 10 percent to 20 percent, introduce nonlinear effects into the response equation of a hot-wire which cannot be neglected as opposed to the standard hot-wire technique (Hinze (1975); Bruun (1972), and Muller (1982)). Following the method described by Muller, an improved data reduction method taking into account triple-velocity products was introduced. The truncation error of the series expansion of the response equation, which is built into the resulting Reynolds stresses, is reduced from third to fourth order. The correction due to included triple-velocity products is not uniform across the shear layer. The corrected and uncorrected Reynolds stresses are shown in figure 1(c). Maximum corrections of the Reynolds stresses near the wall amount to 18 percent, 35 percent, and 15 percent for

$\overline{u^2}$, $\overline{v^2}$, and $-\overline{uv}$ respectively, while in the outer layer the maximum corrections reach the levels of 10 percent, 35 percent, and 20 percent respectively. It appears that the $\overline{v^2}$ is most sensitive to the nonlinear effects of the X-wire response equation. The correction gradually diminishes downstream of the reattachment as the flow recovers from the separation. Only corrected Reynolds stresses are presented in the report.

Errors due to rectification of the anemometer signal cannot be accounted for. This problem occurs roughly for $y < h$ and $x < 1.2X_r$ where the instantaneous velocity vector occasionally reverses its direction or falls outside of the angle formed by the X-wire sensors. Tutu and Shevray (1975) estimated that shear stress incurs error of 28 percent for turbulence intensities greater than 30 percent which roughly agrees with the presently applied correction. It is not attempted to correct triple-velocity products since the correction implies knowledge of all fourth-order moments.

Due to the aforementioned accuracy problems encountered in high intensity turbulent flows, the results of the present experiment should be used with caution in the separated shear layer region ($0 < x < 7h$), where local turbulent levels exceed 30 percent. Figure 1(b) shows contours of $\sqrt{\overline{u^2}}/U = 0.3$, roughly the boundary of quantitative accuracy and qualitative usefulness of the hot-wire measurements, respectively. It appears that maxima of all Reynolds stresses falls in the high-uncertain region (see fig. 3(b)–(d)) This uncertainty of the data, however, does not significantly alter the general conclusions about the separated shear layer downstream of the step.

The boundary layers on the top and bottom walls of the tunnel merge for $x > 50h$, hence the profiles of different turbulent quantities are contaminated by interaction of the two layers.

Results

In the present study, a low-viscosity oil was used to visualize the flow pattern in the separated region and to determine the mean reattachment length on the bottom wall of the wind tunnel. Flow reattachment occurs at about $x/h = 6.8$ on the centerline. It was observed that the reattachment line is not a straight line in the spanwise direction but curves upstream near the side walls because of interaction with the side wall boundary layers. The reattachment line was nominally straight over 65 percent of the wind-tunnel width.

Wall Pressure Coefficient and Wall Shear Stress

Distributions of the wall-pressure coefficient, $C_p = 2(p - p_o)/\rho U_o^2$, along the top and bottom walls are shown in figure 2(a). Most of the pressure recovery on the step-side of the tunnel occurs within $10h$ of the step while on the top wall it takes about $20h$. The separated shear layer is influenced by the strong adverse pressure gradient, by the streamline curvature and by the presence of a highly turbulent recirculating flow beneath it. Castro and Haque (1987) argued that the re-entrainment of the recirculated fluid into the shear layer dominates the stabilizing curvature influence on the flow. They were studying the flow behind a normal plate, but the comment should also apply to the backstep flow where the curvature is less. After the flow reattaches, the recovering boundary layer evolves under zero pressure gradient. The maximum pressure coefficient is about 0.18.

The distribution of skin-friction coefficient, $C_{f0} = 2\tau_w/\rho U_o^2$, plotted against x/X_r is shown in figure 2(b). The wall shear stress, τ_w, was measured directly using laser-oil interferometry (LOI) throughout the separating/reattaching region. Downstream of the reattachment point, the skin friction coefficient, $C_f = 2\tau_w/\rho U_e^2$ (note that the local free-stream velocity U_e was used for normalization), was also estimated from the Clauser chart, by fitting mean velocity profiles to the logarithmic law of the wall. Note that Jovic and Driver (1994, 1995) showed that the log-law is violated in the near field of reattaching flows. The Ludwieg-Tillmann correlation was also used to estimate skin friction.

Agreement in C_f between the three different methods is good to within 5 percent sufficiently far downstream of reattachment, $x > 20h$ approximately.The discrepancy between the C_f distributions estimated by the two latter methods and the LOI technique, shown in figure 2(c), clearly demonstrate that the Clauser chart and the Ludwieg-Tillmann correlation are not appropriate techniques to determine C_f in reattached/recovery flows.

Separated Shear Layer and Reattachment Region

Mean flow– The sudden change of boundary condition as the no-slip and impermeability conditions are abruptly removed at the step leads to a sudden acceleration of the flow near $y = 0$, producing an inflection point in the mean velocity profile (see fig. 3(a)). The presence of an inflection point leads to a Kelvin-Helmholtz instability and the actual rollup of spanwise vortices immediately downstream of the step. This behavior is clearly documented in a flow visualization movie by Pronchick and Kline (1983). The rolled-up vortices do not occur across the entire separated shear layer but are confined to a thin internal layer imbedded in the original boundary layer (fig. 1). The streamlines shown in figure 3(e) were obtained by integrating inwards from a reference streamline near the boundary-layer edge, the inclination of the streamline to the (known) line $y = \delta$ being assumed equal to that in the upstream boundary layer (i.e., no change in entrainment rate). The reason for this indirect approach is that hot-wire measurements in the recirculation region are not reliable enough to permit integration out from y = 0. It is seen that the average radius of curvature of the streamline $\psi = 0.5$ (which starts near mid-layer in the upstream boundary layer and is not shown in fig. 3(e)) is about $60h$ over the interval $0 < x/h < 5$, after which the curvature reverses but has generally smaller values. A typical value of δ/R is therefore somewhat less than the 0.03 which Plesniak, Mehta, and Johnston (1994) found to produce significant alteration of turbulence in a mixing layer, suggesting that curvature effects in the present separated flow are not large, except possibly near the surface for a short distance near the reattachment point. This is, however, much smaller curvature than that of the normal plate studied by Castro and Haque.

Reynolds stresses– The profiles of Reynolds stresses in the separated shear layer are shown in figure 3(b)–(d). These quantities, and higher-order products of velocity components, are shown in a lab-fixed Cartesian (x, y) coordinate system, not streamline coordinates. Effects of the introduced perturbation (sudden expansion and change of boundary conditions) on the shear layer are obvious. Figure 3 shows that all three measured Reynolds stresses increase significantly in mid-layer ($y = h$), displaying a slope discontinuity in their profiles. Above the discontinuity, for larger y, the flow remains virtually unaltered by the increased turbulence production in the internal layer. This can be seen from figure 3(f), where the shear stress profiles of figure 3(d) are replotted against stream function and the gradual outward propagation of the internal mixing layer is clearly seen: the shear stress on a given streamline outside the internal layer continues to change at about the same slow rate as in the upstream boundary layer. A plot of the value of stream function at the outer edge of the internal mixing layer shows that the growth rate for $x/h > 2$ is approximately double that for $x/h < 1$: evidently the internal layer can propagate more rapidly once its stress-producing eddies grow to a size comparable with those in the outer part of the boundary layer.

Reliable values of stream function cannot be obtained in the lower part of the internal mixing layer, but further insight into the multi-layer structure of the separated shear layer can be obtained from a plot of the u-component skewness $S_u = \overline{u^3}/\overline{(u^2)}^{3/2}$ (fig. 3(g)). S_u takes large values near the free-stream edges of any shear layer (negative on the high-velocity side and positive on the low-velocity side) and goes through zero in the

maximum-intensity region of a mixing layer. The line A-A connecting the left-hand zeroes in figure 3(g) therefore marks the high-intensity region of the mixing layer, and the lines B-B and C-C joining the two sets of minima mark the outer edge of the mixing layer, and the edge of the original boundary layer, respectively, the definition of "edge" being somewhat qualitative. Note that the high-intensity region (or the peak in shear stress) moves inwards with respect to y (fig. 3(d),(g)) but outwards with respect to ψ (fig. 3(f)).

The sharp demarcation between the internal and external layers appears to indicate that the two layers contain large eddy structures with different dynamics, which communicate only through the - presumably small-scale - mixing at the interface. The turbulent stresses shown in figure 3(b)–(d) increase in the downstream direction, attaining almost symmetric distributions about the local peak of each quantity (the profiles in fig. 3(f) are far from symmetrical because $\partial\psi/\partial y = U$ changes rapidly with y). If the step wall were removed, the evolving shear layer would be expected to attain the self-similar structure of a plane mixing layer. In the reattachment region, the presence of the wall is felt by the flow one or two step heights upstream of the mean reattachment point, roughly where all the turbulent stresses reach maxima. The same behavior was observed by Wood and Bradshaw (1982) in the case of a mixing layer constrained by a solid wall, and by Chandrsuda and Bradshaw (1981); Eaton and Johnston (1980); and Troutt et al. (1984) among others in the case of backward-facing step.

There is an unresolved question about the reason for this rapid destruction of the turbulent energy downstream of reattachment acquired in the separated shear layer: note that streamline curvature becomes destabilizing in the reattachment region. According to Troutt et al. (1984), the decay of the Reynolds stresses in the reattachment region coincides with the inhibition of vortex pairing due to the close proximity of the bottom wall. Pronchick and Kline (1983), based on their flow visualization, observed a large number of different instantaneous events and divided them into the two major categories: (i) "overriding" eddies that pass over the reattachment zone mostly unaltered and (ii) "interacting" eddies which are significantly altered after interaction with the wall. They divided the latter group further into the three subgroups: (1) recirculated backflow - an eddy is recirculated after suffering major distortion, (2) downstream interaction - an eddy is torn in two so that one portion convects downstream while the other one provides backflow, (3) lifted backflow - part of a recirculating flow (eddy) is lifted by another overriding eddy or an interacting eddy. All three processes lead to the reduction of turbulent length scales. The presence of such eddies with different origins in different parts of the reattachment region give rise to a "discontinuity of history" which results in a reduction of the correlation between velocity components - i.e., a reduction in shear stress.

Comparison with a Plane Mixing Layer

The separated shear layer is influenced by the strong adverse pressure gradient, the short development length, the presence of a highly turbulent recirculating flow beneath it and a sheared turbulent boundary layer above it, and possibly by the streamline curvature. Thus, the separated shear layer cannot be expected to resemble a plane mixing layer exactly. As indicated in the two sections above, it appears that the separated boundary layer initially responds to the perturbation only in a thin layer close to the source of the perturbation (in this case, the step lip) while the rest of the external layer remains unaffected. The internal layer, which develops imbedded in the original boundary layer, must bear some phenomenological similarity to a plane mixing layer. Therefore, similarity of the evolving internal layer to a plane mixing layer is examined in this section, and we begin by defining suitable scales for the comparison. The vorticity thickness of a mixing layer is commonly defined as $\Lambda = \Delta U/(\partial U/\partial y)_{max}$, where $\Delta U = U_e - U_{min}$ and U_e is the shear layer edge velocity. The minimum velocity, U_{min}, on the low-speed side of the present shear layer is not evaluated directly due to the inherent deficiency of the

hot-wire technique in the reversed flow regions. U_{min} is obtained indirectly by fitting the measured velocity profile to the well established velocity profile in the regular mixing layer, given by $0.5\,[1 + tanh\,(\eta)]$, where $\eta = (y - y_c)/\Lambda$ with y_c representing the location of the velocity gradient maximum. This trial-and-error procedure was complete when the best fit to a given analytic velocity profile was established.

The parameters ΔU and Λ were used as the normalization parameters for further assessment of the similarity of the two flows. The growth of the shear layer vorticity thickness is shown in figure 4(a) where the solid line represents the vorticity thickness growth taken from Castro and Haque (1987). The quantity $\Lambda/2\delta_0$ (fig. 4(b)) expresses the half-thickness of the internal mixing layer as a fraction of the original boundary layer thickness. Figure 4(b) shows that the internal layer indeed grows within the original boundary layer and that it apparently spreads across the entire shear layer before the flow reattaches at about $x/h = 7$. The present data do not show a strictly linear increase in Λ as is the case for a plane mixing layer. The initial growth rate of the internal mixing layer appears to be higher than that of a plane mixing layer, while in the reattachment region the vorticity thickness actually decreases. Similar behavior of the vorticity thickness was observed by Castro and Haque (1987). Figure 4(c) shows $(\Delta U)/U_e$. The maximum value of about 1.1 indicates that $U_{min} = -0.1\,U_e$ which is in good agreement with the laser measurements of Driver and Seegmiller (1985). It decreases quite rapidly near reattachment, evidently because of the distortion of the velocity profile by the induced pressure gradient. Once this starts to happen, further resemblance between the step flow and a mixing layer cannot be expected. The mean velocity profiles in self-similar coordinates are shown in figure 5(a). It is seen that the mean velocity within the internal layer collapses on the self-similar velocity profile of the plane mixing layer: this has been largely forced by the fitting procedure explained above.

The profiles of the Reynolds stresses are shown in figure 5(b)–(d) in similarity coordinates. Initially, the normalized stresses decrease from the initial high values adjusting from the boundary layer to an internal mixing layer structure. Apparently, the Reynolds stress distributions fail to recover to those of the self-similar profiles of Bell and Mehta (1990). The observed overshoot of the stresses (for $x > 6h$) can be attributed to the slow response of turbulence to the reduction of the mean rate of strain across the shear layer. The mean rate-of-strain field reduces rapidly in the reattachment region due to the local acceleration of the flow in the presence of the wall. The profiles of the Reynolds stresses in the separated shear layer would eventually coincide with those of a regular plane mixing layer providing that the separated flow had a sufficient streamwise length for its development. However, the $u = 0$, $v = 0$ boundary condition at the wall gives birth at reattachment to a boundary layer, which starts to interact with the internal mixing layer.

Higher-order fluctuating velocity products such as $\overline{u^2 v}$ and $\overline{uv^2}$ (others are omitted for brevity) show a high degree of similarity to those in a plane mixing layer (see fig. 6). The restriction of the growth of large structures by the presence of the bottom wall leads to the reduction of triple velocity products close to the wall (a negative lobe of the distributions) as observed in the experiment of Wood and Bradshaw. Near, and downstream of, reattachment, several further processes may affect the triple products: break-down of the large structures, flow interaction with recirculating parts of the torn structures and re-entrainment of the same. The lobes in the outer region reduce at a much slower rate suggesting that the large structures in the outer layer remain almost unaffected.

The shear correlation coefficient $R_{uv} = \overline{uv}/\left(\sqrt{\overline{u^2}}\sqrt{\overline{v^2}}\right)$, which represents a measure of the efficiency of turbulent mixing, and $\overline{v^2}/\overline{u^2}$, are compared with the plane mixing layer data of Bell and Mehta (1990) in figure 7. In the initial stages of the separated shear layer development, R_{uv} attains a value of 0.6 in the mid layer, which is significantly

larger than in the plane mixing layer. It appears that the turbulent mixing near the step is higher in the central portion of the shear layer ($-1 < \eta < 1$). However, R_{uv} approaches 0.5 in the mid layer of the flow for increasing x. This shows that the structural parameter of the separated shear layer approaches that of the self-similar plane mixing layer. On the high-velocity side ($\eta > 0$) of the separated shear layer (in the outer layer), for $\eta > 1.5$ and $x < 2h$ ($x > 2.5\delta_o$), R_{uv} attains a constant value of 0.45 which is a value typical for a zero-pressure-gradient turbulent boundary layer. This suggests that the external flow is unperturbed for $x < 2h$ and that it retains its similarity to the upstream boundary layer. Downstream of this x location, it appears that the external flow region changes its boundary-layer character and approaches that of a mixing layer due to the stronger interaction of the internal and external layers.

A similar argument applies to the anisotropy parameter, $\overline{v^2}/\overline{u^2}$. The competing mixing-layer like structure appears to prevail gradually over that of the outer boundary-layer like structure for $x > 2h$. The data show that $\overline{v^2}/\overline{u^2}$ profiles are somewhat lower than in the self-similar plane mixing layer. Close to reattachment, the profiles on the low-velocity side resemble that of a boundary layer suggesting that fluctuations of the transverse v-velocity component are attenuated faster than the u component as the flow approaches the wall. On the high-velocity side (for $\eta > 1.5$) and for $x < 2h$, the given ratio is initially about 0.4 which is a characteristic value for a plane boundary layer. Further downstream, the ratio gradually approaches the distribution of an ordinary plane mixing layer, indicating that the structure of the mixing-layer-like flow prevails over that of a boundary layer.

Eddy viscosity and mixing length, shown in figure 8(a),(b) respectively, evolve in a similar fashion to all of the above turbulent quantities. They are low at the first few stations, but approach the self-similar distribution of a plane mixing layer for $x > 5h$. Reattachment occurs at $x = 6.8h$.

Time-averaged triple products of the velocity fluctuating components constitute turbulent diffusion terms in the Reynolds stress and turbulent kinetic energy balance equations. Transport velocities of turbulent kinetic energy, $V_k = -K_1\left(\overline{u^2v} + \overline{v^3}\right)/K_2\left(\overline{u^2} + \overline{v^2}\right)$, and shear stress, $V_{uv} = \overline{uv^2}/\overline{uv}$, normalized by ΔU are shown in figure 9. Values of approximation constants, in case when w velocity component is not measured, have been usually set to $K_1 = K_2 = 0.75$. However, the DNS data of the back-step flow (Le, Moin, and Kim (1993)) indicate that the above values overestimate corresponding terms, and that the values $K_1 = 0.6$ and $K_2 = 0.7$ provide a better approximation. The data show that the evolving V_k and V_{uv} nominally resemble those of the plane mixing layer. It appears that the fluxes of the turbulent energy and the shear stress are slightly larger in the central portion of the separated shear layer where V_k and V_{uv} exhibit a self-similar character. In the reattachment region V_{uv} rapidly becomes more negative for $\eta < -1$ as $-\overline{uv}$ approaches zero near the wall.In summary, the data indicate that the perturbation introduced by the separation of the original turbulent boundary layer (TBL) at the step lip does not affect the separated shear layer across the entire thickness instantaneously. Instead, an internal mixing layer is generated, emanating from the step lip, imbedded in the external TBL, spreading in the transverse direction, and carrying information about the new boundary condition across the flow. The results indicate that the internal mixing layer experiences an "adjustment phase" in the near field (for $x < 2h$), while the external boundary layer structure remains unaltered. For larger x, it appears that external and internal layers interact more vigorously, leading to a dominant mixing-layer-like structure across the entire shear layer. The overshoot of Reynolds stresses at locations close to the reattachment (in mixing layer similarity coordinates), when compared with the plane mixing layer profiles, can be attributed to the slow response of turbulence to a change of the mean rate of

strain. It should be emphasized that it cannot be expected that the mixing layer will fully resemble a self-similar plane mixing layer due to its restricted developing length, presence of the wall, adverse pressure gradient and presence of the highly turbulent recirculating region below the separated shear layer. However, the above findings point to a very strong qualitative similarity of the internal layer to a plane mixing layer.

This thin internal layer has a turbulence structure resembling that of a plane mixing layer. Above this is an external layer unaffected by the perturbation and strongly resembling the original boundary layer. By about $x = 2h$ the internal layer has filled the inner layer of the original boundary layer and commences strong interaction with the outer external layer while the whole separated shear layer moves towards the wall.

Recovery region

In the recovery region, the mixing-layer-like structure of the separated shear layer encounters a solid wall at reattachment and begins to recover to a structure characteristic of a plane TBL. As in the case of the flow downstream of separation, the response of the turbulence structure to the imposed new boundary condition is not instantaneous across the entire flow but is achieved rather gradually in y as well as in x. The results show that an internal layer forms downstream of reattachment as a result of a sudden imposition of the no-slip boundary condition. Initially, the internal layer is dominated by the external layer dynamics carrying the memory of the upstream, mixing-layer-like, flow structure. However, the near-wall structure within the evolving internal layer recovers to that of an equilibrium plane TBL, as shown below, although recovery is far from complete at the last test station. Three different basic flow structures, namely that of the mixing layer, and those of the wall and wake layers of the plane TBL, compete in the recovery region downstream of reattachment. It is clear that this type of flow deviates strongly from an equilibrium turbulent flow structure in the "near field," i.e., the region just downstream of reattachment for $X_r < x < 20h$ ($X_r = 6.8h$).

Mean Flow

Profiles of mean U-component velocity in the recovery region, measured with normal and crossed hot wires, are shown in wall coordinates in figure 10(a). It is apparent that the velocity profiles close to reattachment do not collapse on the universal law of the wall. This is consistent with the results of Jovic and Driver (1994, 1995). Note that the u_τ used was obtained from the direct measurements of τ_w using the laser oil-film interferometry technique. The profiles exhibit smaller velocity gradients, suggesting larger turbulence length scales as discussed by Bradshaw and Wong (1972). The large "wake" contribution to the mean velocity profiles is not produced by an adverse pressure gradient - pressure gradient is negligible in the recovery region as seen in figure 2 - but is generated by the mixing-layer-like flow upstream of reattachment. This "mixing layer" contribution gradually decays with x as the outer flow is increasingly influenced by the spreading of the newly developing wall layer. This feature of the flow during the recovery phase will be discussed more in the next section. For $x/h > 20$, the mean velocity profile rises to follow the universal log-law over a range of y that gradually increases downstream, although even at the last measurement position, $x = 51h$, the profile still dips below the log law; the "wake" component is much smaller than in an equilibrium TBL and is still decreasing.

Reynolds Stresses

Distributions of the three measured Reynolds stresses in wall coordinates are shown in figure 10(b)–(d). All three stresses attain maxima in the outer layer of the recovering boundary layer downstream of the mean reattachment point. The peaks have decreased somewhat from the values in the separated shear layer but are still several times larger than those in an equilibrium TBL. In the reattachment and recovery regions, the flow accelerates near the wall, resulting in the gradual reduction of the velocity gradients

across the outer part of the flow and in an increase of the gradients near the wall. Simultaneously, all the Reynolds stresses monotonically decrease across the entire recovering boundary layer.

Measurements very close to the wall revealed that the normal stress $\sqrt{\overline{u^2}}$ does not scale on the wall variables during the initial stages of the flow recovery, as seen in figure 10(b). $\sqrt{\overline{v^2}}$ (fig. 10(c)) is also nonuniversal, at least for $yu_\tau/\nu > 30$, but less strongly. $-\overline{uv}$ is of course forced to collapse just outside the buffer layer, where the total shear stress is still closely equal to the wall shear stress. nonuniversality of $\sqrt{\overline{u^2}}$ and $\sqrt{\overline{v^2}}$ can be attributed to the "splat effect," i.e., the $v = 0$ boundary condition redistributes fluctuations to u and w components induced by the constraint of the large-scale eddies of the former mixing layer, for values of y much less than the typical wavelengths of those eddies. However this does not explain the milder nonuniversality of $\sqrt{\overline{v^2}}$. The u-component turbulence intensity exhibits a plateau, $u_{rms}/u_\tau \approx 4.5$, for $40 < yu_\tau/\nu < 100$ at $x = 9.87h$. u_{rms}/u_τ is attenuated for smaller normal distances from the wall while it increases for larger distances until it reaches a maximum in the outer layer. The plateau region can be interpreted as a region where the wall and the external-layer influences overlap. In other words, the value of y at the inflection point is related to the thickness of the internal layer. This will be discussed in more detail below, with reference to the higher-order statistics, skewness and flatness, and the quadrant analysis of the shear stress. It appears that the plateau and the associated inflection point propagate away from the wall with downstream distance, indicating the thickening of the internal layer and the outward spreading of the wall influence.

In the near field of reattachment, the normal stresses decay rapidly, while further downstream the rate of decay is rather slow. Figure 11(a) shows the variation with x of the maximum value of u_{rms}/u_τ in the outer layer and its value in the internal layer at $yu_\tau/\nu \approx 20$. It is seen that the turbulence intensities in the two layers, the internal boundary layer and external layer, are initially proportional. At $y^+ \cong 20$, however, u_{rms}/u_τ falls to a value of about 3.0 at $x \approx 20h$ and remains constant for the rest of the recovery region, suggesting that the turbulence structure recovers to that of an equilibrium TBL in a very thin layer close to the wall, regardless of high turbulence levels in the external layer. At the same x location ($x \approx 20h$), the turbulence intensity attains a maximum value of about $3.5u_\tau$ in the outer layer, or in terms of the free-stream velocity, U_e, and the local skin friction coefficient: $u_{rms}/U_e = 3.5\sqrt{C_f/2}$. We can infer a rough general rule that any flow perturbation (in the mid layer) equal to or greater than this threshold level will be sufficient to alter the near-wall boundary layer structure significantly.

At $x \approx 20h$, all Reynolds stresses attain their characteristic equilibrium values (in wall units) near the wall. It appears that C_f has nominally recovered (fig. 2(b)), and the law of the wall for the mean velocity profile has reached as far out as $y^+ = 100$ (fig. 10(a)), at the same x location. Based on these characteristic features, it can be concluded that the internal layer qualifies as a quasi-equilibrium layer for $x > 20h$. Most likely, the first and the second derivatives of the u_{rms}/u_τ distribution are equal to zero at $y^+ \cong 20$ at this x location. It appears that once the quasi-equilibrium internal layer forms, the law of the wall holds almost independently of the external flow conditions, providing $u_{rms}/u_\tau \leq 3.5$ or $u_{rms}/U_e = 3.5\sqrt{C_f/2}$, where u_{rms} represents a maximum turbulence intensity in the external shear layer. The implication is that, in the case of an equilibrium turbulent boundary layer with $C_f = 0.003$, a free-stream turbulence level of the order of 15 percent, and greater, affect the near-wall structure for $y^+ < 20$. In the outer region, the turbulence intensity continues to decay, as seen in figure 11(a), indicating that the turbulence in that region has not approached an equilibrium state even at the last measuring station, $x = 51h$.

The decay of the maximum shear stress, $-\overline{uv}/U_e^2$, and the maximum turbulent kinetic energy, k/U_e^2, is plotted on a log-log scale in figure 11(b). The peak values of both quantities lie approximately along straight lines for $x > 30h$. The peak shear stress decays approximately as $x^{-1.33}$, though its asymptotic value is nominally unity (not zero) while the turbulent energy decays somewhat slower, as $x^{-1.27}$, suggesting slightly faster shear stress recovery. It appears that the rate of energy decay of the present experiment is approximately same as that of the homogeneous turbulence energy-decay rate for x > 30h (Gibson and Dakos (1993)).

In summary, two regions are identified, the near-field $X_r < x < 20h$ and the far-field $x > 20h$. In addition, two distinct layers in the transverse direction of the reattached boundary layer can be identified downstream of the reattachment region. One is very thin, of the order of 20 to $100\nu/u_\tau$ in the near-field, and is identified as an internal boundary layer. The internal layer is dominated by the external layer dynamics in the near-field region, attaining a quasi-equilibrium state by $x \approx 20h$. The outer layer is characterized by a strong memory of the upstream perturbation, i.e., it is characterized by the mixing-layer type of Reynolds- stress production and the large "mixing-layer contribution" seen in the mean velocity profiles. However, for $x > 20h$ the inherited mixing-layer structure of the external layer comes under the increasing influence of the boundary-layer-like structure of the internal layer.

Triple Products

Profiles of $\overline{u^2v}$, $\overline{v^3}$, $\overline{uv^2}$, and $\overline{u^3}$, normalized by U_e^3, are shown at the different measuring stations in figure 12. Since we are no longer concerned specifically with the internal wall layer, these and later quantities are plotted against y/δ instead of y^+. Magnitudes of the normalized triple velocity products near reattachment are about 20 times greater than those of an equilibrium TBL. This in its own right shows the importance of an accurate modeling of turbulent transport (diffusion) terms in the balance equations of Reynolds stresses. Beside high magnitudes, it is striking to observe presence of large negative lobes in $\overline{u^2v}$ and $\overline{v^3}$ in the attached region at least as far as $x = 20h$, despite the attenuating effect of the solid surface. This shows that the flow still has a very strong memory of the upstream mixing-layer-like flow. It appears that $\overline{u^3}$ is much less sensitive to the newly imposed boundary conditions, judging by its slow rate of decay near the wall as seen in figure 12(d). The large eddies are affected by the proximity of the wall exerted through the $u = 0$ and $v = 0$ boundary condition. The turbulent fluxes associated with the diffusion of turbulent kinetic energy normal to the wall are severely attenuated close to the wall ($y/\delta < 0.1$ say).

The local minimum and maximum values of the triple products occur at approximately 0.2δ and 0.6δ with the zero point at about 0.35δ: compare the behavior of the u-component skewness upstream of reattachment in figure 3(g). The reduction of the triple products near the wall suggests that the large eddies break down or get flattened, producing eddies of smaller length scales. This is consistent with the flow visualization observations of Pronchick and Kline (1983), and with the above findings for the normal stress. The negative lobes of $\overline{u^2v}$, $\overline{v^3}$, and positive lobes of $\overline{uv^2}$ disappear for approximately $x > 25h$, when the triple products resemble those of an equilibrium TBL near the wall. The difference between the two distances, $20h$ and $25h$, the former being deduced from the normal stress ($\sqrt{\overline{u^2}}$) and the latter from the triple products, indicate that the contribution of the turbulent transport (diffusion term) to the Reynolds stresses for $x > 20h$ is not significant.

Turbulence Structural Parameters, Higher Order Statistics and the Quadrant Analysis

The structural parameters of the recovering flow are compared with those of the upstream undisturbed TBL in figures 13–15. Structural parameters $\overline{v^2}/\overline{u^2}$ and R_{uv} are

shown in figure 13. The low values of both parameters near the wall in the initial stages of the recovery region indicate relatively stronger attenuation of the v-velocity component when compared to the u-velocity component. This is consistent with the observations made above for the Reynolds stresses and triple velocity products in the near field. In the outer layer, values of $\overline{v^2}/\overline{u^2}$ and R_{uv} appear to be generally larger than the distribution characteristic for an undisturbed TBL. $\overline{v^2}/\overline{u^2}$ increases while R_{uv} decreases with increasing x, attaining constant values of about 0.5 and 0.42 respectively. The trend of increasing $\overline{v^2}/\overline{u^2}$ suggests somewhat slower recovery of the v component when compared to the u component in the outer layer. The mildly decreasing trend of R_{uv} indicates a faster rate of recovery of the shear stress (or reduced efficiency of maintenance of shear stress) compared to that of the turbulent kinetic energy (not shown here). This is consistent with the rates of decay of the shear stress and the turbulent kinetic energy presented in figure 11.

The ratio $-\overline{uv}/\overline{v^2}$ (fig. 13(c)) shows rather clearly how the internal boundary layer starting at the reattachment point spreads out into the former mixing layer. $-\overline{uv}/\overline{v^2}$ is just $R_{uv}\sqrt{\overline{u^2}/\overline{v^2}}$ but as a diagnostic of shear-stress behavior it has the advantage over R_{uv} that it is not contaminated by u and w component fluctuations resulting from the "splat effect" of wall constraint mentioned above, which contributes to turbulent kinetic energy but not to $-\overline{uv}$ or $\overline{v^2}$). The value at $y/\delta \approx 0.15$ changes more slowly than the remainder of the profile, because of conflicting effects: close to the surface, (the closest data point is at very roughly $y^+ = 35$, so the fact that $-\overline{uv}/\overline{v^2} \sim 1/y$ in the viscous sublayer is immaterial) $-\overline{uv}/\overline{v^2}$ rises slowly from nominal zero at reattachment, but even at $x/h = 51.18$ the undisturbed boundary layer trend is approached only for $y/\delta = 0.03$ approximately. A rising tide of $-\overline{uv}/\overline{v^2}$ starts to fill up the original profile, whose inner part happens to be almost linear on the semi-log plot of figure 14(c). When this tide reaches $y/\delta = 0.15$ (somewhere between $x/h = 15.13$ and $x/h = 20.29$) the peak in $-\overline{uv}/\overline{v^2}$ near $y/\delta = 0.5$ starts to decrease. Remarkably, the peak is still decreasing strongly at the last station, $x/h = 51.18$, and is well below the boundary-layer value to which it must revert downstream. A possible explanation of the decrease is that as the internal boundary layer grows, it starts to interfere with the large eddies in the outer layer, whose structure is qualitatively that of a mixing layer: evidently, the interaction between two different eddy structures produces a less efficient structure than either - i.e., it reduces the shear stress for a given turbulent intensity.

The relatively large positive u-component skewness S_u for $y < 0.3\delta$, shown in figure 14(a), indicate that the u-component is lower than its mean value more often than not. However, the condition $\bar{u} = 0$ implies the presence of rare but large positive spikes of u-component, which contribute to the long tail of the velocity probability distribution and tend to produce a large flatness factor also. There are two types of motions which can be associated with positive u-spikes, depending upon the sign of the v-component. One is the type of event which occurs in quadrant I (Q_1) of the (u, v) plane, i.e., $u > 0$ and $v > 0$, which like a Q_3 event is called "interactive" motion, and the other is the Q_4 event with $u > 0$ and $v < 0$, which is usually called a "sweep" (see Willmarth and Lu (1972); Wallace, Eckelmann, and Brodkey (1972) for a discussion of quadrant analysis). In the early stages of the flow recovery, surprisingly, the S_v profiles cross zero at two y locations, $y \approx 0.03\delta$ and $y \approx 0.3\delta$ as seen in figure 14(c). For $y < 0.03\delta$, positive S_v and S_u suggest the presence of positive u and v spikes associated with quadrant I events (interactive motion). This type of motion possibly occurs when a sweep ($u > 0$, $v < 0$) is deflected by the wall and is being ejected back into the flow ($u > 0$, $v > 0$).

Simultaneous large values of F_u and F_v near the wall (see fig. 14(b),(d)) indicate large excursions of the fluctuating velocity components from their mean. Note that the flatness factor is roughly equal to $3/\gamma$, where γ is the intermittency factor (Corrsin and Kistler (1955)). Hence, the large values of F_u and F_v in the inner layer indicate lower intermittency factor which is produced by the large structures which, on the other hand, communicate between the outer and inner layer of the recovering boundary layer.

It appears that the S_v cross-over point closer to the wall coincides with the plateau observed in the streamwise turbulence intensity $\overline{u^2}$ (fig. 10(b)), i.e., it roughly corresponds to the inflection point near the wall. This first zero-crossing of S_v gradually moves away from the wall while the second crossing (further away from the wall) moves towards the wall at the downstream stations, until S_v becomes positive across the entire boundary layer at about $x = 28h$. Relatively large negative values of S_v for $0.03\delta < y < 0.3\delta$ for a flow in the early stages of the recovery indicate a behavior quite different from a plane TBL. Positive S_u and negative S_v show that Q_4 dominate in this y interval. The sweeps intermittently transfer high momentum fluid to the inner layer, producing high normal stresses, while shear stress remains surprisingly low (see fig. 10(d)). Initially, both skewnesses, S_u and S_v, change sign at $y \approx 0.3\delta$. This location corresponds to the distance where all Reynolds stresses attain their maximum values. Ueda and Hinze (1975) found that the location where S_u change sign coincide with the location where $\overline{u^2}$ attains a local maximum value in the wall region of an equilibrium TBL. Simpson, Chew, and Shivaprasad (1981) found that S_u crosses zero at $y \approx 0.4\delta$ where $\overline{u^2}$ has a local peak in case of the separating turbulent boundary layer. For $y > 0.3\delta$, negative S_u and positive S_v indicate occurrence of large negative and large positive u and v peaks, respectively, suggesting that Q_2 dominates farther away from the wall. It appears that the higher order statistics of u- and v-components in the inner layer approach those distributions of a plane TBL for $x > 25h$ coinciding with the distance deduced from the turbulent diffusion fluxes.

Beside the qualitative observations made above for the higher order statistics, better understanding of the physics of the recovering boundary layer can be gained through a quadrant analysis of the measured shear stresses. The fractional contributions to the Reynolds shear stress from each quadrant in the (u, v) plane are determined for two locations, $x = 9.87h$ and $38.55h$, and they are compared with the corresponding distributions measured in the upstream plane TBL. The results are shown in figure 15. At $x = 9.87h$ (fig. 15(a)) the turbulence near the wall is still in a disordered state and the shear stress is still small for $y < 0.05\delta$ (compared to the turbulent energy, say), so that contributions from the four quadrants almost cancel and the customary normalization by $-\overline{uv}$ is not very meaningful. It is more useful to normalize by the Q_2 contribution ($u < 0$, $v > 0$), i.e., ejections from near the surface, which can be regarded as locally-generated turbulence as distinct from the Q_4 sweeps imposed from above, and this is done in figure 16. Compared with the upstream boundary layer there are now stronger sweeps in the inner layer throughout the recovery region, and the negative contributions, Q_1 and Q_3, increase greatly as y decreases. It is curious that Q_3 (incoming low-speed fluid) is smaller than Q_1 (high-speed fluid moving away from the surface, which would be expected to be a rarer event). Possibly the Q1 contributions are the return flow from the "splat effect." By $x/h = 38.55$ (figs. 15(b) and 16(c)) the quadrant contributions look much more like those in the upstream boundary layer.

The fraction of time the uv signal spends in each quadrant is also of interest, the relevant quantity being the departure from 1/4 (fig. 17). In the upstream boundary layer, sweeps from above (Q_4) occupy more time than ejections from

below (Q_2), both near the surface and in the outer intermittent region, and Q_1 and Q_3 occupy shorter times except near the outer edge. At $x/h = 9.87$ (fig. 17(b)), Q_4 sweeps, though now making a larger contribution to uv than Q_2 in the first 30 percent of the shear layer thickness, are shorter than the Q_2 events, whereas Q_4 events become much longer than Q_2 in the outer part of the flow, occupying nearly half the total time. The percentage of time occupied by Q_1 and Q_3 events is roughly the same as in the upstream boundary layer. The broad outer-layer peak in Q_4 time is still present at $x/h = 38.55$, where the quadrant contributions to uv have nearly returned to the boundary-layer distribution. Once more we see the long persistence of the mixing layer structure in the outer layer.

Transport of the Turbulent Kinetic Energy and Shear Stress

The balance of the turbulence kinetic energy at four representative streamwise locations ($9.87h$, $11.84h$, $20.29h$, and $38.55h$) is shown in figure 18. Distributions at six other additional locations are not shown, for brevity, but will be used in the discussion below. The turbulent kinetic energy equation for two-dimensional flows may be written as follows

$$U\frac{\partial k}{\partial x} + V\frac{\partial k}{\partial y} = -\frac{\partial}{\partial x}\overline{u\left(k + \frac{p}{\rho}\right)} - \frac{\partial}{\partial y}\overline{v\left(k + \frac{p}{\rho}\right)} - \left(\overline{u^2} - \overline{v^2}\right)\frac{\partial U}{\partial x} - \overline{uv}\frac{\partial U}{\partial y} - \varepsilon$$

Contribution by fluctuating pressure-velocity covariances to the turbulent transport (diffusion term) is typically small in wall bounded flows and was therefore neglected. However, this approximation may be quite crude in the reattachment region of separated flows where large pressure and velocity fluctuations take place.

All terms of the transport equation were evaluated from the measured turbulent quantities except the rate of dissipation, which was obtained by difference of all the other terms. The uncertainty of individual terms is rather difficult to estimate; however, the terms containing gradients with respect to x are clearly more uncertain on a percentage basis than those containing gradients with respect to y though the latter are larger. The uncertainty of the dissipation when determined from the difference is rather high. Since the spanwise velocity component was not measured, the following approximations are introduced. The turbulent kinetic energy, k, was approximated by $0.7\left(\overline{u^2} + \overline{v^2}\right)$, turbulent diffusion in the streamwise direction, $\overline{uk}$, and in the transverse direction, $\overline{vk}$, were approximated by $0.6\left(\overline{u^3} + \overline{uv^2}\right)$ and $0.6\left(\overline{u^2v} + \overline{v^3}\right)$ respectively as suggested by the DNS data for the separated flow, as indicated above.

At reattachment, part of the mixing-layer-like flow is deflected upstream (at least in a time-average sense), bringing highly-turbulent fluid close to the wall. The turbulent kinetic energy balance in a true mixing layer has very large diffusion terms, the loss by diffusion in the central part of the layer being almost as large as the dissipation, with correspondingly large gains near the edges. In the reattachment region, the near-equality of gain by diffusion and loss by dissipation near the wall makes the energy balance unlike that in the inner layer of a boundary layer (production = dissipation) or in any part of a mixing layer. It is seen that the contributions to the turbulent energy by the production and convection are negligibly small in this part of the flow. Although the large eddies which carry out the turbulent diffusion are distorted by the $v = 0$ boundary condition at the surface, gain by diffusion is a major term in the energy balance near the wall as far downstream as $x/h \approx 15$ (fig. 18(a) and (b)), and there is still significant gain by diffusion near the wall at $x/h = 38.55$. It takes a very long time for the flow to regain energy equilibrium (production approximately equal to dissipation, as it is over most of the thickness of a constant-pressure TBL).

It was found that contributions from the three terms, longitudinal turbulent diffusion, $\partial\overline{uk}/\partial x$, production by the normal stresses, $-\left(\overline{u^2}-\overline{v^2}\right)\partial U/\partial x$, and the mean flow transport are significant downstream of reattachment, in contrast to a regular TBL where contributions by these three agents are negligibly small. Production by the normal stresses near the wall is negative, since $\partial U/\partial x$ is positive due to the flow acceleration and $\overline{u^2}$ is larger than $\overline{v^2}$. Note that advection is small - rapid changes in mean flow do not necessarily mean rapid changes in turbulence. This negative production of turbulent energy is nearly equal to the shear production $-\overline{uv}\partial U/\partial y$, in the inner layer (which is still of the order of magnitude of $u_\tau^3/(\kappa y)$ as predicted by the law of the wall) so net production is much smaller than dissipation in the inner layer, at least as far as x/h = 12 (fig. 18(b)). These features lead to the conclusion that turbulence models which use equilibrium assumptions are not applicable in the near field of reattachment. Note that the k-equation terms shown in figure 18 were made dimensionless by U_e^3/δ where U_e is a boundary layer edge velocity and δ is a local boundary layer thickness.

The distributions of all the terms of the k-equation in the outer portion of the flow strongly resemble the distributions of the same terms in an ordinary plane mixing layer (fig. 18). Even though the magnitude of each term reduces in the downstream direction, this similarity is retained even up to about $20h$. This shows that the mixing-layer-like structure is still present, but decays gradually in the outer part of the flow. On the other hand, the competing wake-like structure of a regular TBL asserts its presence through the boundary condition $u = 0$ and $v = 0$ at the wall. It affects the mean-velocity gradients, production of turbulence and the turbulent transport through the confinement and break up of large eddies produced in the separated region. As a result, the peak of the production shifts from the central region of the layer to the wall region where the velocity gradient begins to dominate and the shear stress gradually increases. Transport by the turbulent diffusion gradually decreases in the outer region (see fig. 18(b),(c)). while the maximum loss moves towards the wall. The peak of turbulent diffusion in the central region of the flow occurs approximately at 0.5δ. The peak of the diffusion is surprisingly large, almost as large as the secondary peak in production even at x/h = 38.55. Apparently, large eddies transfer turbulent energy from the central, energy-rich, region toward the wall and outwards to the boundary layer edge as can be seen in figure 18(a),(b). The data suggest that an accurate prediction of the separated/ reattached flow will require a good model for the turbulent diffusion terms.

The production peak occurs at about 0.45δ in the transverse direction and is larger than the near-wall production in the near field (up to $20h$). Downstream of this location, the production in the wall region rapidly increases. It appears that the competing outer layer/mixing-layer like structure ceases to affect wall structure by about $x = 20h$ when the familiar wall mechanisms prevail in the production of the wall turbulence. By the streamwise distance of about $x = 30h$, the transport terms of the turbulent kinetic energy further decrease in the outer part of the flow as seen in figure 18(b)–(d), gradually approaching the structure of an equilibrium constant-pressure TBL.

The balance of the shear stress, $-\overline{uv}$, in four streamwise locations ($9.87h$, $11.84h$, $20.29h$, and $38.55h$) is shown in figure 19, again with the terms made dimensionless by U_e^3/δ. The shear stress transport equation for two-dimensional flows may be written as follows

$$U\frac{\partial -\overline{uv}}{\partial x}+V\frac{\partial -\overline{uv}}{\partial y}=\frac{\partial}{\partial x}\left(\overline{u^2v-\frac{p}{\rho}v}\right)+\frac{\partial}{\partial y}\left(\overline{uv^2-\frac{p}{\rho}u}\right)$$
$$+\overline{v^2}\frac{\partial U}{\partial y}+\overline{u^2}\frac{\partial V}{\partial x}-\overline{\frac{p}{\rho}\left(\frac{\partial u}{\partial y}+\frac{\partial v}{\partial x}\right)}$$

The turbulent diffusion due to the pressure-velocity correlations, $\partial(\overline{vp/\rho})/\partial x$ and $\partial(\overline{up/\rho})/\partial y$, and the production by the normal stress, $\overline{u^2}(\partial V/\partial x)$, were neglected. It appears that the advection term is smaller than for the *k*-equation. The three terms which dominate the transport of shear stress are production, $\overline{v^2}(\partial U/\partial y)$, combined longitudinal and transverse turbulent diffusion, and the pressure-strain "redistribution" term. In the central portion of the recovering flow, the maximum shear-stress production occurs at the same location as the maximum production of turbulent energy. In the near-wall region, the gain by diffusion and the loss by the pressure-strain term are not balanced as would be expected from the behavior of the *k*-equation near the wall. The shear-stress diffusion term is of the same magnitude and sign (gain) as the production term in the wall region. The production of the shear stress has significantly increased near the wall by $x = 20h$ (see fig. 19(b)). Distributions of diffusion and pressure-strain terms in the wall region resemble those in a plane TBL by about x = 30*h*, which is consistent with the behavior of the *k*-equation. In the outer part of the flow, all three terms decrease significantly beyond 30*h* so that by $x = 38.55h$ (see fig. 19(c)) the distribution of all terms strongly resembles that of a regular TBL. The faster recovery towards local equilibrium is partly illusory: the "rapid" part of the pressure-strain term acts in direct opposition to the production term, and is often so modelled: if the two terms are merged to give a net production, the shear-stress balance looks much more like the energy balance, with the "slow" part of the pressure-strain term playing the same part as energy dissipation.

Derived Quantities and their Implications for Modeling

In the recovery region, the shear stress and mean streamwise velocity, measured in the Cartesian coordinate system, were used to evaluate Prandtl's mixing length, $l = \sqrt{-\overline{uv}}/(\partial U/\partial y)$, and the eddy viscosity, $\nu_t = -\overline{uv}/(\partial U/\partial y)$. Though lacking physical meaning, these two quantities have been successfully used as the basis of data correlations in turbulence models for calculating slowly-evolving flows. However, such correlations fail in more complex flow configurations, such as separating/reattaching flows, where the Reynolds stresses respond slowly to the rapid changes of the mean rate of strain. nondimensional mixing-length, l/δ, and eddy-viscosity, $\nu_t/(U_e\delta_1)$ (where δ_1 is the local displacement thickness), are shown in figure 20(a),(b) respectively, compared with the distributions in the upstream fully developed TBL. The values of the Reynolds number Re_θ in the recovery region for the given Re_h are typically over 9000 compared to 3600 in the upstream boundary layer, but mixing length and eddy viscosity are not expected to depend significantly on Reynolds number in this range. Near the wall the mixing length is a linear function of the normal distance from the wall. However, the slope is significantly larger than the value of $\kappa = 0.41$ typical for a zero-pressure-gradient equilibrium boundary layer. At the initial stations ($x/h < 20$) the mixing length reaches a maximum value at $y/\delta \approx 0.2$ (see fig. 20(a)) and then drops sharply, rather than becoming nearly independent of y as in a regular TBL. The drop suggests the presence of two distinct structures with different origins, one being associated with the developing internal TBL and the second one being associated with the inherited mixing-layer-like structure in the external part of the flow.

The mixing-length slope in the linear inner region gradually decreases with downstream distance (fig. 21(a)), while the nondimensional mixing length in the outer part of the flow rises well above the value of 0.085 characteristic of a zero-pressure gradient equilibrium TBL remaining approximately constant at about 0.20 in the outer region for $x > 30h$. Similarly, the eddy viscosity, $\nu_t/(U_e\delta_1)$, deviates both in the wall and the outer flow regions from

the distribution of the upstream TBL (see fig. 20(c)). It appears that, as in the case of the mixing length, the slope near the wall is larger than in the upstream TBL. The slope gradually decreases downstream approaching the value of κu_τ. Maximum values of the normalized eddy viscosity are shown in figure 21(b). It is seen that the nondimensional eddy viscosity in the outer part of the flow rises initially, reaching the value of 0.075 at approximately $x = 20h$. Subsequently, it begins to decay at a very slow rate. It is seen that even at the last measuring station, $x = 51h$, the maximum eddy viscosity is about four times larger than the value of 0.017 in an equilibrium TBL. These high values of the mixing length and eddy viscosity in the outer parts of the flow far downstream indicate the slow response of the Reynolds stresses to changes in the mean rate of strain. However, a recovery trend can be clearly observed.

The dissipation length scale put forward by Townsend (1961) and cast in somewhat modified form by Bradshaw, Ferriss, and Atwell (1967) on the argument that $-\overline{uv}/k$ is usually well-behaved, is defined as $L_\varepsilon = (-\overline{uv})^{3/2}/\varepsilon$. It can be easily shown that $L_\varepsilon \equiv l$, for a flow in energy equilibrium. Dissipation obtained by difference of the other terms in the balance equation of the turbulent kinetic energy was used to calculate L_ε. The scatter in the dissipation length scale, as seen in figure 22, can be attributed to the uncertainty of the rate of dissipation. Near the wall $y < 0.1\delta$, L_ε increases as κy, as in the case of an equilibrium boundary layer. This observation contrasts with the conclusions about Prandtl's mixing length, but the explanation is simply that the inner layer is far from energy equilibrium. The data show that L_ε increases at a higher rate for $y > 0.1\delta$. In the outer layer, L_ε attains peak values which are four to five times larger than in an equilibrium TBL. Cutler and Johnston (1989) observed a threefold increase of the same quantity in the recovery region behind a fence. The same feature is observed in recovering boundary layers perturbed by a concave, destabilizing, curvature (Hoffmann, Muck, and Bradshaw (1985); and Smits, Eaton, and Bradshaw (1979)) and in the case of streamline divergence of developing boundary layers (Saddoughi and Joubert (1991)). The spectacular increase of the dissipation length scale in the mid-layer is associated with the reduced dissipation in the central portion of the recovering boundary layer.

The data indicate that Prandtl mixing length and the dissipation length parameter gradually recover as the flow evolves downstream, but are still far from the equilibrium plane boundary layer distributions at the last measuring station. Hunt, Spalart, and Mansour (1987) proposed a model for the dissipation length

$$L_\varepsilon = \left(\frac{-\overline{uv}}{\overline{v^2}}\right)^{3/2}\left(\frac{A_b}{y} + A_s\frac{\partial U/\partial y}{\overline{v^2}^{1/2}}\right)^{-1}$$

invoking the local turbulence parameters, in an attempt to predict a wider range of wall-bounded complex flows. The model underestimates the peak value in mid-layer (not shown here). In addition, the model fails to capture the decay rate of the dissipation length scale in the streamwise direction.

It appears that P/ε, the ratio of the turbulence energy production rate to its dissipation rate, is an important parameter used for improvement of baseline turbulence models for predictions of complex flows (Coakley and Huang (1992)). Three different forms of P were determined from the data,

$$P_1 = -\left(\overline{u^2} - \overline{v^2}\right)\frac{\partial U}{\partial x} - \overline{uv}\frac{\partial U}{\partial y}$$

$$P_2 = -\overline{uv}\frac{\partial U}{\partial y}$$

$$P_3 = ak\frac{\partial U}{\partial y}$$

and appropriate ratios are shown in figure 23(a)–(c). The structural parameter $a = 0.3$. It is obvious that P_3 is not an

appropriate representation of turbulent kinetic energy production near the wall because the ratio P/ε overshoots unity near the wall. It appears that all three forms of P are identical in the outer flow region since the production due to the normal stresses is negligibly small, while the shear stress and kinetic turbulent energy are proportional. The ratio P/ε dips below unity near the wall, while it overshoots unity in the outer flow region. For large streamwise distances, it approaches unity across the entire boundary layer as it is expected since the flow approaches equilibrium conditions.

Conclusions

The results presented and discussed in the previous sections led to the following conclusions about the response and recovery of the turbulence structure of the separated flow downstream of a backward-facing step.

The results suggest a two-layer structure of the separated boundary layer downstream of the step. The internal layer, imbedded in the original boundary layer, grows immediately from the step edge while a second layer, the outer layer, remains largely unaffected by the disturbance at the step, thus resembling the original boundary layer. The internal layer behavior is similar to that of a plane mixing layer; however, it fails to resemble a mixing layer exactly, because of the additional effects of adverse pressure gradient, the high turbulence levels on the low-speed side, the sheared turbulent "boundary layer" on the high-speed side, the curvature, and the short development length before the flow reattaches. The boundary between the internal layer and the outer region, fed by the original boundary layer, is marked by a clearly identifiable kink in the profiles of all the measured turbulence quantities. The large structures of the two layers appear to have independent dynamics interacting through the small scales which reside in the interface between the two layers. Only the presence of the small scales between the two layers can support a sudden change of gradients detectable in the relevant profiles. Two regions are identified in the separated shear layer: the near field, $x < 2h$, where the mixing-layer-like internal layer adjusts to the new boundary conditions, and the far field, $x > 2h$, where vigorous interaction between the internal and external layers takes place. The results indicate that the two layers merge before the flow reattaches.

In the recovery region, the new boundary conditions imposed on the flow in the reattachment region, $u = 0$ and $v = 0$, restrict further growth of the large structures of the mixing-layer-like flow, and promote a new internal boundary layer downstream of reattachment. Based on the rate of recovery of the internal boundary layer, two regions are identified downstream of reattachment: the near field, which ends at $x \approx 20h$, where the structure of the internal layer attains a quasi-equilibrium state, and the far field for $x > 20h$ approximately.

The results indicate that the structure near the wall becomes wall-dominated when the maximum u_{rms}/u_τ in the external layer decreases to a value of about 3.5. The x position where this occurs is a function of two parameters, Re_h and a perturbation strength, δ/h. For this experiment (Re_h = 37,000 and δ/h = 0.82) this position is $x \approx 20h$. If the external perturbation (in the mid layer) exceeds this threshold level (which can be also cast in the form $u_{rms}/U_e > 3.5\sqrt{C_f/2}$) the near-wall structure will be strongly altered by the external outer dynamics. It appears that, once recovered, the internal layer controls the skin friction coefficient.

Longitudinal turbulent diffusion and production of the turbulent energy by the normal stresses (both negligible according to the boundary-layer approximation) play a significant role in the balance of the turbulent kinetic energy in the near field region. Turbulent diffusion and dissipation are balanced in the internal boundary layer up to about $x = 20h$, suggesting that energy equilibrium concepts of turbulence modeling are not applicable in this region. The importance of the turbulent diffusion in the

balance of turbulent kinetic energy and shear stress transport equation suggests that an accurate prediction of the separated/reattached flow will require a good model for the turbulent diffusion terms. In the far field, $x > 20h$, the internal layer spreads away from the wall, remaining self-similar (when scaled on the wall variable) but interacting vigorously with the external layer. The turbulence quantities in the outer layer decay at a slow rate and the external layer still has a memory of the upstream disturbance even at the last measuring station of $51h$.

In the near field ($X_r < x < 20h$), the nonequilibrium state of the flow structure of the internal boundary layer yields a linear variation of the mixing length and eddy viscosity with y near the wall. The slopes are, however, larger than the von Karman constant, $\kappa = 0.41$, for the mixing length and κu_τ for the eddy viscosity. After the internal layer has attained equilibrium (in the far field, $x > 20h$), the mixing length and eddy viscosity distributions resemble those of a plane TBL within the developing internal layer. Mixing length and eddy viscosity in the external layer of the flow exceed the values of a regular TBL by up to four times even at the last measuring station.

References

1. Adams, E. W.; and Johnston, J. P.: Effects of the separating shear layer on the reattachment flow structure. Part 1 and 2. Exp. Fluids, vol. 6, 1988a, pp. 400–408.

2. Bell, J. H.; and Mehta, R. D.: Development of a two-stream mixing layer with tripped and untripped boundary layers. AIAA J., vol. 28, 1990, pp. 2034–2042.

3. Bradshaw, P.; Ferriss, D. H.; and Atwell, N. P.: Calculation of boundary-layer development using the turbulent energy equation. J. Fluid Mech., vol. 28., 1967, p. 593.

4. Bradshaw, P.; and Wong, F. Y. F.: The reattachment and relaxation of a turbulent shear layer. J. Fluid Mech., vol. 52, 1971, p. 113.

5. Browne, L. W.; Antonia, R.; and Shah, D. A.: Selection of wires and wire spacing for X-wires. Exp. Fluids, vol. 6, 1988, pp. 286–288.

6. Bruun, H. H.: Hot-wire data corrections in low and high turbulence intensity flows. J. Phys. E: Sci. Instrum., vol. 5, 1972, pp. 812–818.

7. Champagne, F. H.; Sleicher; and Wehrmann, O. H.: Turbulence measurements with inclined hot-wires Part 1 and 2. J. Fluid Mech., vol. 28, 1967, p. 153.

8. Chandrsuda, C.; and Bradshaw, P.: Turbulence structure of a reattaching mixing layer. J. Fluid Mech., vol. 110, 1981, p. 171.

9. Castro, I. P.; and Haque, A.: The structure of a turbulent shear layer bounding a separation region. J. Fluid Mech., vol. 179, 1987, p. 439.

10. Cherry, N. J.; Hillier, R.; and Latour, M. E. M. P.: Unsteady measurements in a separated and reattaching flow. J. Fluid Mech., vol. 144, 1984, p. 13.

11. Coakley, T. J.; and Huang, P. G.: Turbulence modeling for high speed flows. AIAA Paper 92-0436, 30th Aerospace Sciences Meeting and Exhibit, Reno, Nev., Jan. 6–9, 1992.

12. Corrsin, S.; and Kistler, A. L.: NACA Rep. no. 74-04, 1955.

13. Cutler, A.; and Johnston, J. P.: The relaxation of a turbulent boundary layer in an adverse pressure gradient. J. Fluid Mech., vol. 200, 1989, p. 367.

14. Devenport, L. W.; and Sutton, E. P.: Near-wall behavior of separated and reattaching flows, AIAA J., vol. 29, 1991, p. 25.

15. Driver, D. M.; and Seegmiller, H. L.: Features of a reattaching shear layer in a divergent channel flow. AIAA J., vol. 23, 1985, p. 163.

16. Driver, D. M.; Seegmiller, H. L.; and Marvin, J. G.: Time-dependent behavior of a reattaching shear layer. AIAA J., vol. 25, 1987, p. 914.

17. Eaton, J. K.; and Johnston, J. P.: A review of research on subsonic turbulent flow reattachment. AIAA J., vol. 19, 1981, p. 1093.

18. Eaton, J. K.; and Johnston, J. P.: Low frequency unsteadiness of a reattaching turbulent shear layer. In Turbulent Shear Flows 3 (ed., L. J. Bradbury, F. Durst, B. E. Launder, F. W. Schmidt and J. H. Whitelaw). Springer-Verlag, 1982, p. 162.

19. Gibson, M. M.; and Dakos, T.: Production of temperature fluctuations in grid turbulence: Wiskind's experiment revisited. Exp. Fluids, vol. 16, 1993, pp. 146–154.

20. Hinze, J. O.: Turbulence. McGraw Hill, 1975.

21. Hoffman, P. H.; Muck, K. C.; and Bradshaw, P.: The effects of concave surface curvature on turbulent boundary layers. J. Fluid Mech., vol. 161, 1985, p. 371.

22. Hunt, J. C. R.; Spalart, P. R.; and Mansour, N. N.: Proc. Summer Prog., Center for Turbulence Research, Stanford, 1987.

23. Jovic, S.; and Driver. D. M.: Reynolds number effect on the skin friction in separated flows behind a backward-facing step. Exps. Fluids, vol. 18, 1995.

24. Jovic, S.; and Driver, D. M.: Backward-facing step measurements at a low Reynolds number, $Re_h = 5000$. NASA TM-108807, 1994.

25. Kim, H. T.; Kline, S. J.; and Reynolds, W. C.: The production of turbulence near a smooth wall in a turbulent boundary layer. J. Fluid Mech., vol. 50, 1971, p. 133.

26. Kline, S. J.; Reynolds, W. C.; Schraub, F. A.; and Runstadler, P. W.: The structure of turbulent boundary layers. J. Fluid Mech., vol. 30, 1967, p. 741.

27. Kiya, M.; and Sasaki, K.: Structure of a turbulent separation bubble. J. Fluid Mech., vol. 137, 1983, p. 83.

28. Kiya, M.; and Sasaki, K.: Structure of large-scale vortices and unsteady reverse flow in the reattaching zone of a turbulent separation bubble. J. Fluid Mech., vol. 154, 1985, p. 463.

29. Le, H.; Moin, P.; and Kim, J.: Direct numerical simulation of turbulent flow over a backward-facing step. Report TF-58, Thermoscinces Division, Department of Mechanical Engineering, Stanford University, 1993.

30. Ligrani, P.; and Bradshaw, P.: Subminiature hot-wire sensors: development and use. J. Phys. E: Sci. Instrum., vol. 20, 1987, pp. 323–332.

31. Moffat, R. J.: Describing uncertainty in experimental results. Exp. Thermal Fluid Sci. 1, 1988, pp. 3-17.

32. Muller, U.: On the accuracy of turbulence measurements with inclined hot wires. J. Fluid Mech., vol. 119, 1982, pp. 155–172.

33. Murlis, J.; Tsai, H. M.; and Bradshaw. P.: The structure of turbulent boundary layers at low Reynolds numbers. J. Fluid Mech., vol. 122, 1982, p. 13.

34. Nagano, Y.; and Tsuji, T.: Recent developments in hot- and cold-wire techniques for measurements in turbulent shear flows near walls. Exp. Thermal Fluid Sci., vol. 9, 1994, pp. 94–110.

35. Plesniak, M. W.; Mehta, R. D.; and Johnston, J. P.: Curved two-stream turbulent mixing layers: Three-dimensional structure and streamwise evolution. J. Fluid Mech., vol. 270, 1994, p. 1.

36. Pronchick. S. W.; and Kline, S. J.: An experimental investigation of the structure of a turbulent reattaching flow behind a backward-facing step. Stanford UniversityThermosciences Div. Rep. MD-42, 1983.

37. Ruderich, R.; and Fernhholz, H. H.: An experimental investigation of a turbulent shear flow with separation, reverse flow and reattachment. J. Fluid Mech., vol. 163, 1986, p. 283.

38. Saddoughi, S. G.; and Joubert, P. N.: Lateral straining of turbulent boundary layers. Part 1. Streamline divergence. J. Fluid Mech., vol. 229, 1991, p. 173.

39. Simpson, R. L.; Chew, Y. T.; and Shivaprasad, B. G.: The structure of a separating turbulent boundary layer. Part 2. Higher-order turbulence results. J. Fluid Mech., vol. 113, 1981, p. 53.

40. Smits, A. J.; Eaton, J. A.; and Bradshaw, P.: The response of a turbulent boundary layer to lateral divergence. J. Fluid Mech., vol. 94, 1979, p. 243.

41. Townsend, A. A.: The Structure of Turbulent Shear Flow. Cambridge University Press, Cambridge, 1976.

42. Troutt, T. R.; Scheelke, B.; and Norman, T. R.: Organized structures in a reattaching separated flow field. J. Fluid Mech., vol. 143, 1984, p. 413.

43. Tutu, N. K.; and Chevray, R.: Cross-wire anemometry in high intensity turbulence. J. Fluid Mech., vol. 71, 1975, pp. 785–800.

44. Ueda, H.; and Hinze, J. O.: Fine-structure turbulence in the wall region of a turbulent boundary layer. J. Fluid Mech., vol. 67, 1975, p. 125.

45. Wallace, J. M.; Ekelmann, H.; and Brodkey, R. S.: The wall region in turbulent shear flow. J. Fluid Mech. 54, 1972, p. 39.

46. Willmarth, W. W.; and Lu, S. S.: Structure of the Reynolds stress near the wall. J. Fluid Mech., vol. 55, 1972, p. 65.

47. Westphal, R. V.; Johnston, J. P.; and Eaton, J. K.: Experimental study of flow reattachment in a single-sided sudden expansion. NASA CR-3765, 1984.

48. Wood, D. H.; and Bradshaw, P.: A turbulent mixing layer constrained by a solid surface. Part 1. Measurements before reaching the surface. J. Fluid., vol. 122, 1982, p. 57.

49. Yavuzkurt, S.: A guide to uncertainty analysis of hot-wire data. Trans. ASME J. Fluids Engrg., vol. 106, 1984, pp. 181–186.

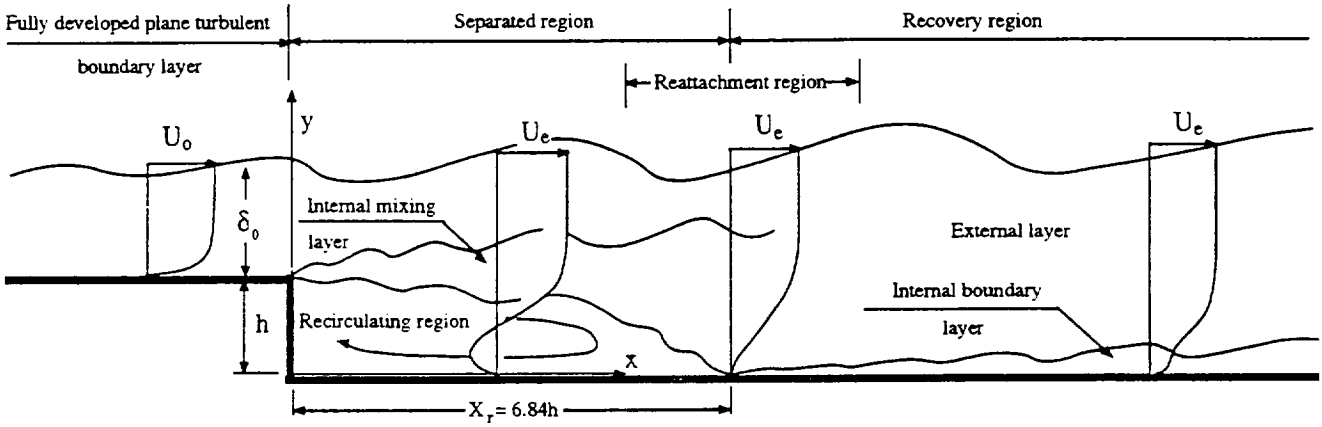

(a)

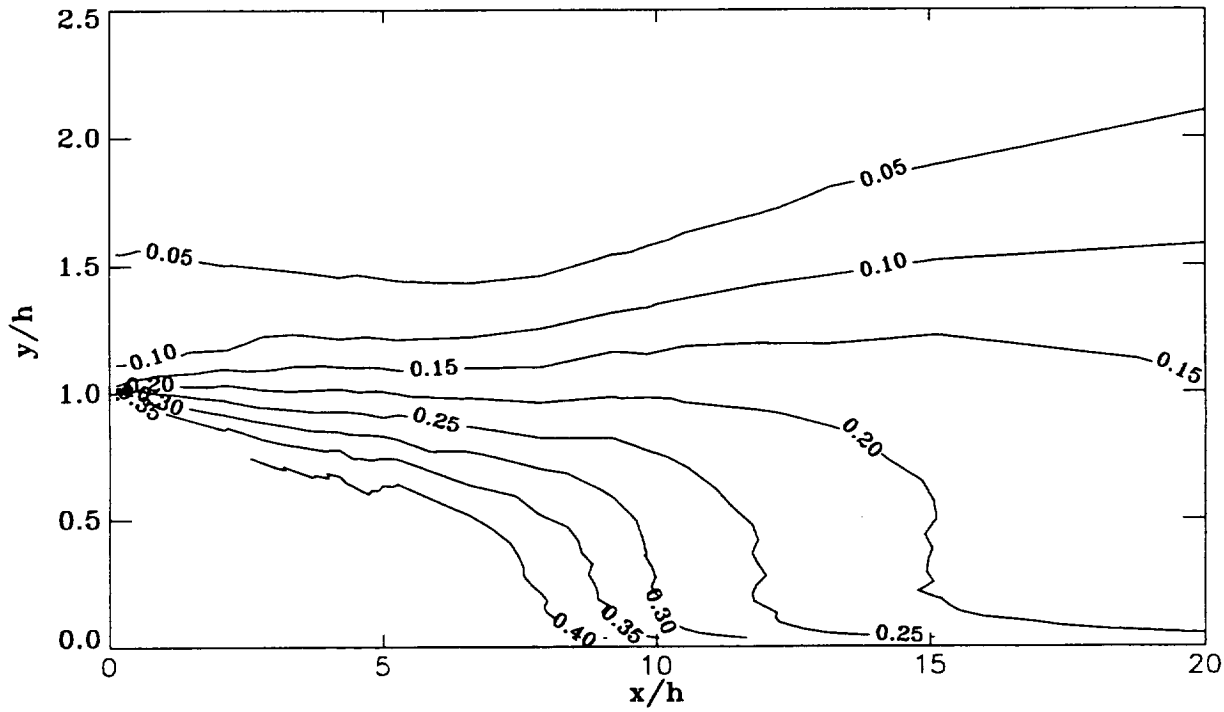

(b)

Figure 1. Flow configuration. (a) Regions of the backstep flow—not to scale, (b) contours of measured relative turbulence intensity.

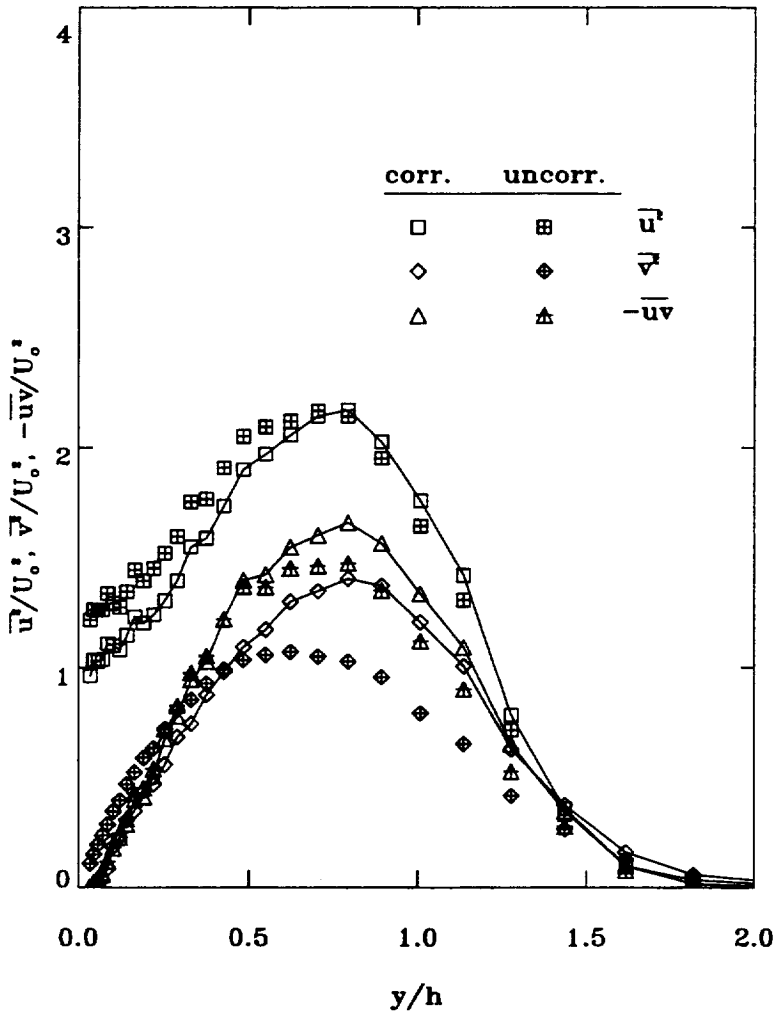

(c)

*Figure 1. Concluded. (c) Comparison of corrected and uncorrected Reynolds stresses at x = 9.21*h. *Solid lines added for clarity.*

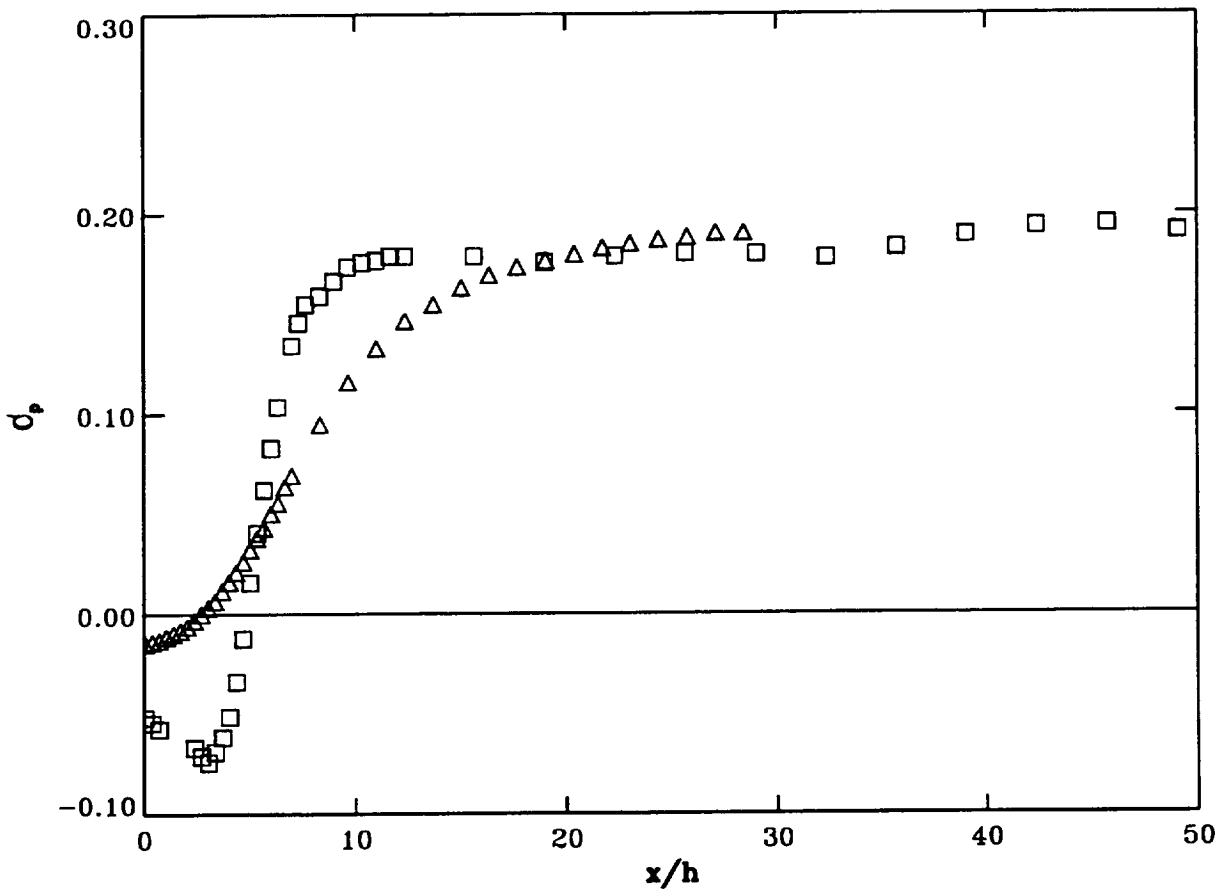

(a)

Figure 2. (a) Pressure coefficient. □, bottom wall; Δ, top wall.

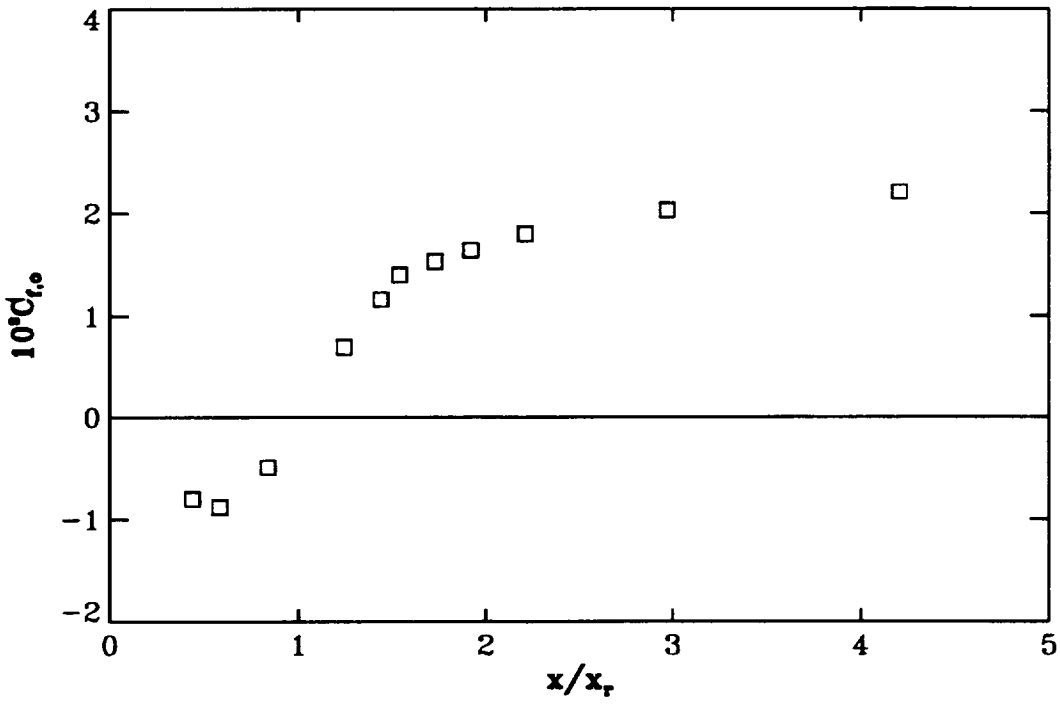

(b)

Figure 2. Continued. (b) Skin friction coefficient along the bottom wall.

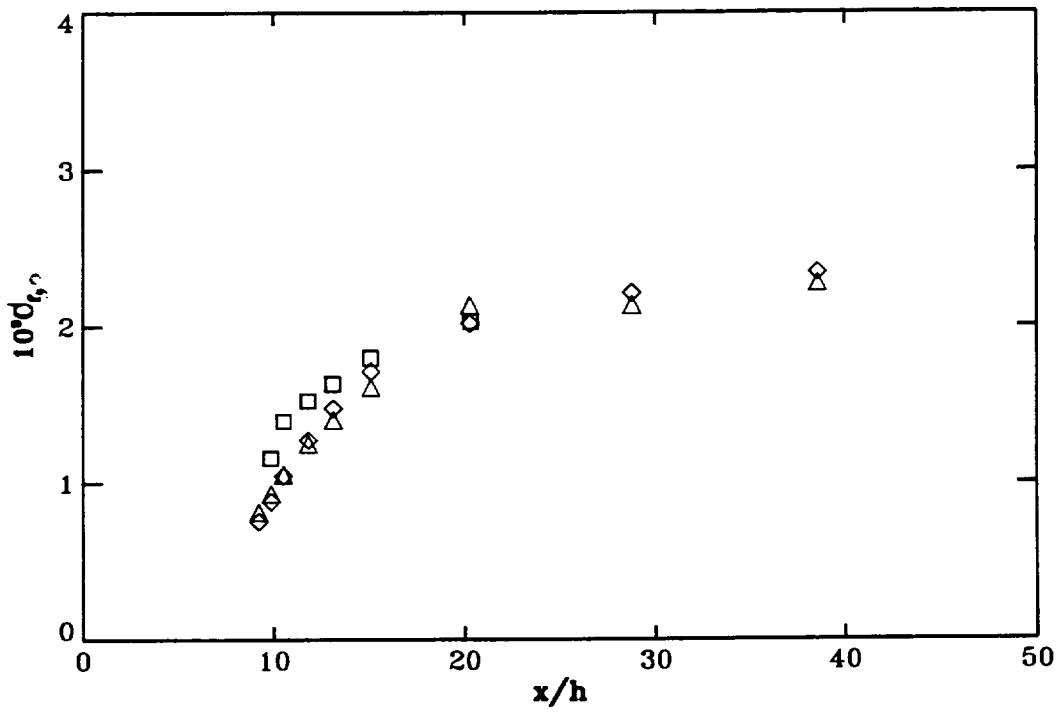

(c)

Figure 2. Concluded. (c) Comparison of C_f determined in three different ways: □, LOI-present experiment; △, Ludwieg–Tillmann; ◇, Clauser chart.

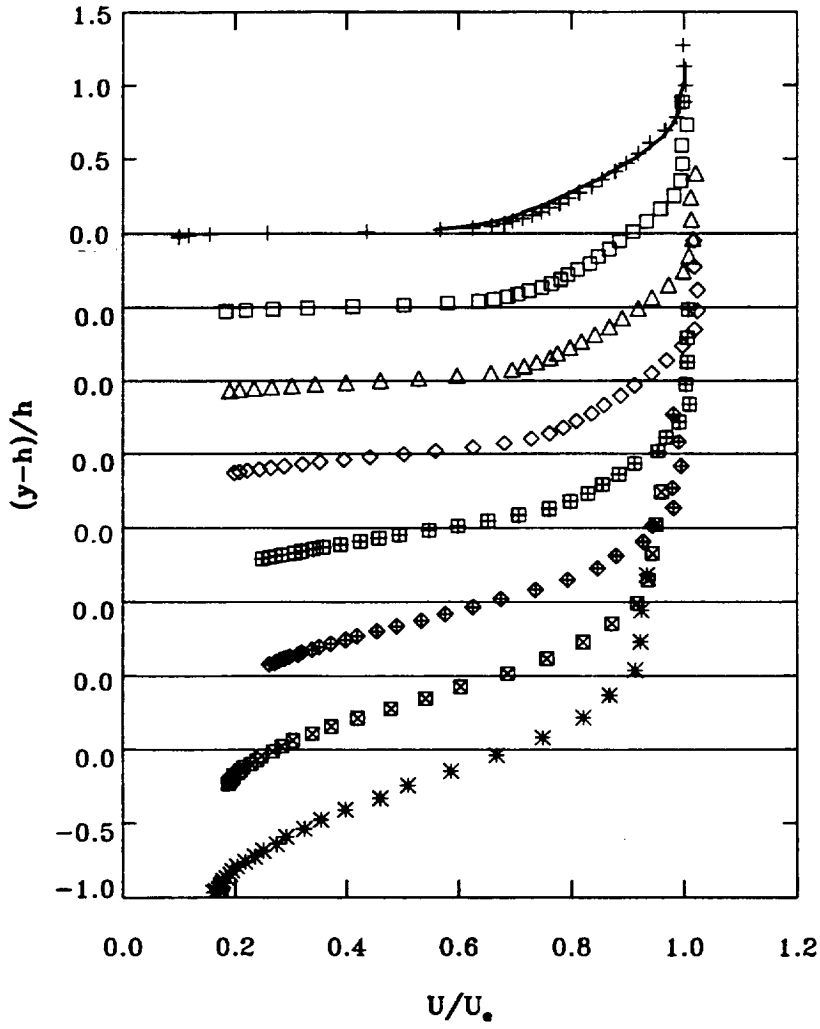

(a)

Figure 3. Development of the internal mixing layer: profiles for −1.05 < x/h < 6.58. All symbols as in figure 3(b). (a) Mean velocity.

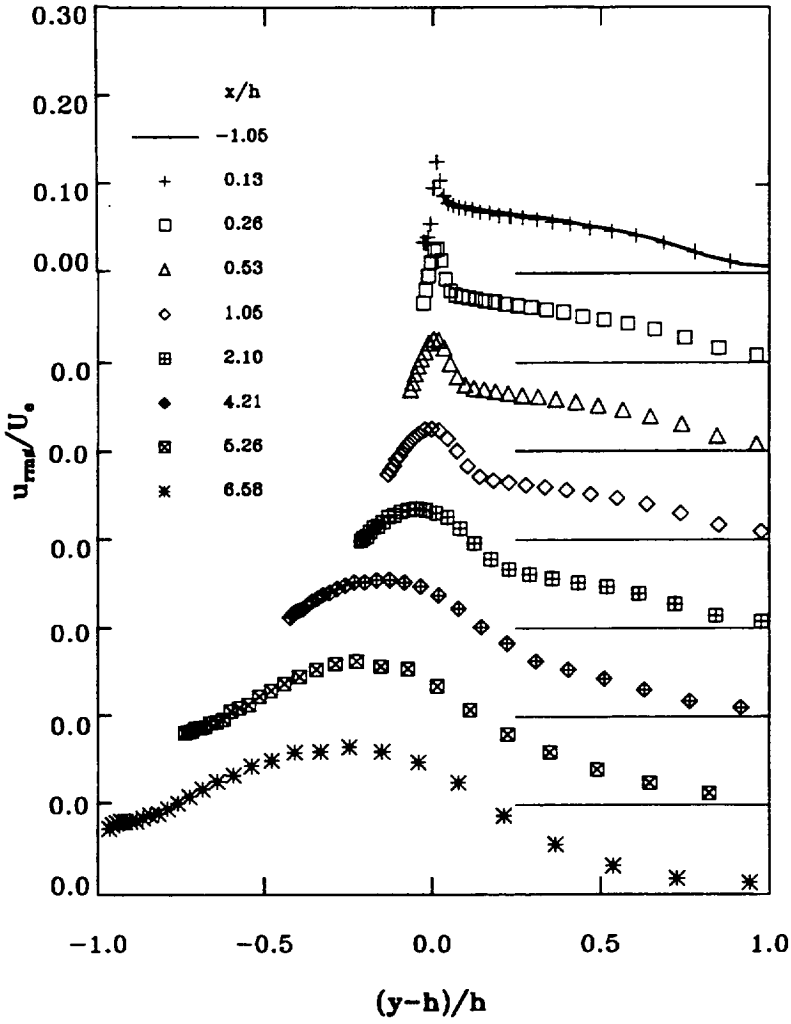

(b)

Figure 3. Continued. (b) $u_{rms} = \sqrt{\overline{u^2}}$.

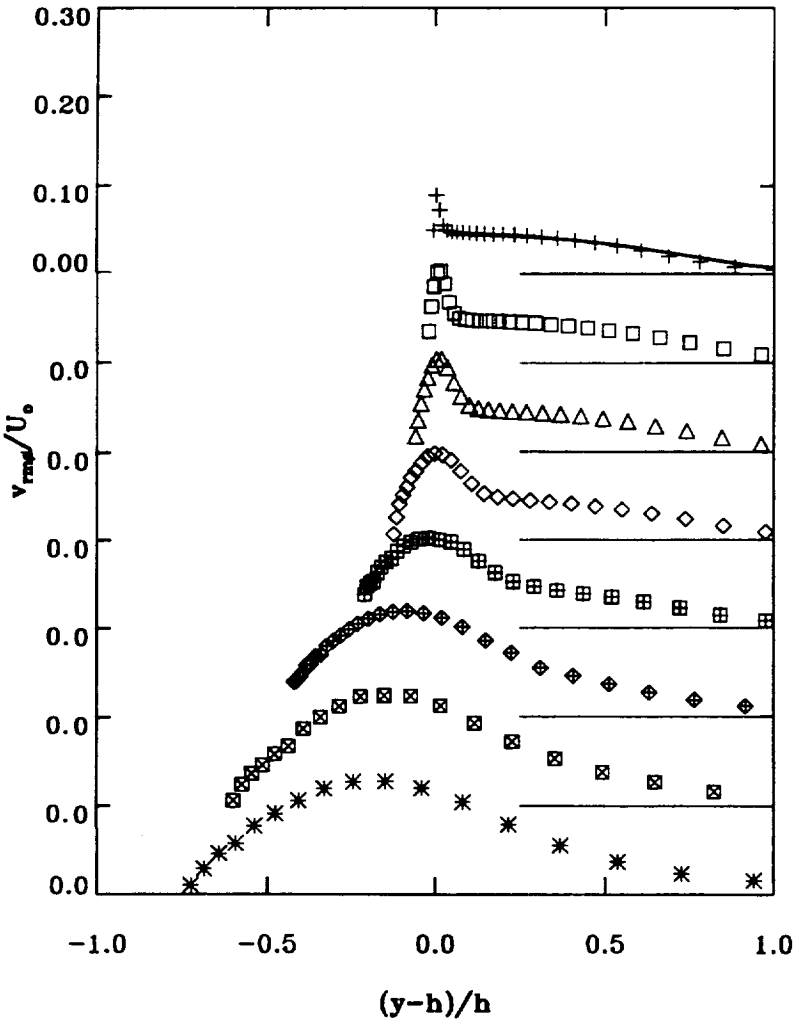

(c)

Figure 3. Continued. (c) $v_{rms} = \sqrt{\overline{v^2}}$ *. All symbols as in figure 3(b).*

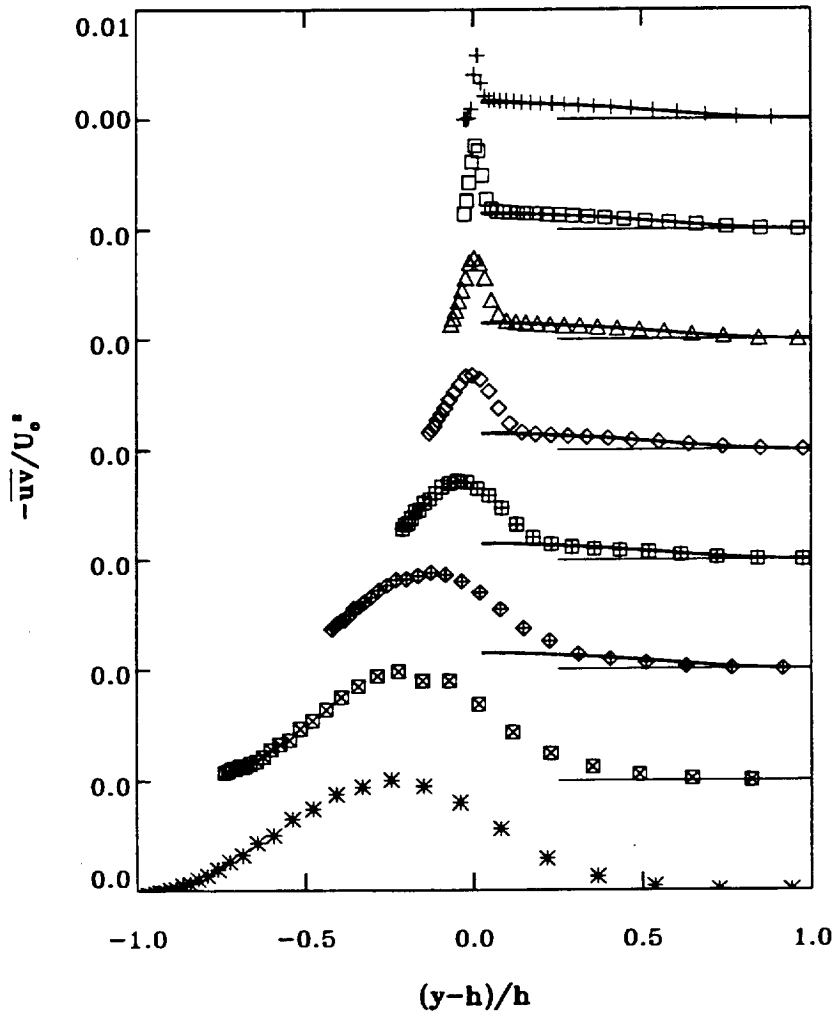

(d)

Figure 3. Continued. (d) $-\overline{uv}$. All symbols as in figure 3(b).

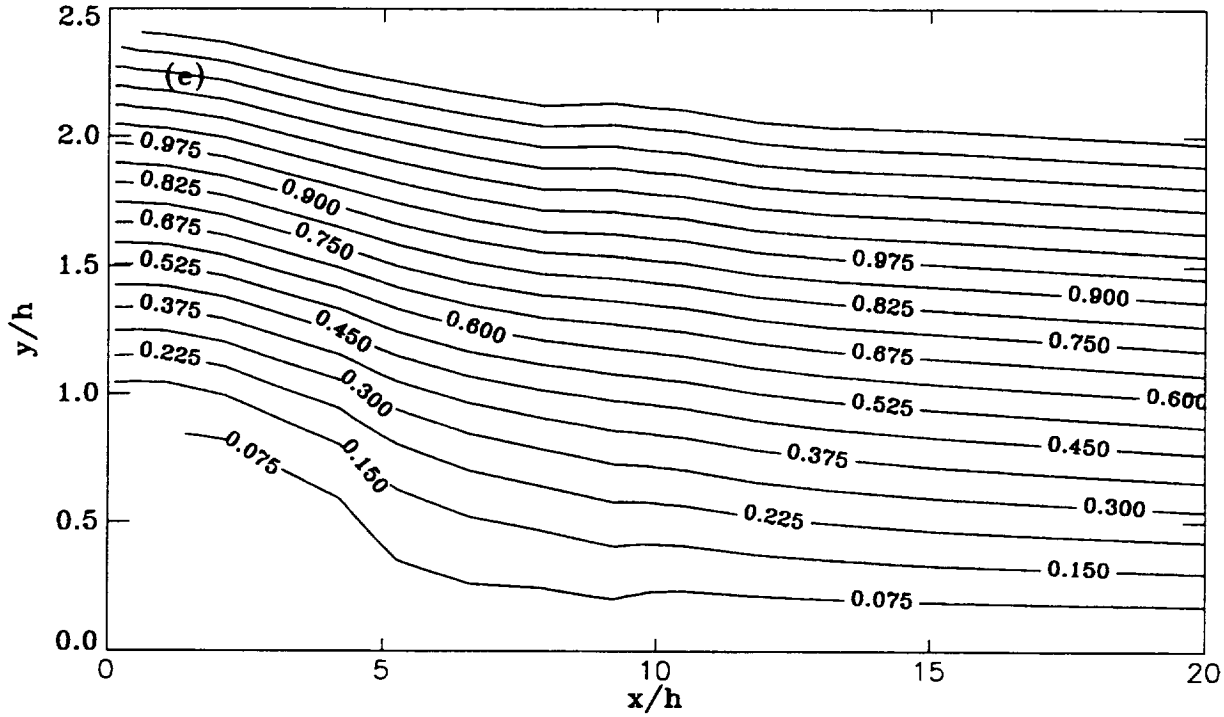

(e)

Figure 3. Continued. (e) Streamlines.

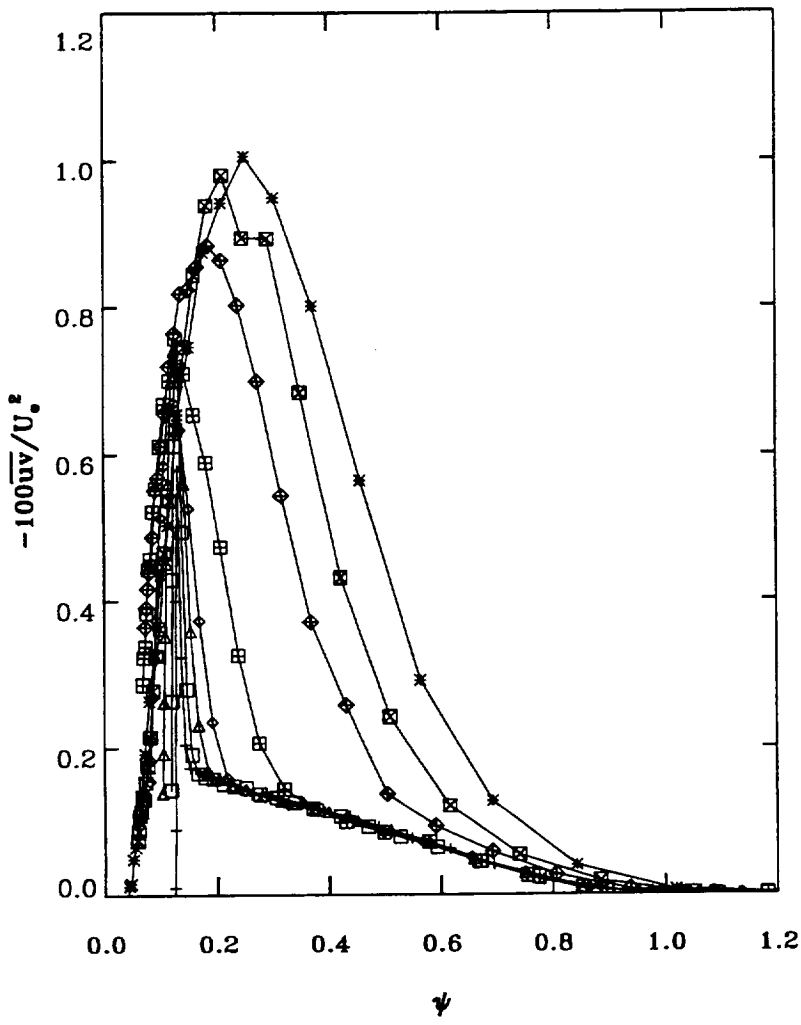

(f)

Figure 3. Continued. (f) Turbulent stress plotted against stream function. Lines added for clarity; symbols as in figure 3(b).

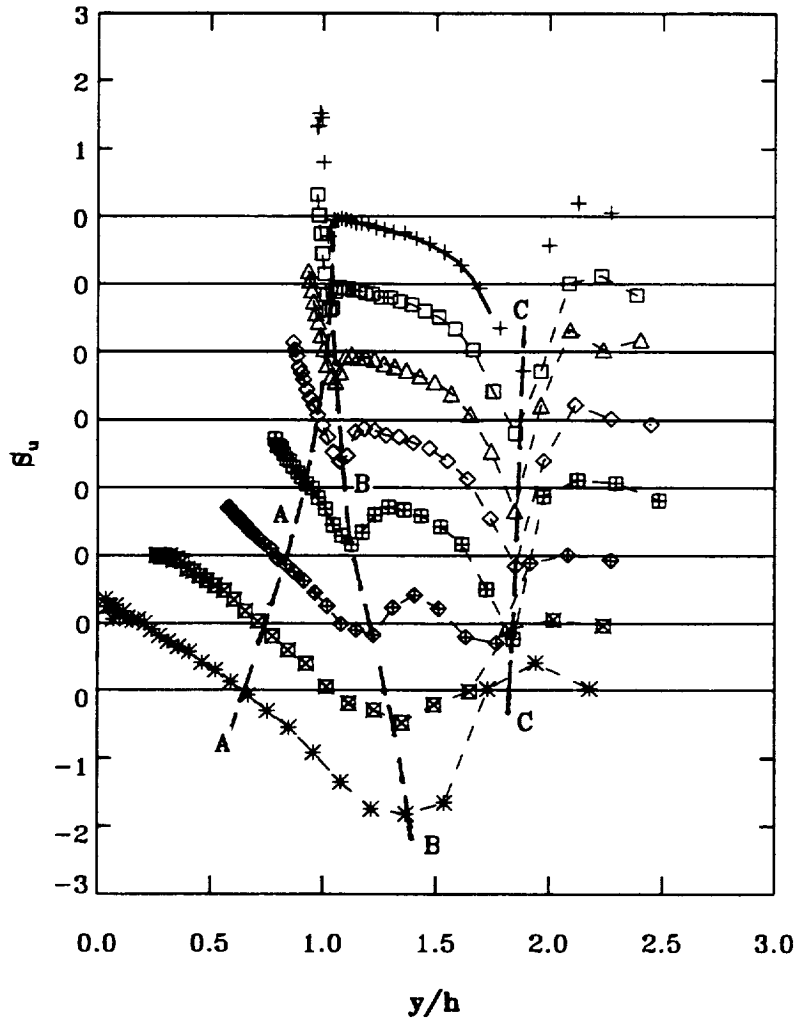

(g)

Figure 3. Concluded. (g) u-component skewness. Lines A-A, B-B, and C-C connect zeros or extrema (see text). All symbols as in figure 3(b). Dash lines added for clarity.

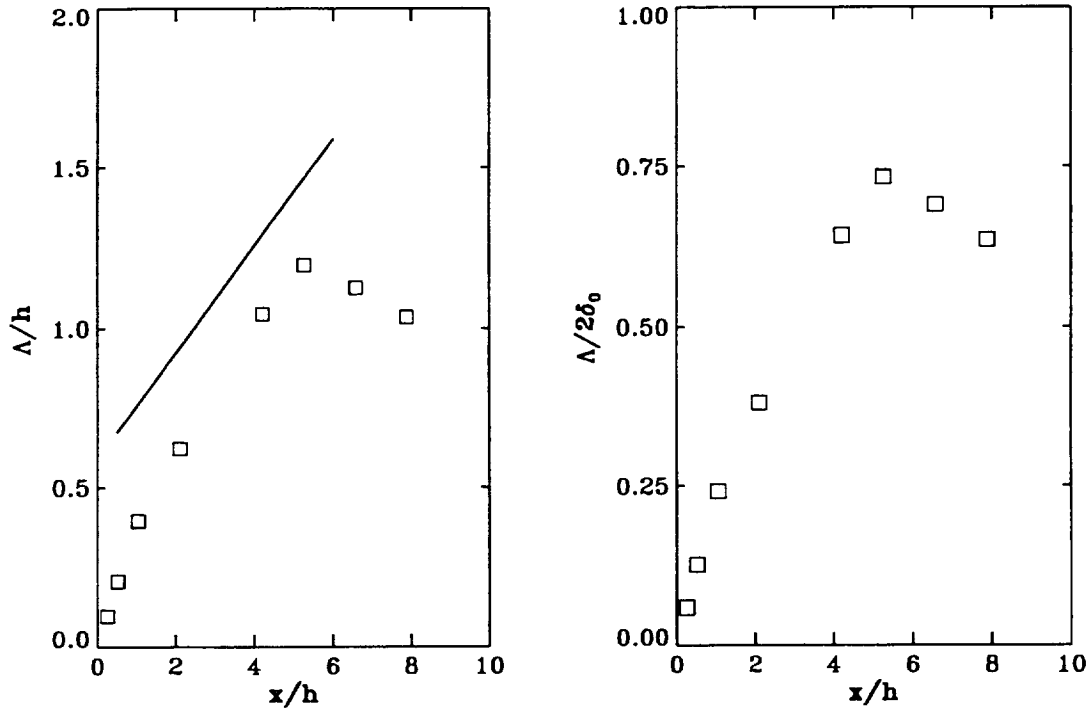

Figure 4. Scaling parameters for internal mixing layer. (a) Shear layer vorticity thickness; solid line depicts plane mixing layer, (b) internal mixing layer growth.

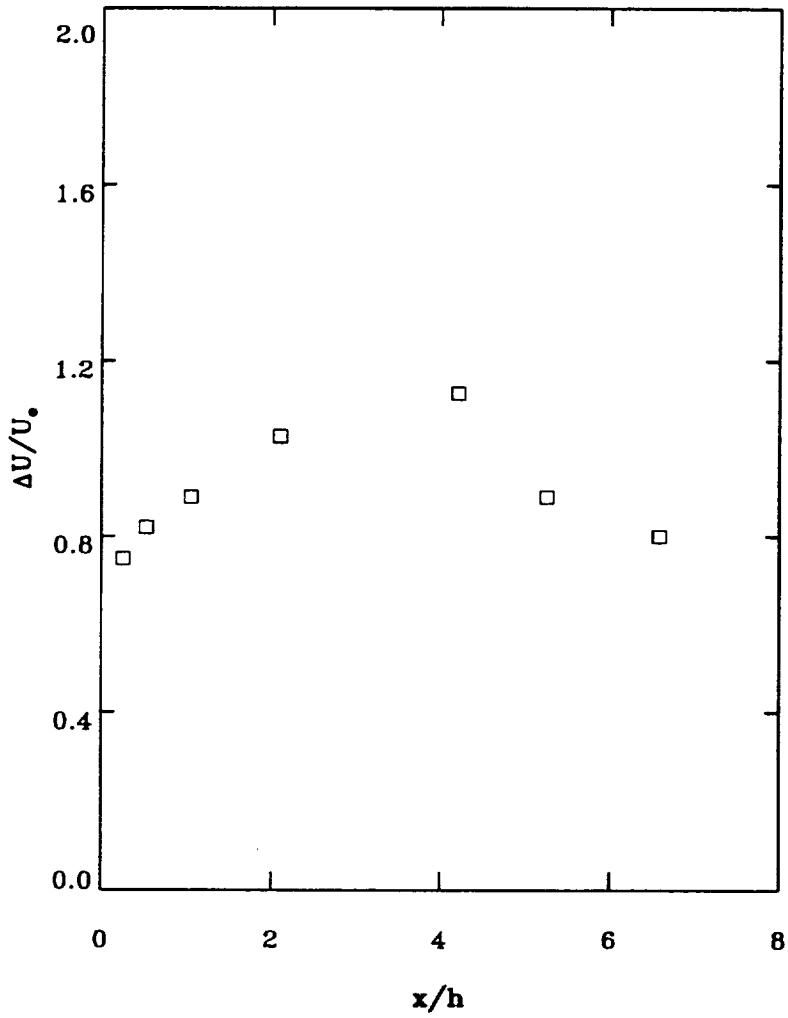

(c)

Figure 4. Concluded. (c) Velocity scale.

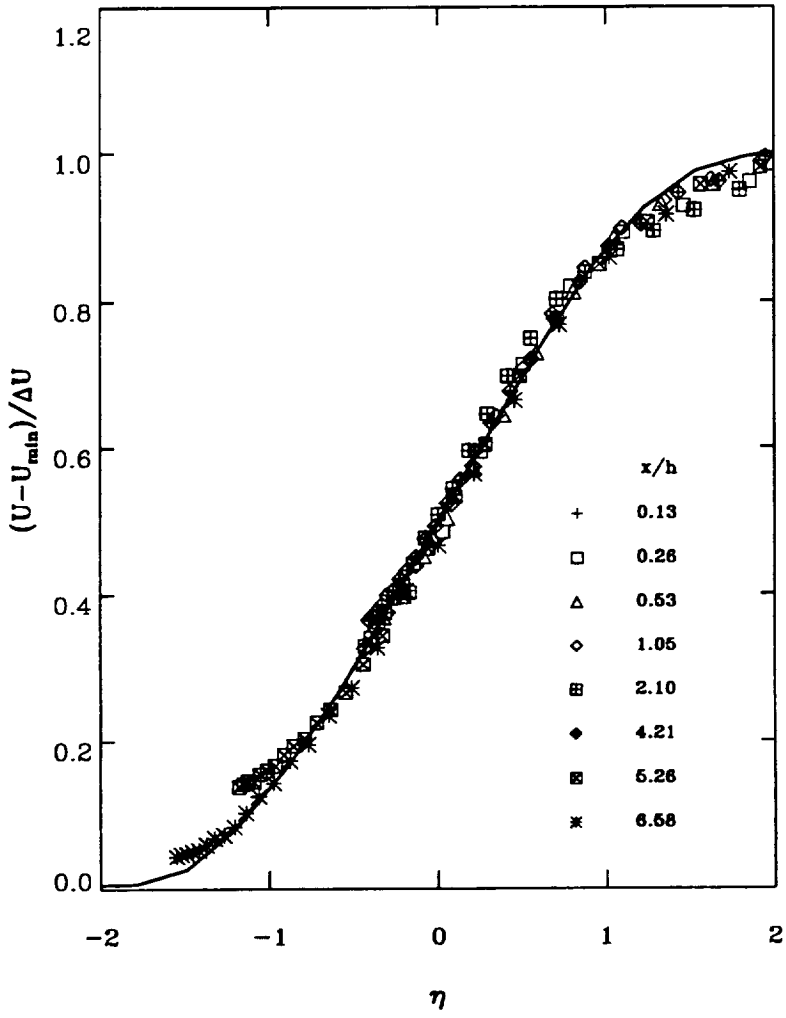

(a)

Figure 5. Profiles of the internal mixing layer in similarity coordinates. In figures 5–9, solid line is self-similar mixing layer from Bell and Mehta (1990). (a) Mean velocity.

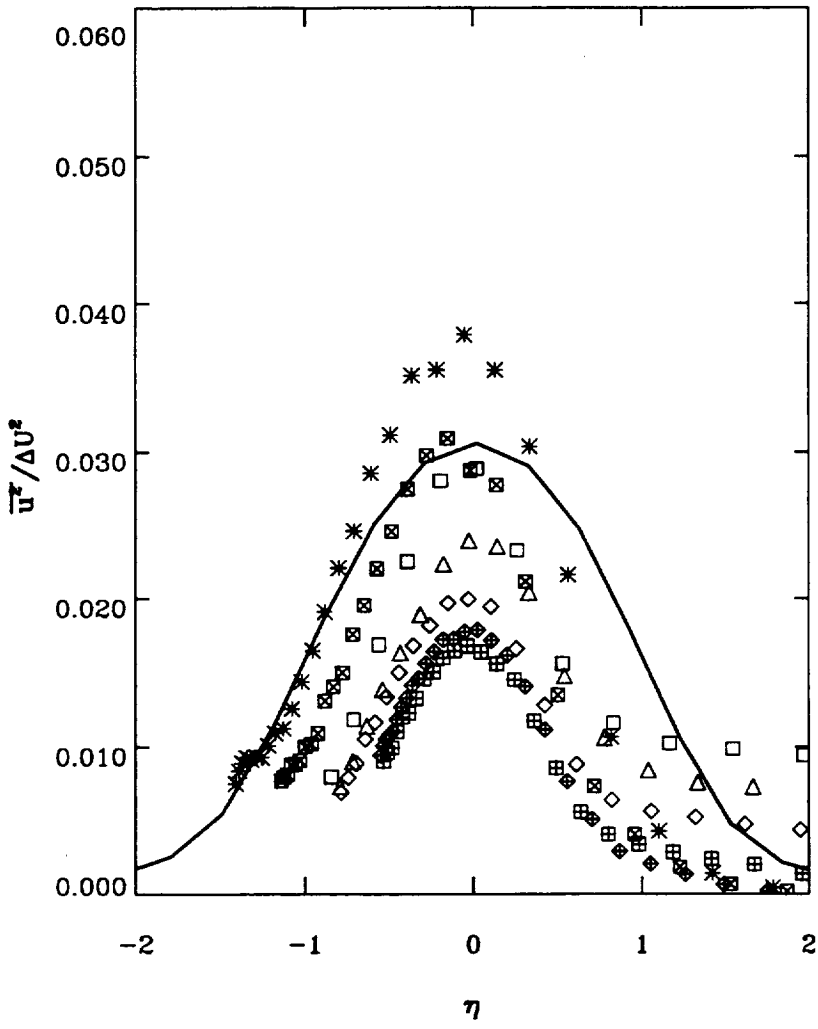

(b)

Figure 5. Continued. (b) $\overline{u^2}$. All symbols as in figure 5(a).

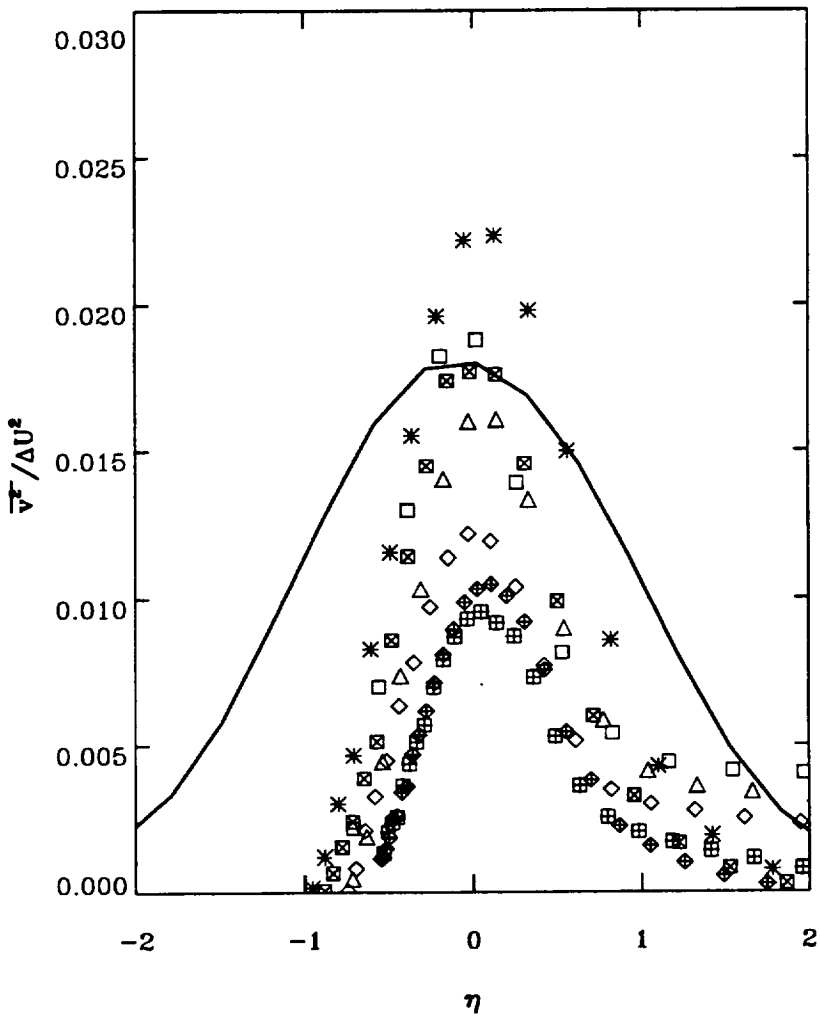

(c)

Figure 5. Continued. (c) $\overline{v^2}$. All symbols are same as in figure 5(a).

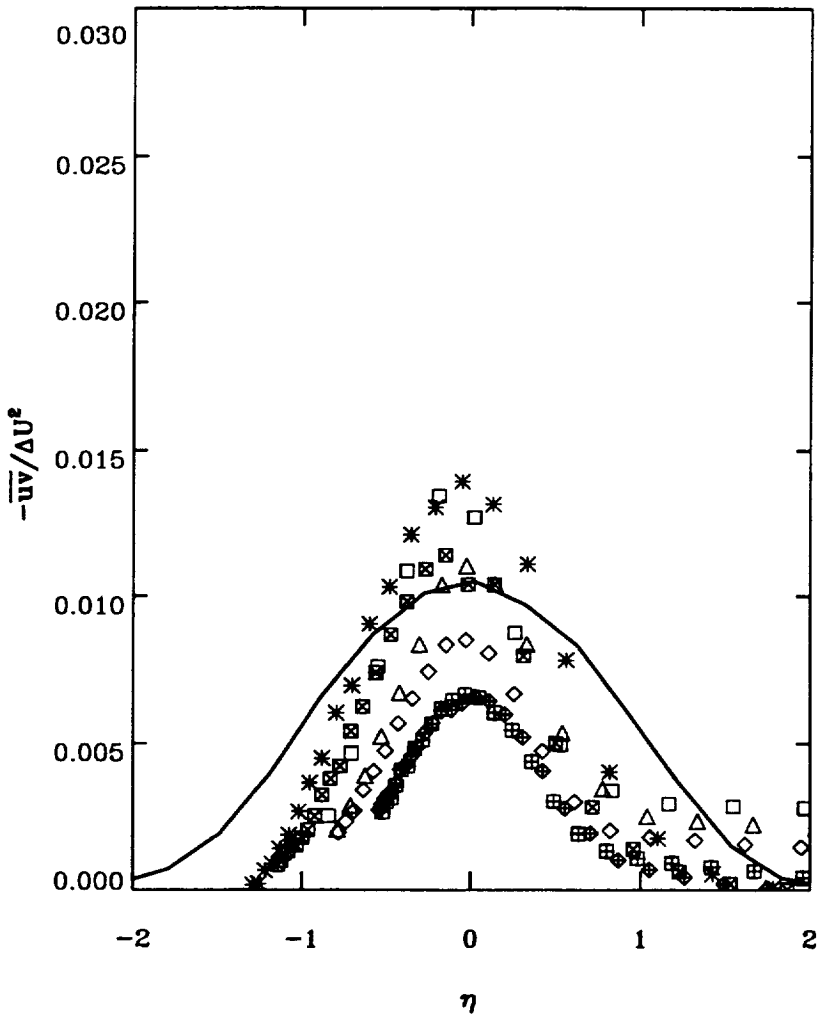

(d)

Figure 5. Concluded. (d) $-\overline{uv}$. All symbols as in figure 5(a).

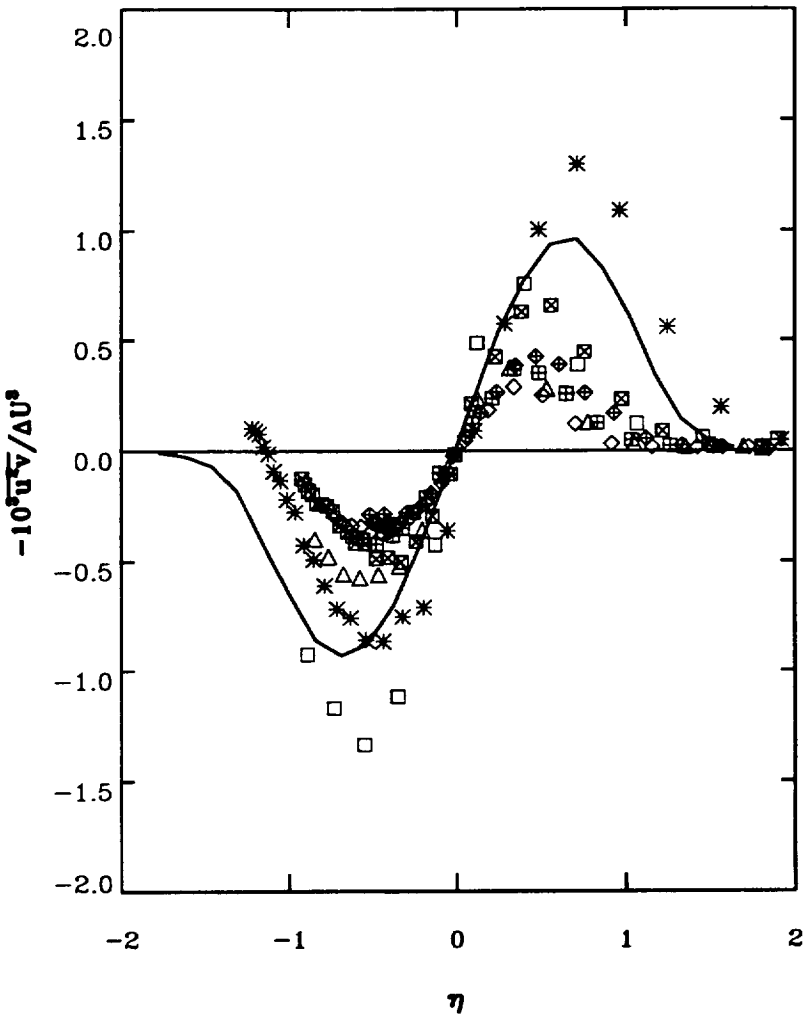

(a)

Figure 6. Profiles of the internal mixing layer in similarity coordinates; triple products. All symbols are same as in figure 5(a). (a) $-\overline{u^2 v}$.

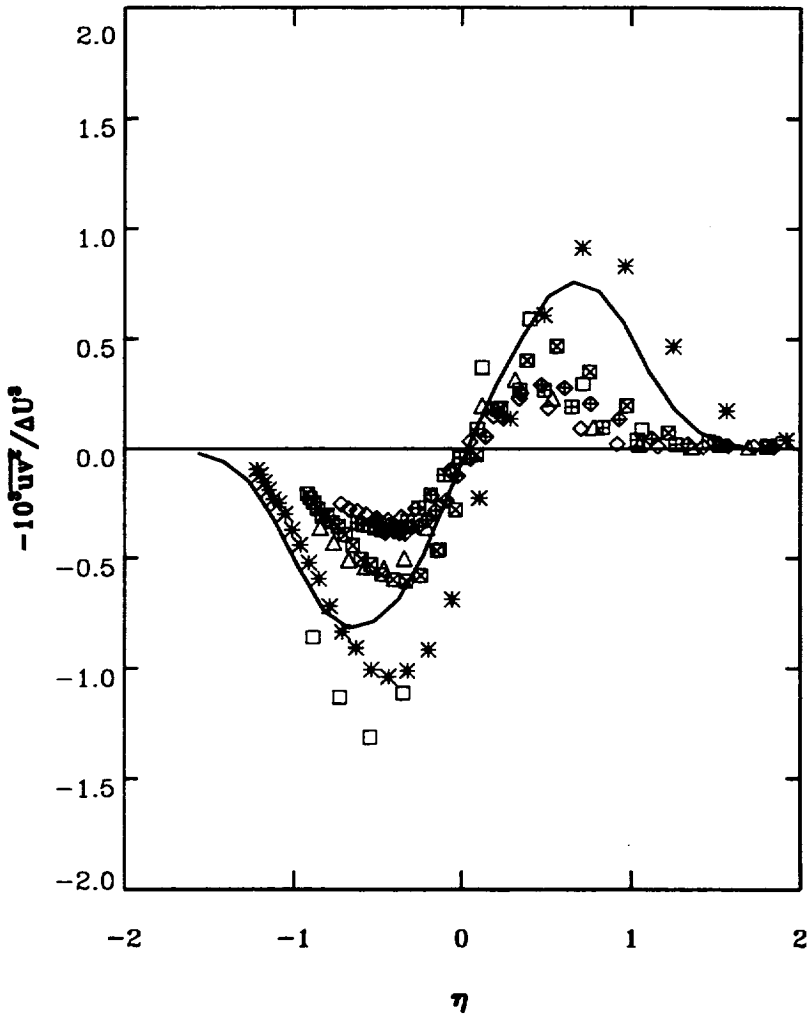

(b)

Figure 6. Continued. (b) $\overline{uv^2}$. All symbols are same as in figure 5(a).

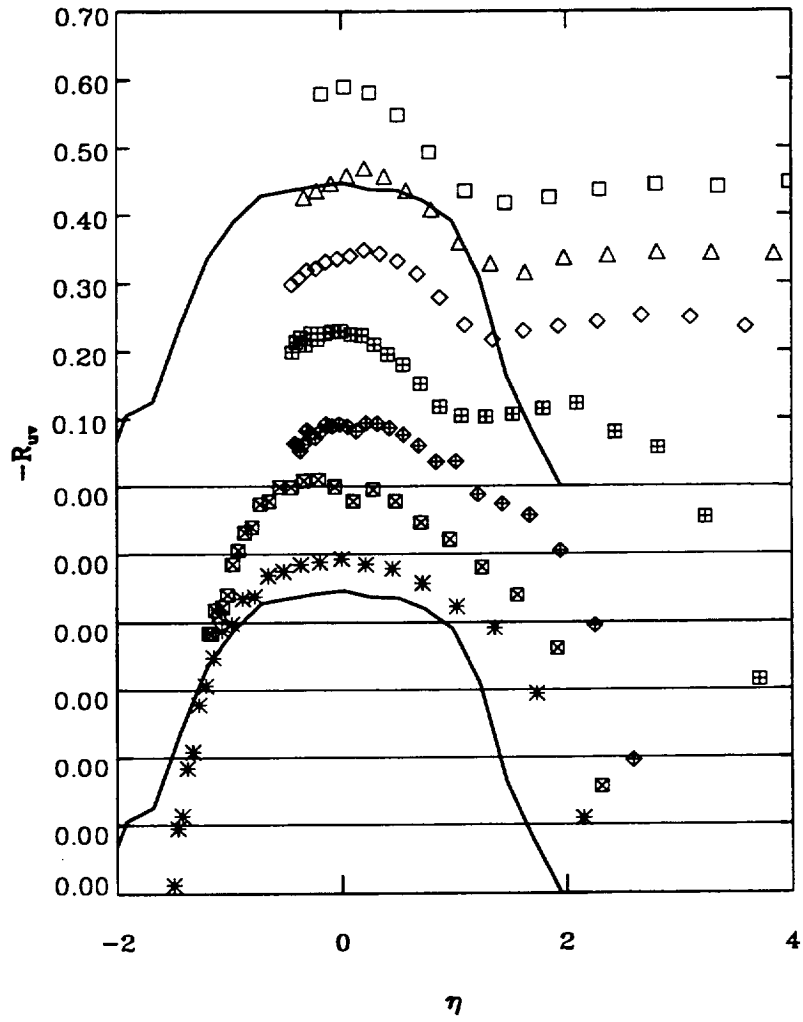

(a)

Figure 7. Profiles of the internal mixing layer in similarity coordinates. (a) Shear correlation coefficient. R_{uv}. All symbols are same as in figure 5(a).

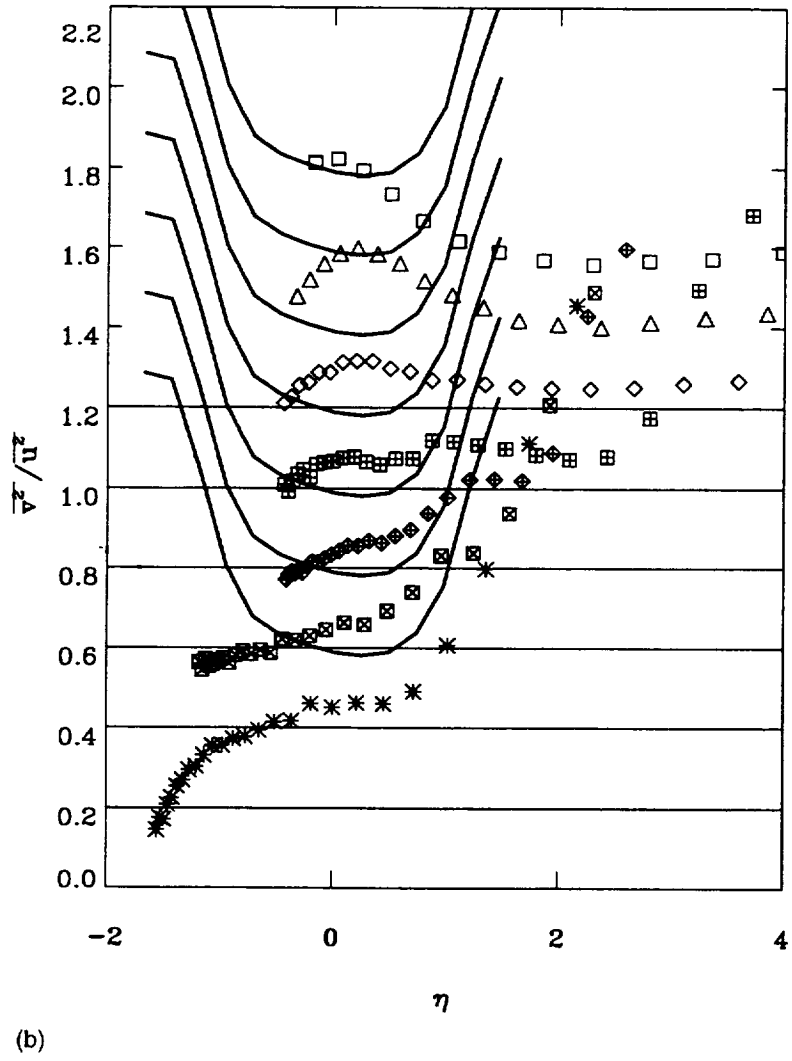

(b)

Figure 7. Concluded. (b) Intensity ration $\overline{v^2}/\overline{u^2}$. All symbols are same as in figure 5(a).

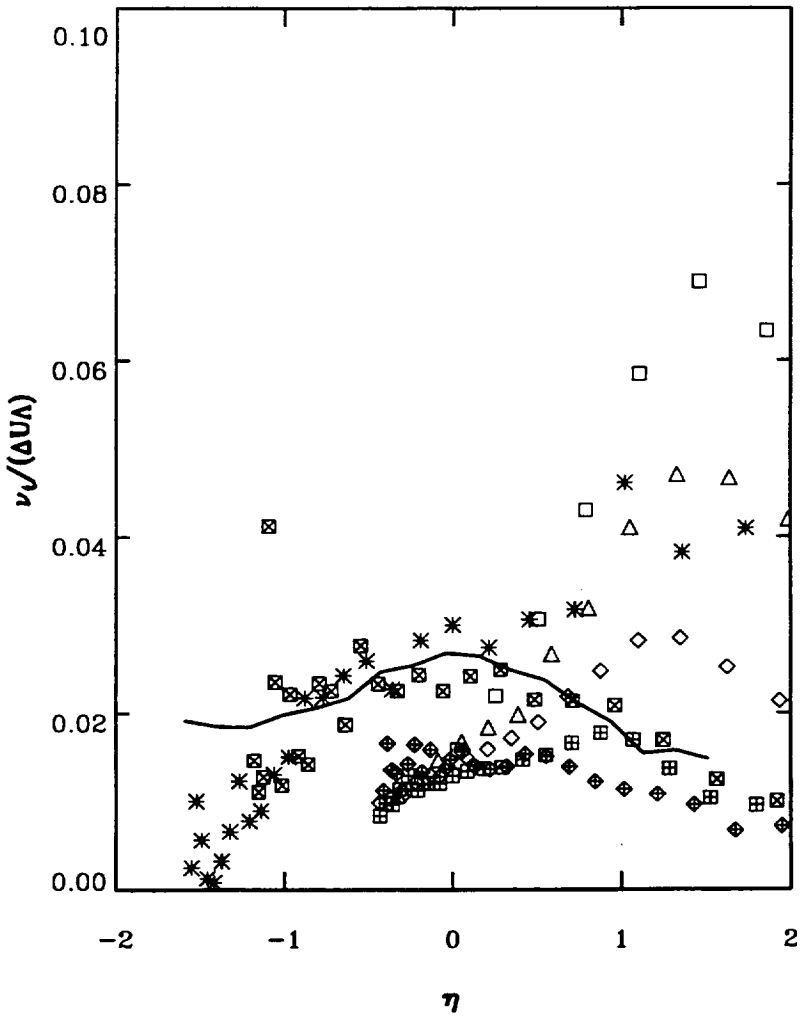

(a)

Figure 8. Profiles of the internal mixing layer in similarity coordinates. (a) Eddy viscosity. All symbols are same as in figure 5(a).

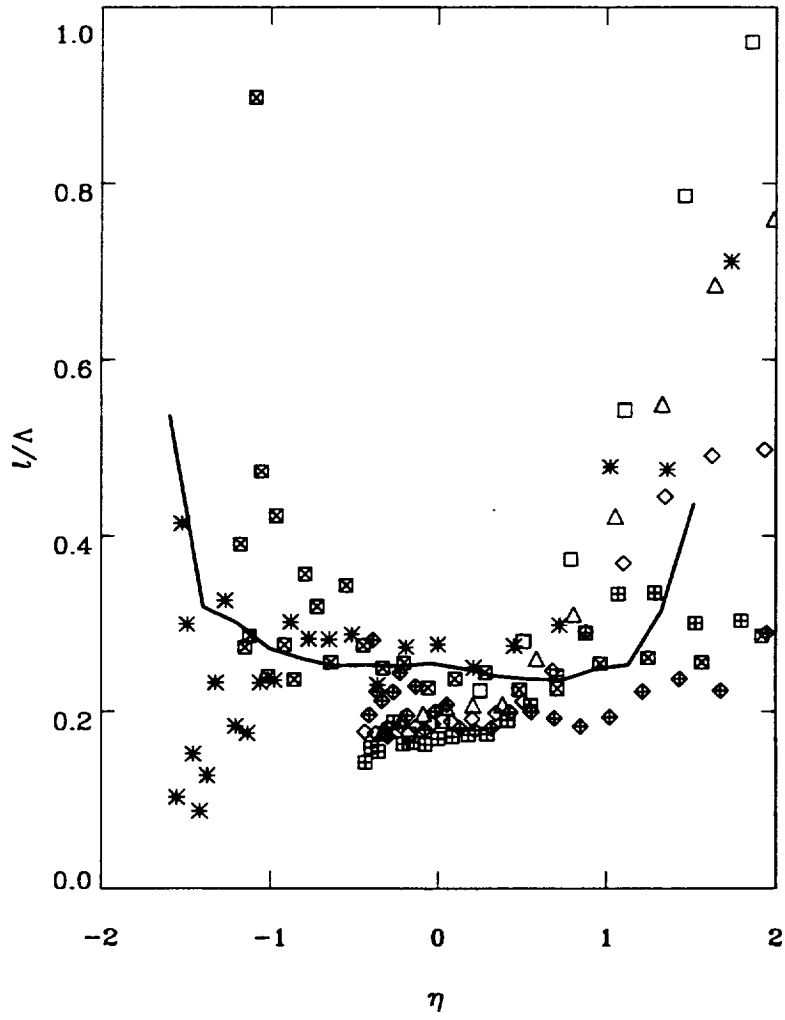

(b)

Figure 8. Concluded. (b) Mixing length. All symbols are same as in figure 5(a).

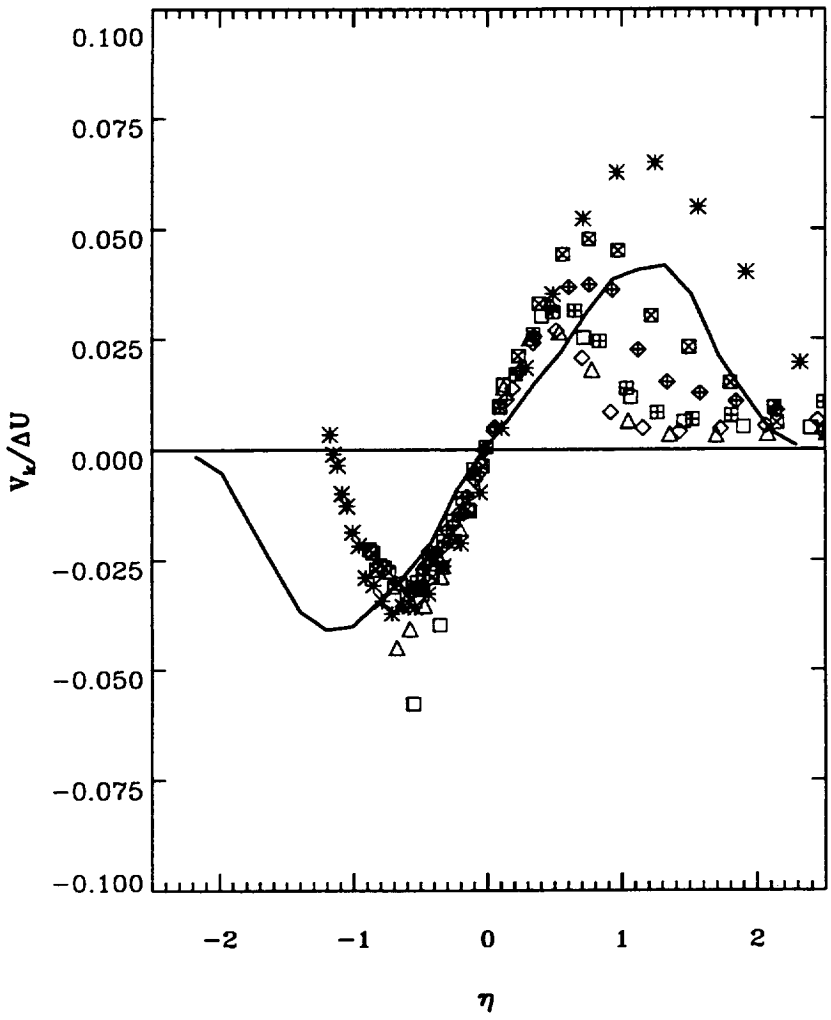

(a)

Figure 9. Profiles of the internal mixing layer in similarity coordinates: triple-product transport velocities. (a) For turbulent kinetic energy $v_k = 0.6\left(\overline{u^2 v} + \overline{v^3}\right) \Big/ 0.7\left(\overline{u^2} + \overline{v^2}\right)$. *All symbols are same as in figure 5(a).*

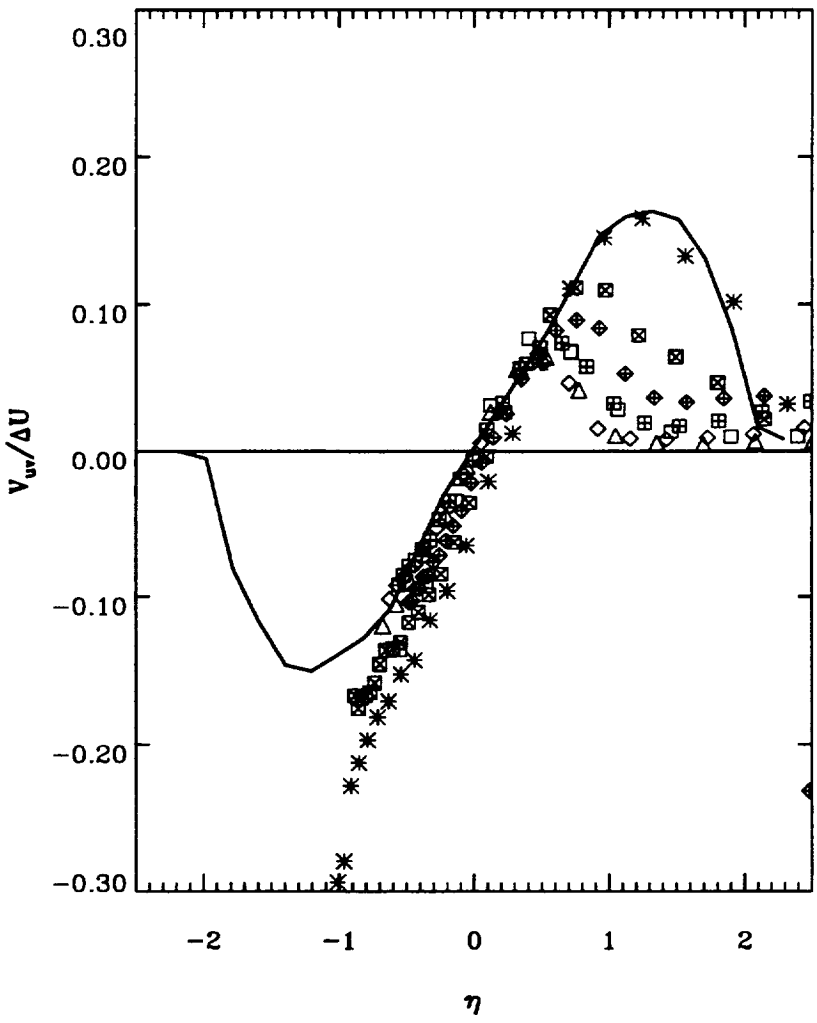

(b)

Figure 9. Concluded. (b) For shear stress $v_{uv} = \overline{uv^2}/\overline{uv}$. *All symbols are same as in figure 5(a).*

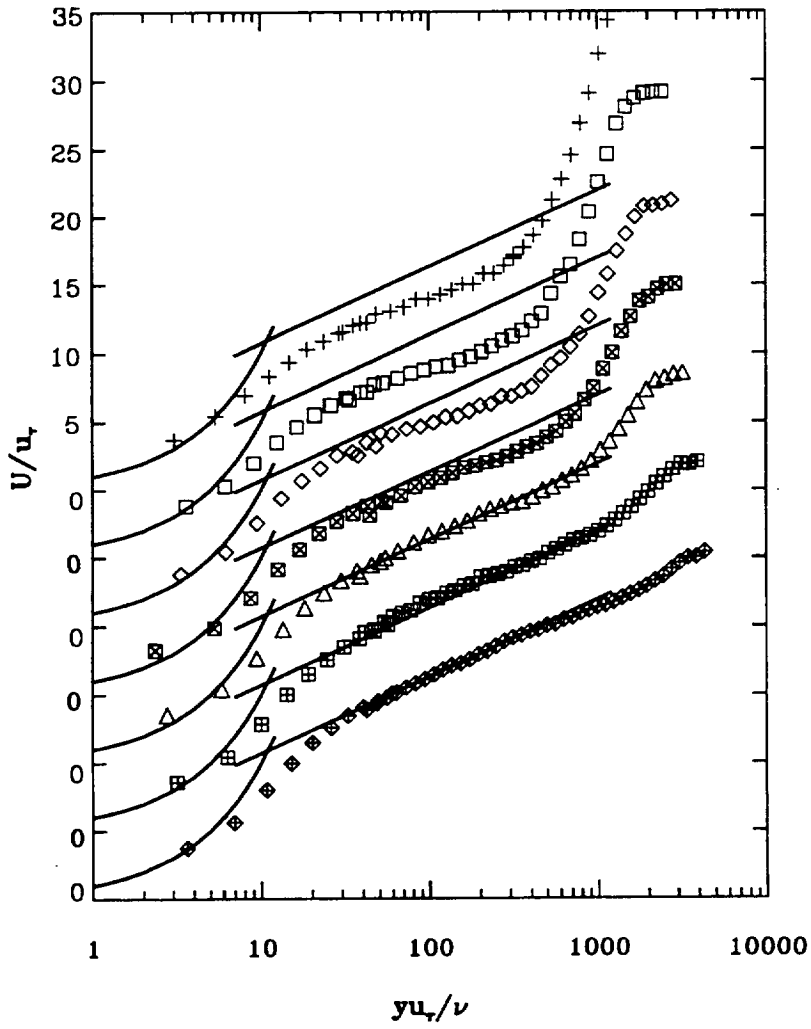

(a)

Figure 10. Profiles of the reattached flow in semi-log coordinates. (a) Mean velocity (symbols are shown in figure 10(b)).

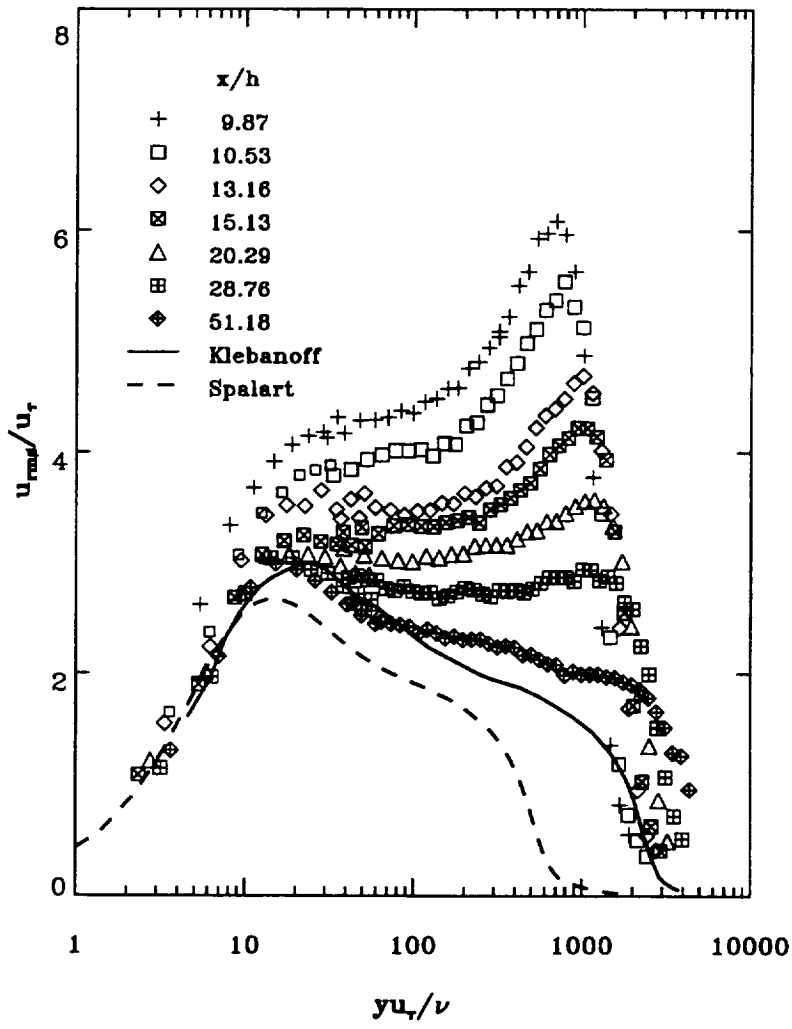

(b)

Figure 10. Continued. (b) Turbulence intensity in the streamwise direction.

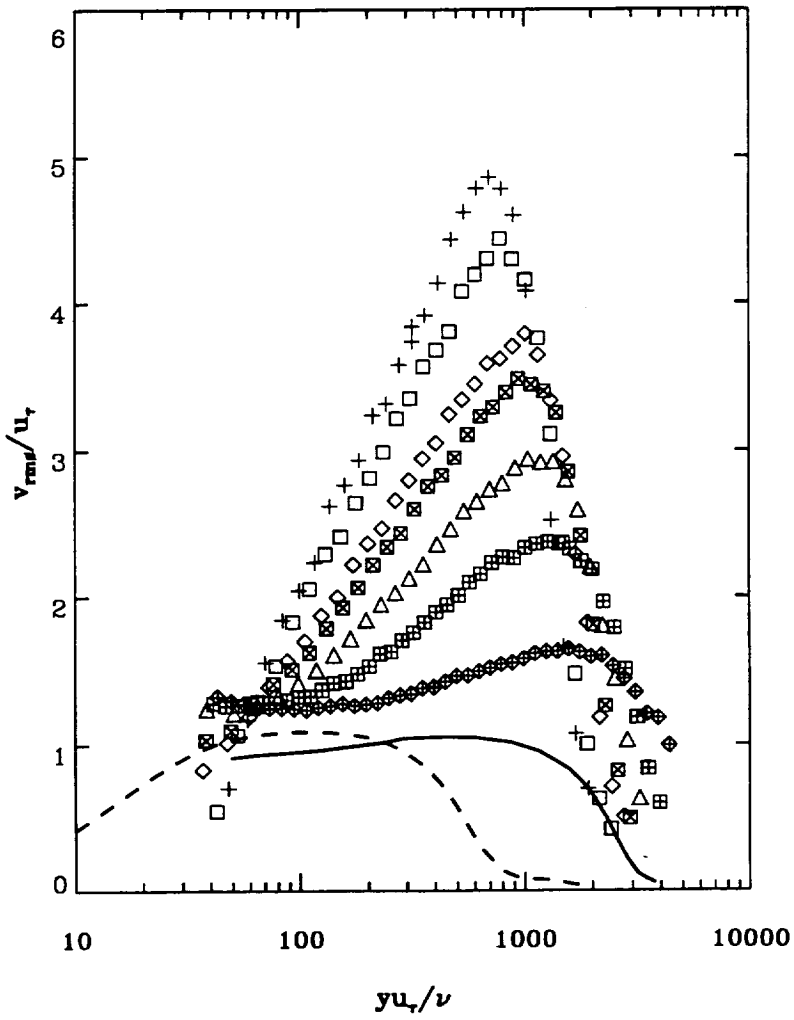

(c)

Figure 10. Continued. (c) Turbulence intensity in the transverse direction. All symbols are same as in figure 10(b).

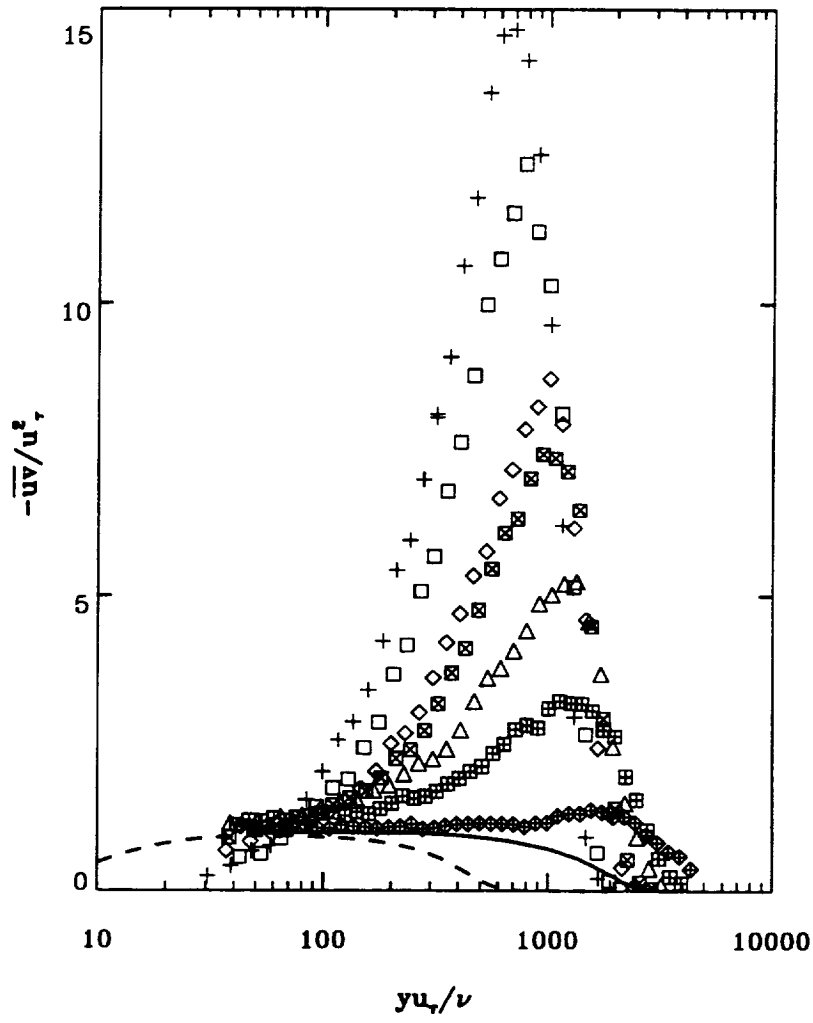

(d)

Figure 10. Concluded. (d) Shear stress. All symbols are same as in figure 10(b).

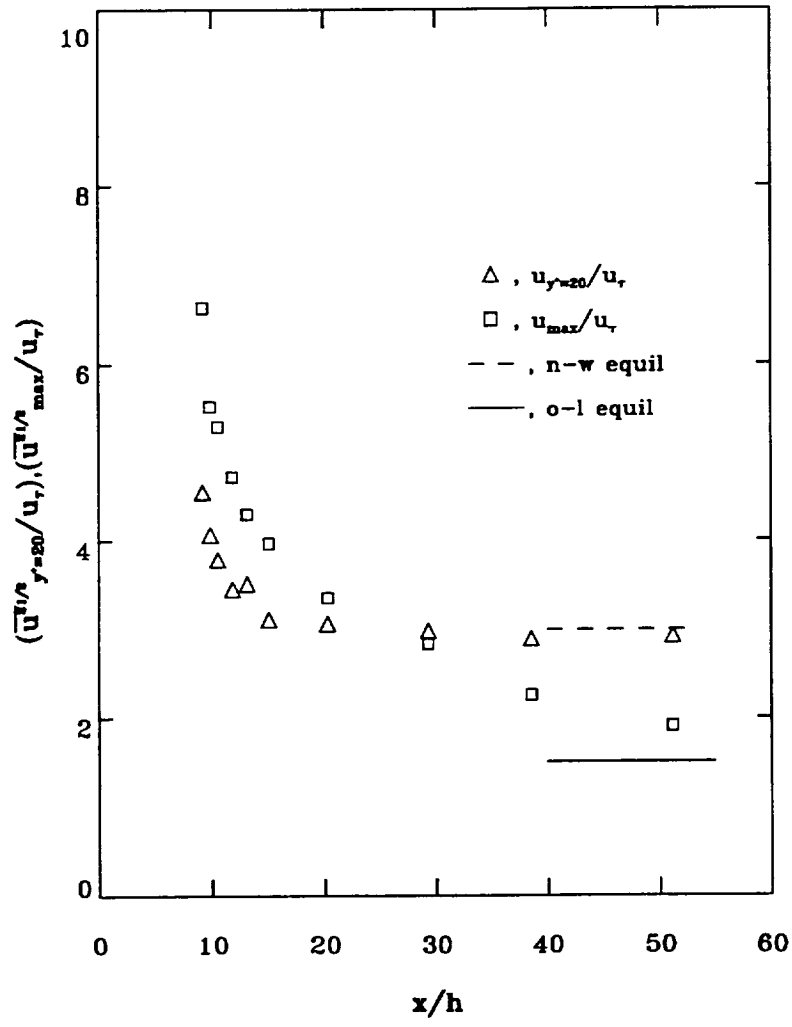

(a)

Figure 11. Development of maximum values in the reattached flow. (a) $u_{rms} = \sqrt{\overline{u^2}}$; local maximum in outer layer, and value at $y^+ = 20$. n–w equil, near wall equilibrium; o–l equil, outer layer equilibrium.

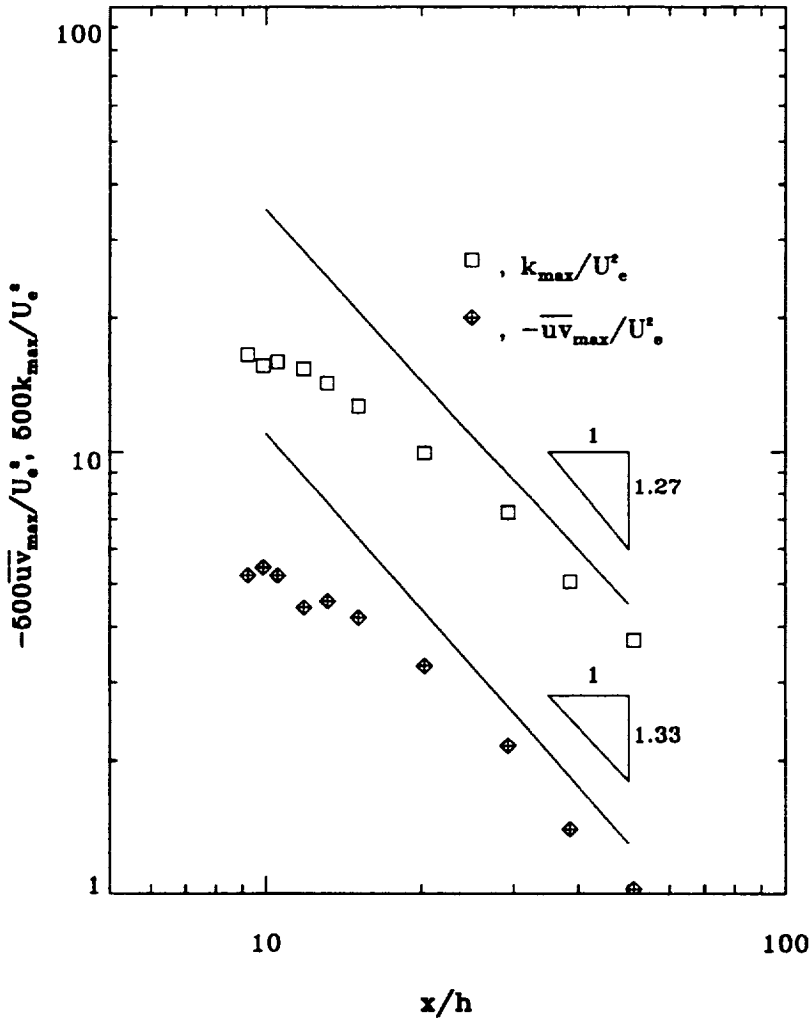

(b)

Figure 11. Concluded. (b) Maximum values of shear stress and turbulent kinetic energy.

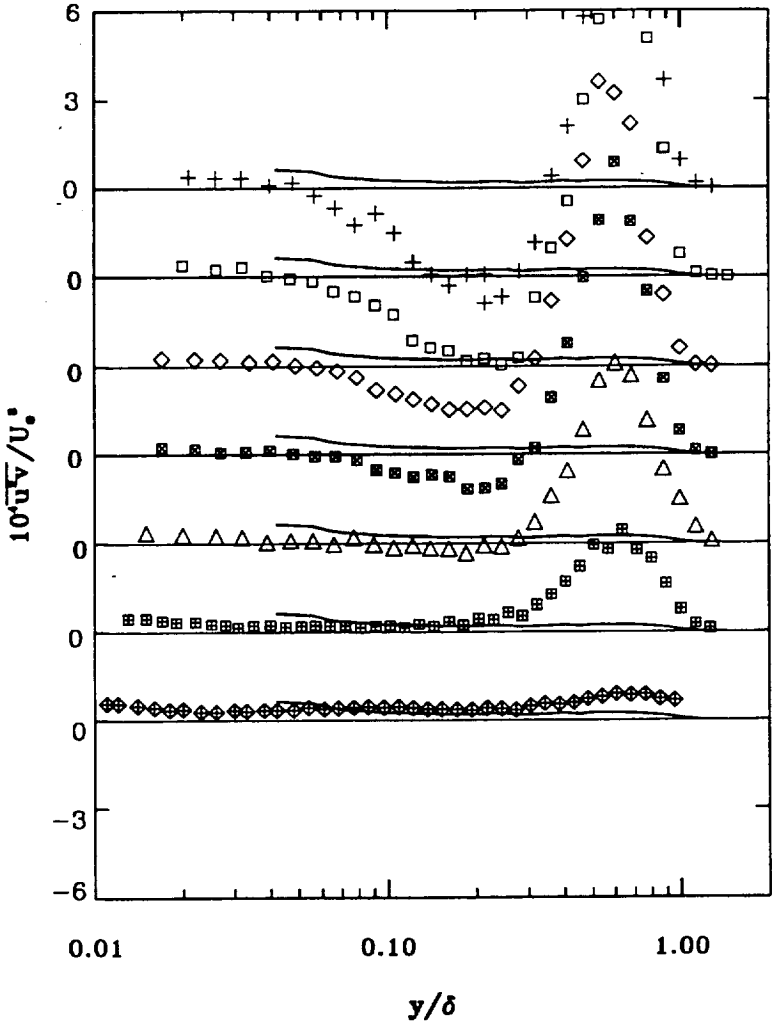

(a)

Figure 12. Profiles of the reattached flow; triple products. In figures 12–15, all symbols are as in figure 10(b). (a) $\overline{u^2v}$.

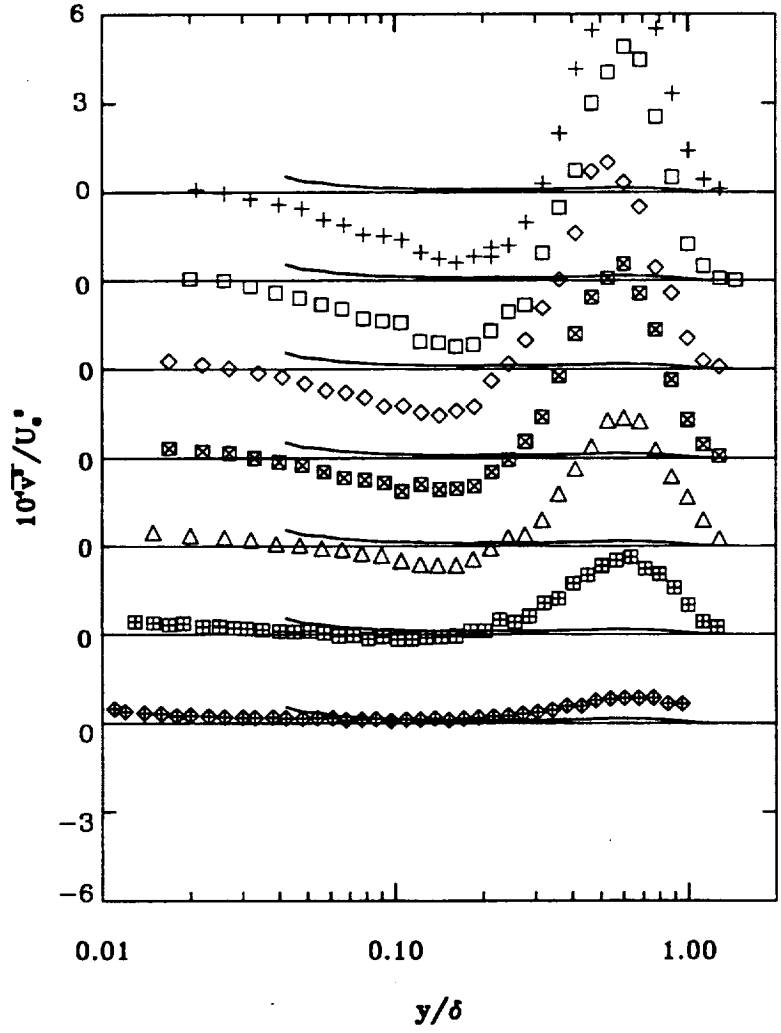

(b)

Figure 12. Continued. (b) $\overline{v^3}$.

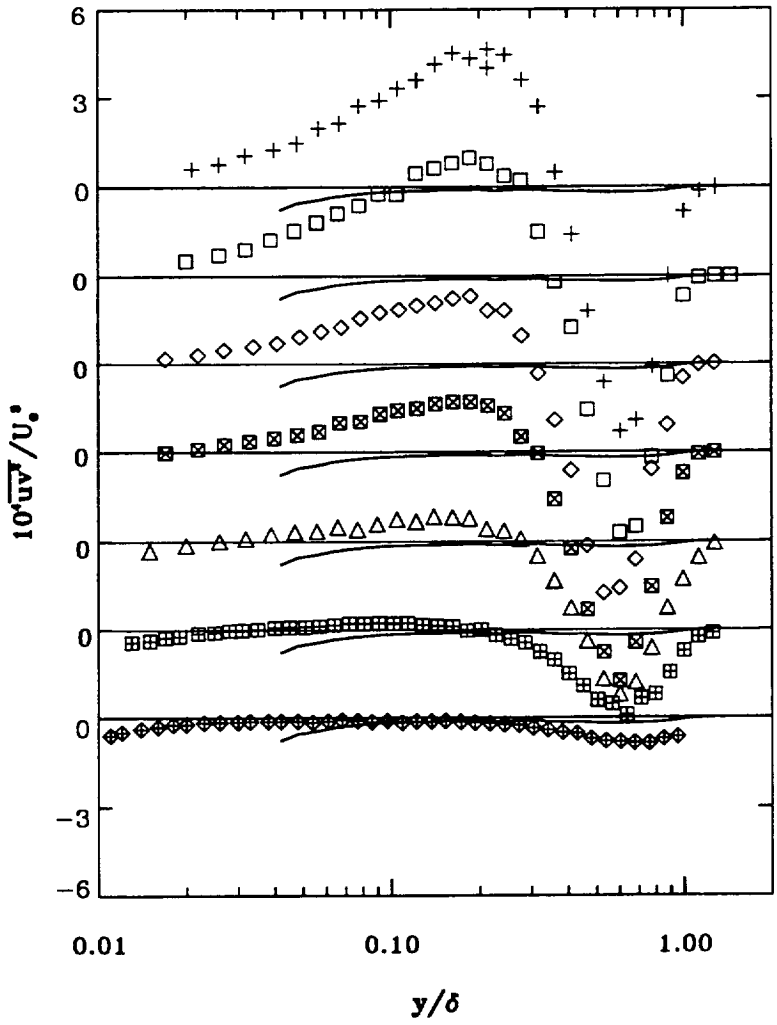

(c)

Figure 12. Continued. (c) $\overline{uv^2}$.

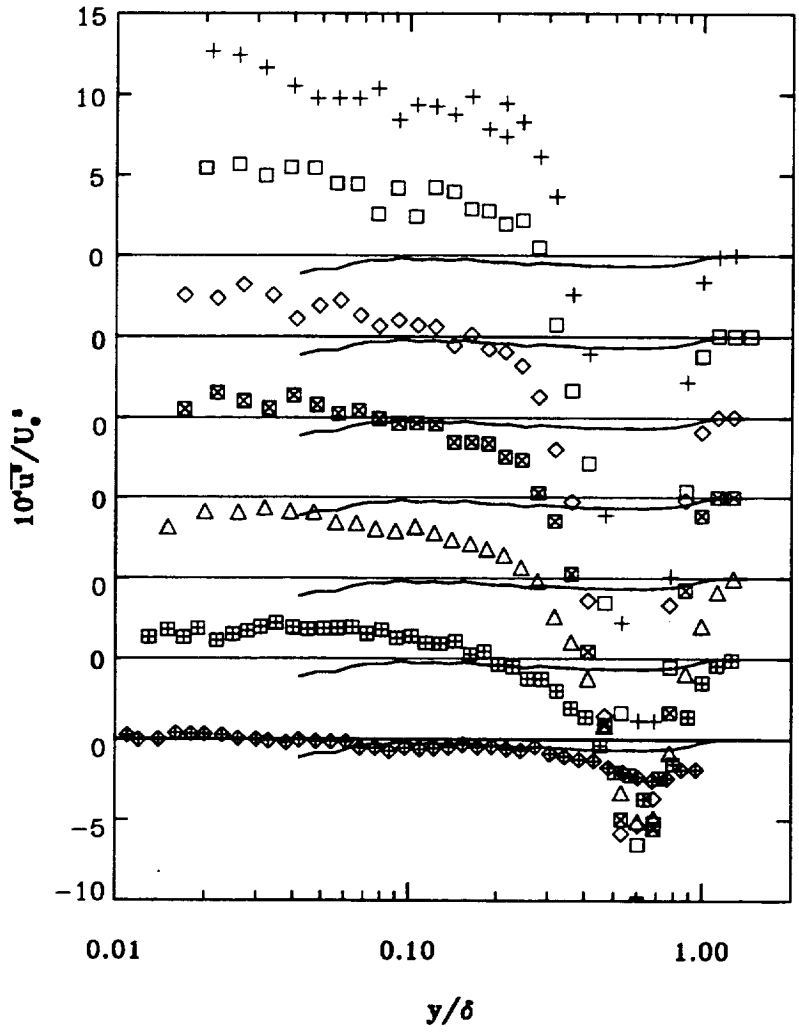

(d)

Figure 12. Concluded. (d) $\overline{u^3}$.

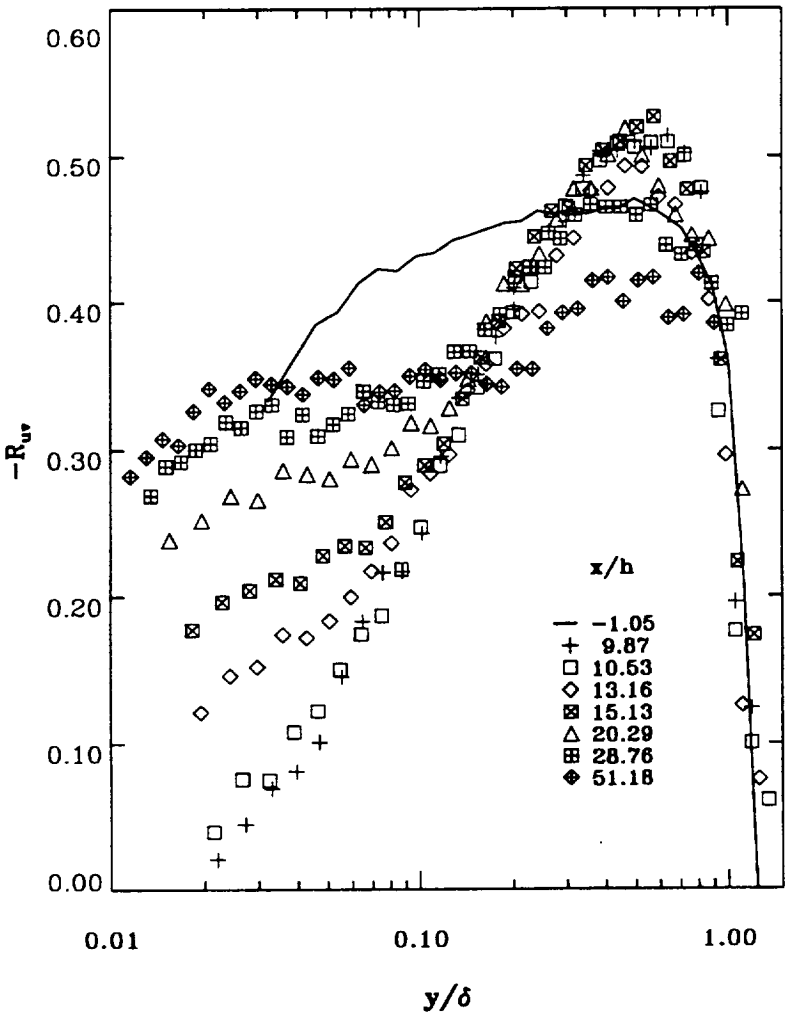

(a)

Figure 13. Development of the internal boundary layer; anisotropy parameters in semi-log coordinates. (a) Shear correlation coefficient R_{uv}.

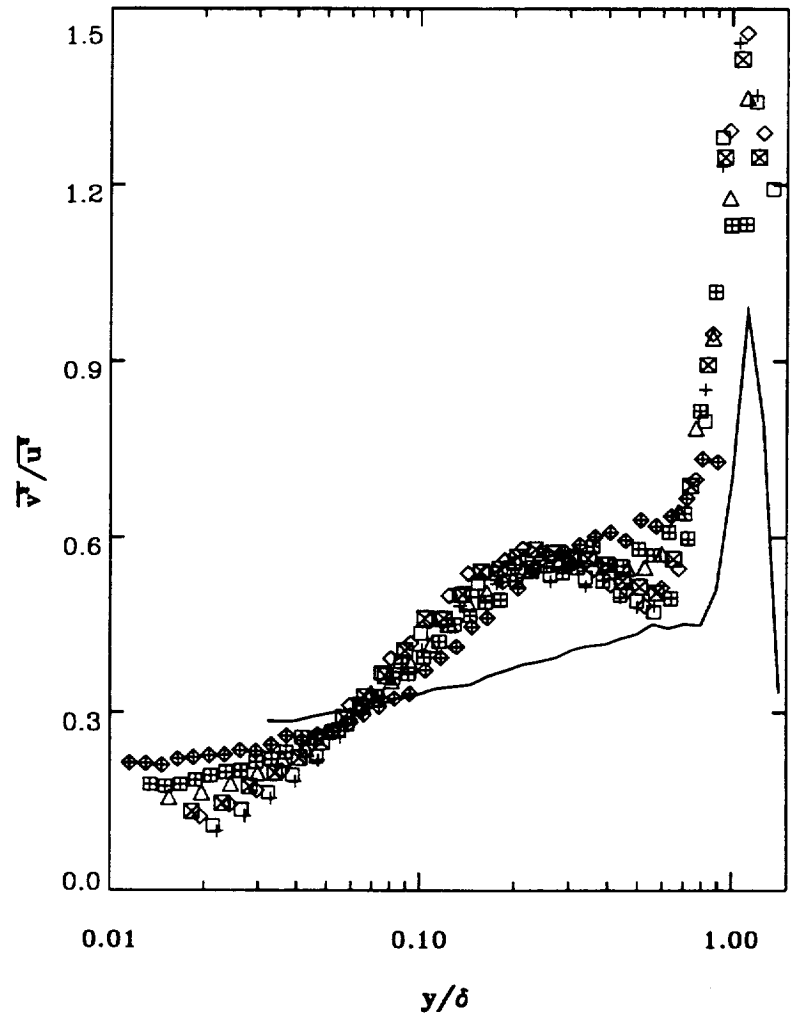

(b)

Figure 13. Continued. (b) Intensity ratio $\overline{v^2}/\overline{u^2}$.

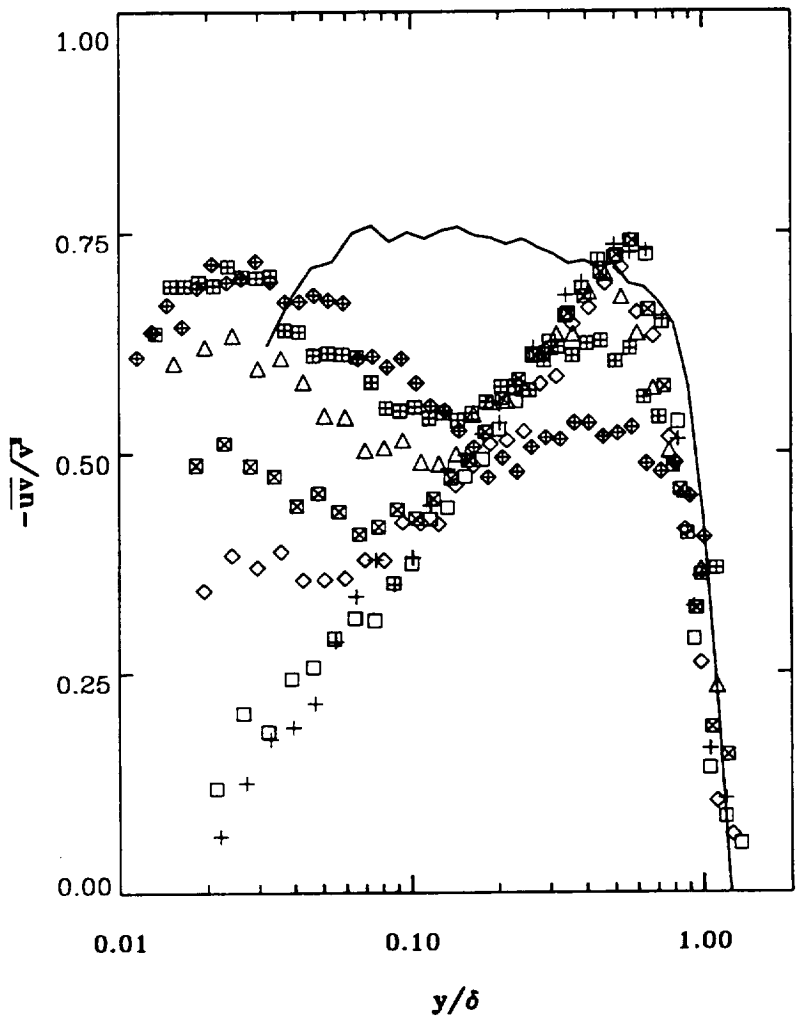

(c)

Figure 13. Concluded. (c) $-\overline{uv}/\overline{v^2}$.

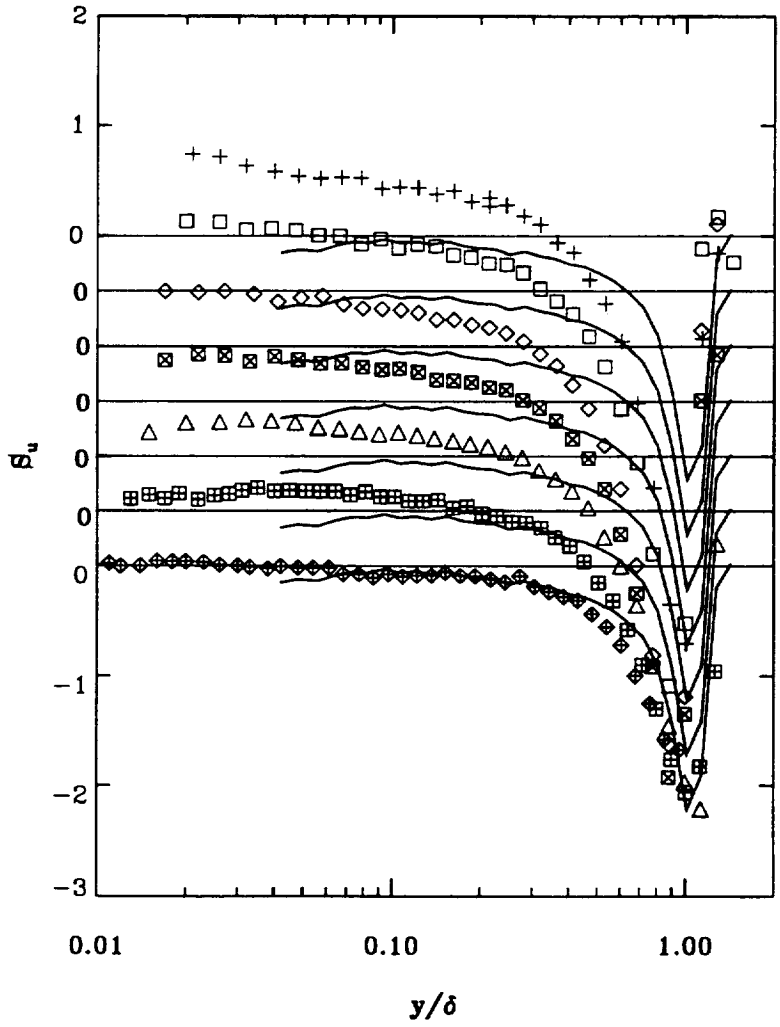

(a)

Figure 14. Development of the internal boundary layer; profiles of skewness and flatness factors. (a) u-component skewness. All symbols are same as in figure 13(a).

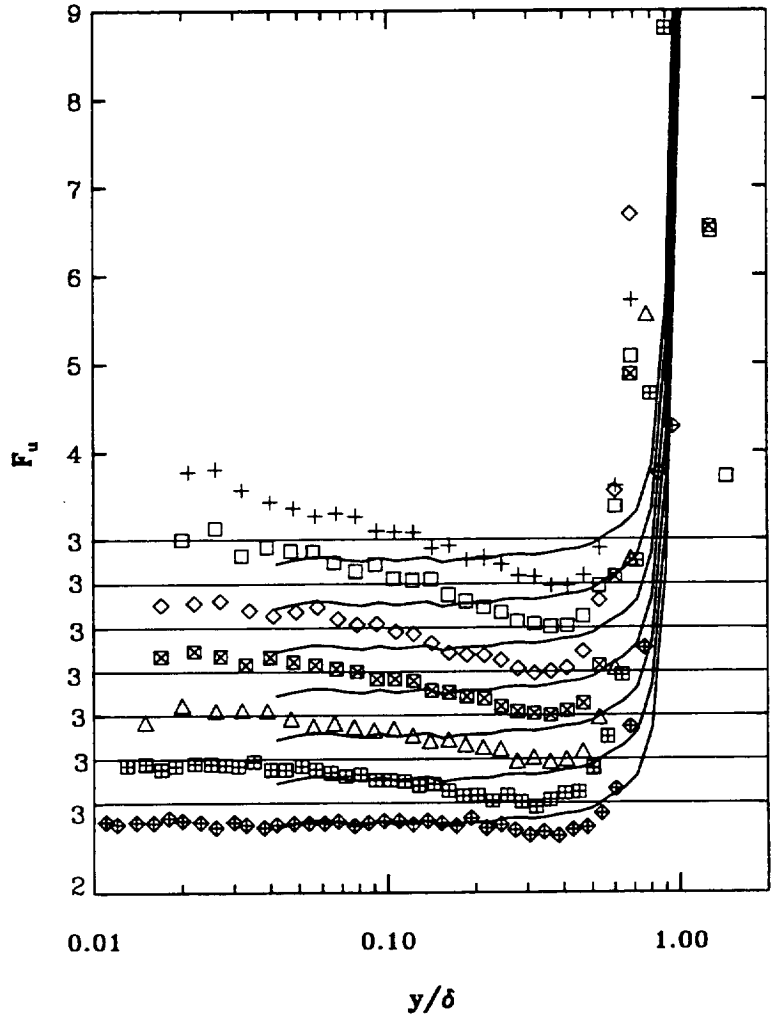

(b)

Figure 14. Continued. (b) u-component flatness.

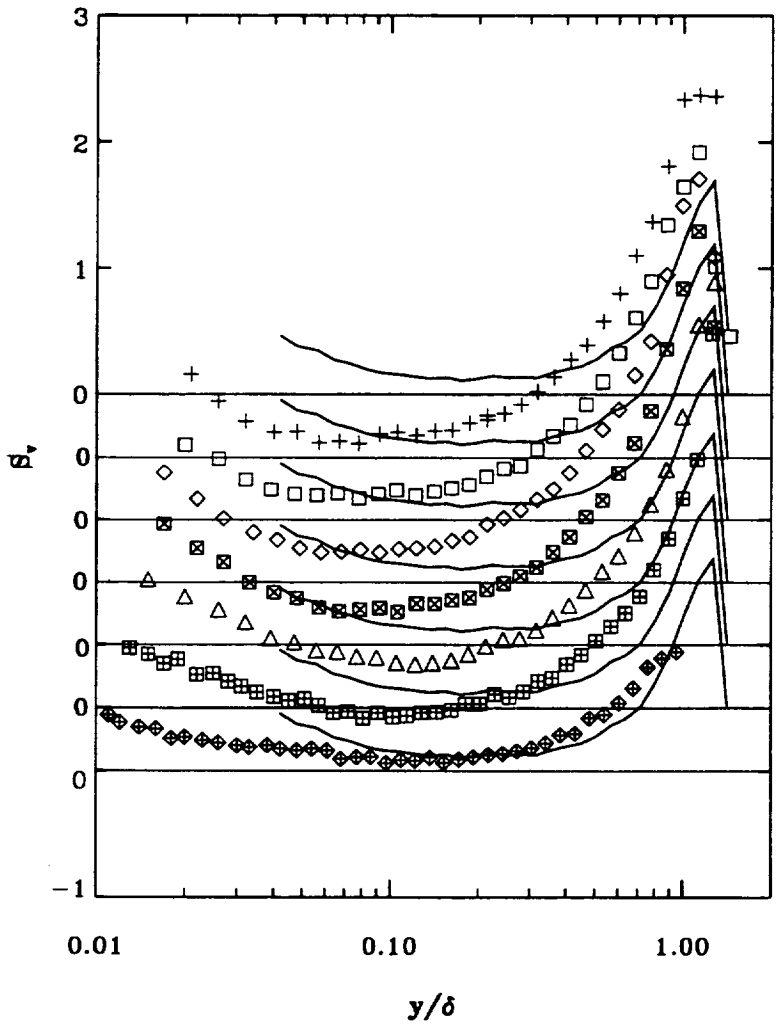

(c)

Figure 14. Continued. (c) v-component skewness.

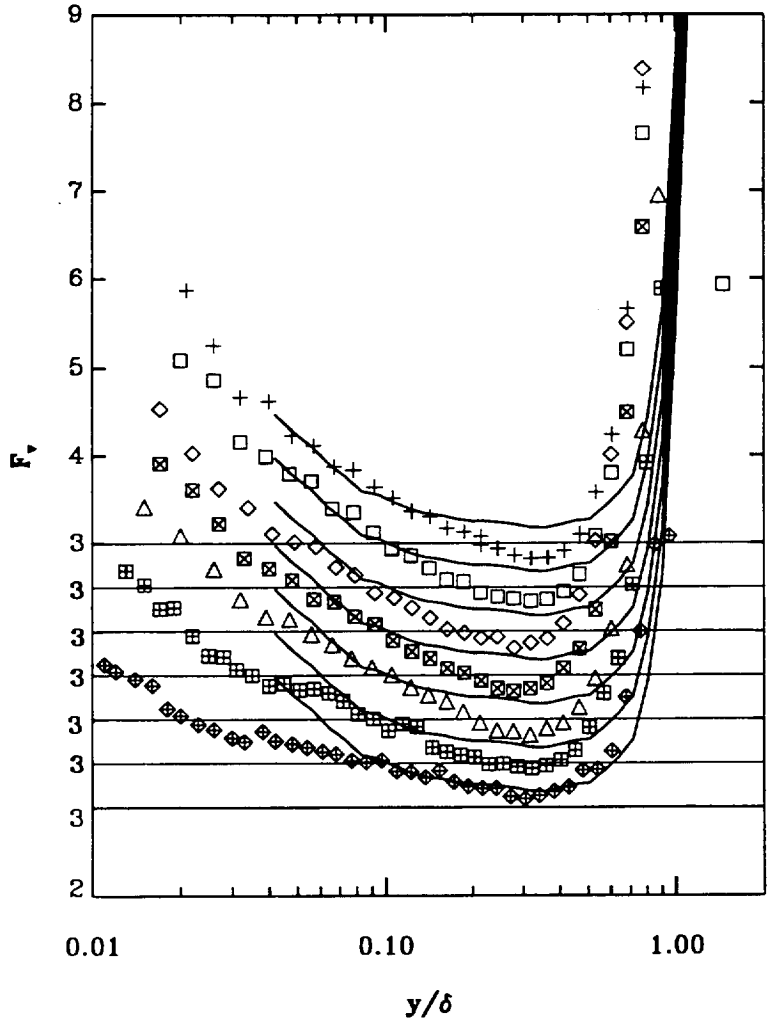

(d)

Figure 14. Concluded. (d) v-component flatness.

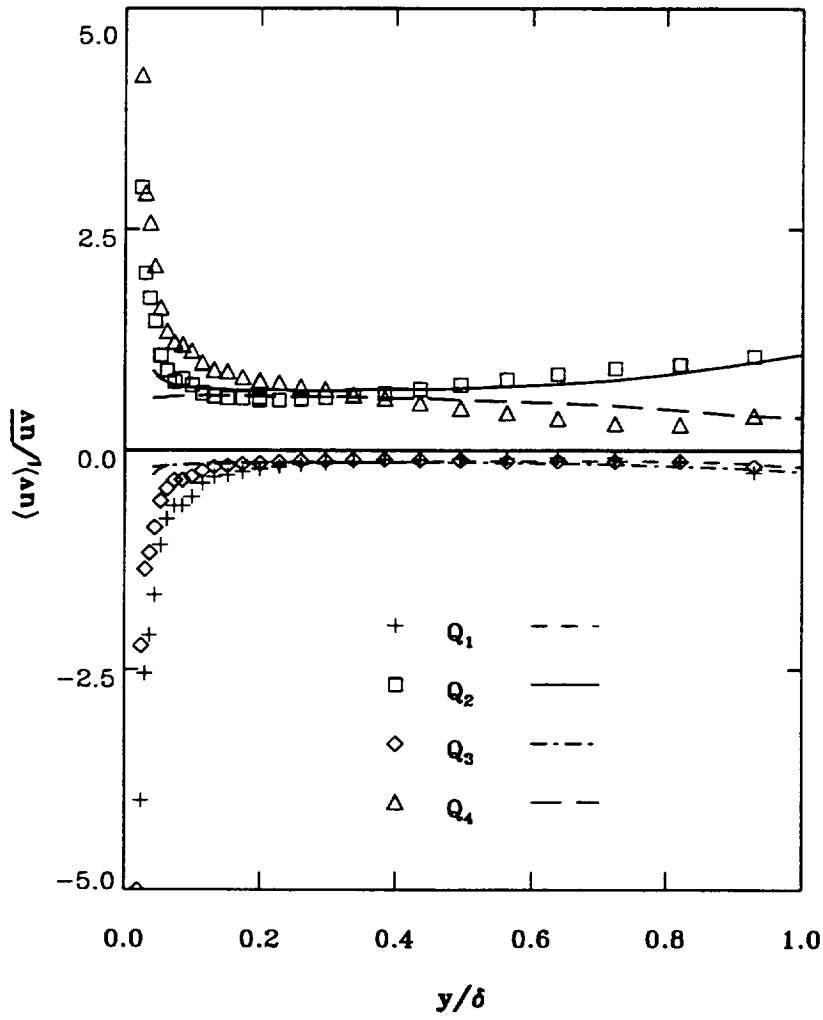

(a)

Figure 15. Development of the internal boundary layer; quadrant distributions of $< uv >_i / \overline{uv}$ *(lines denote boundary layer at x = −1.05h). (a) x = 9.87h.*

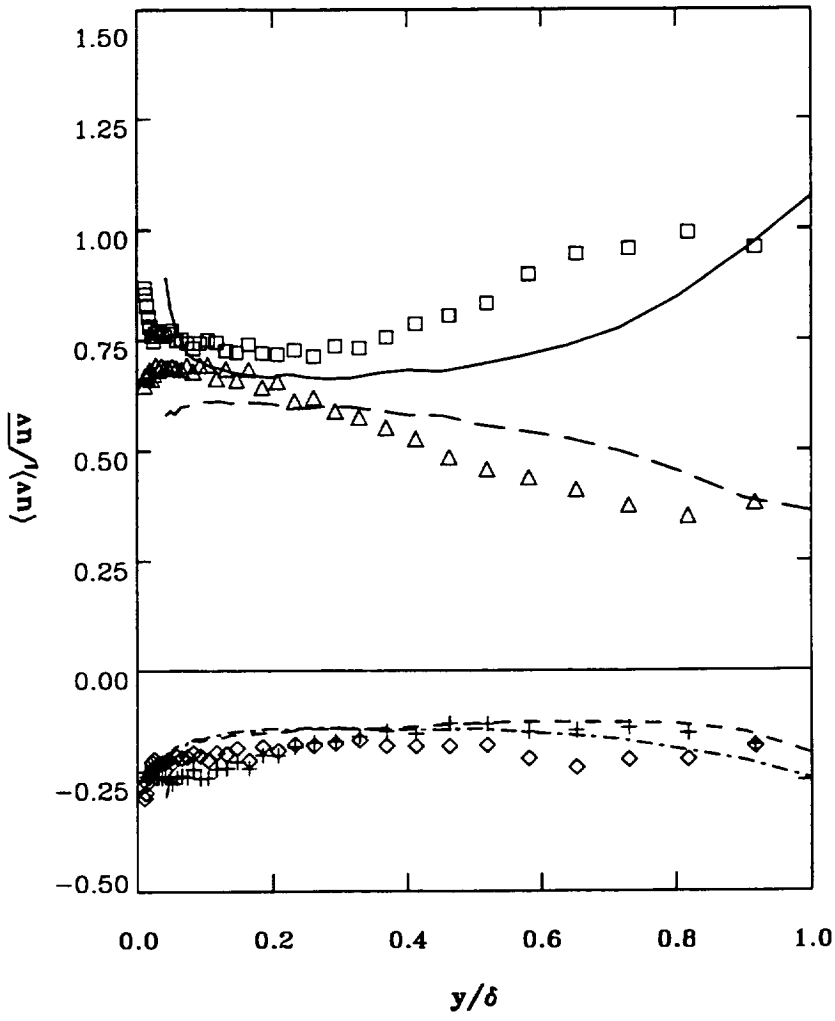

(b)

Figure 15. Concluded. (b) x = 38.55h. All symbols are same as in figure 15(a).

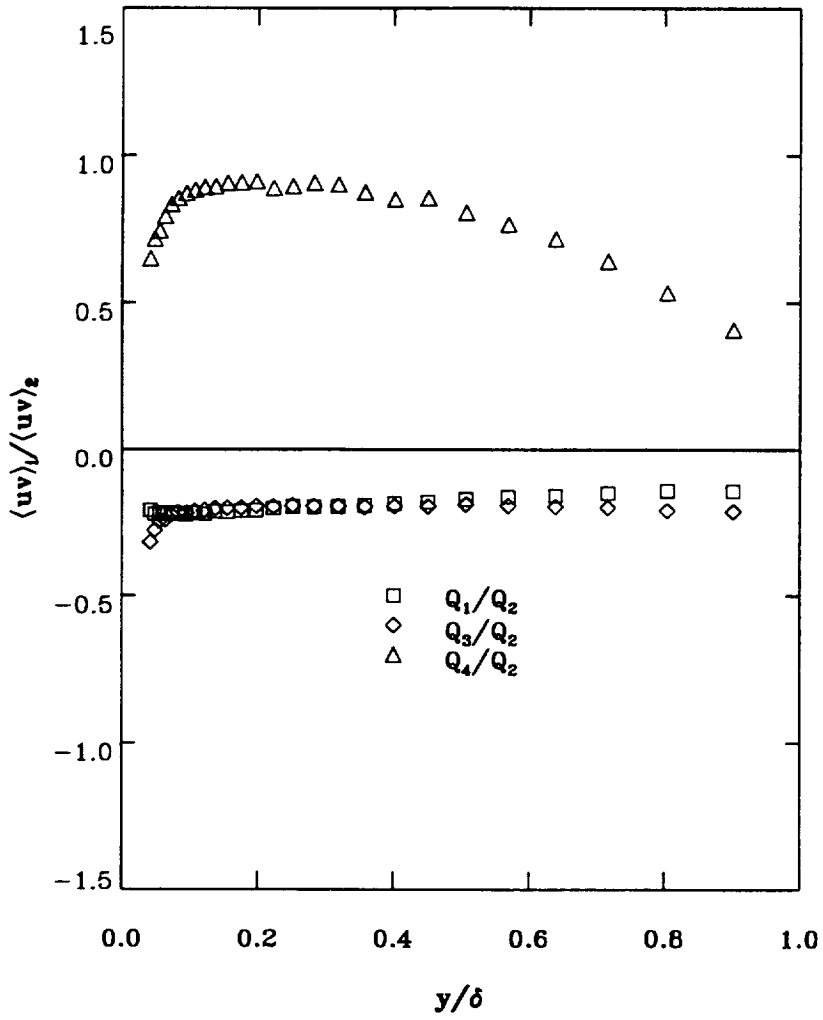

(a)

Figure 16. Development of the internal boundary layer; quadrant distributions of $< uv >_i / \overline{uv}$. *(a)* $x = -1.05h$.

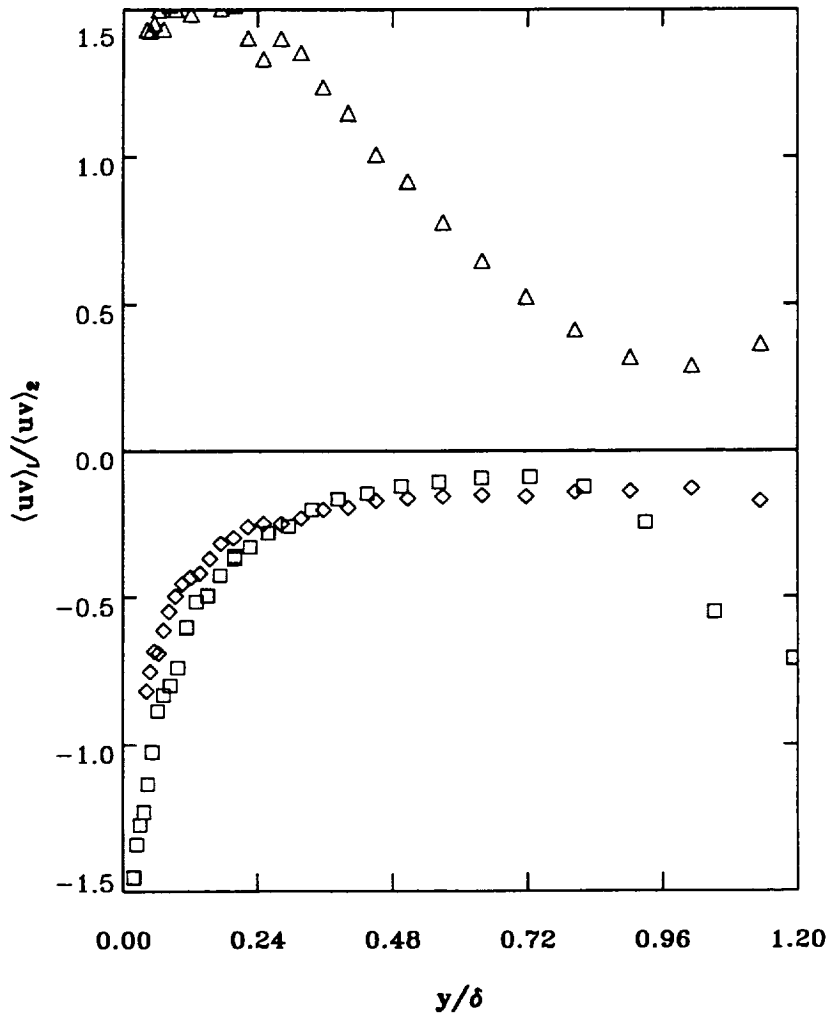

(b)

Figure 16. Continued. (b) x = 9.87h. All symbols are same as in figure 15(a).

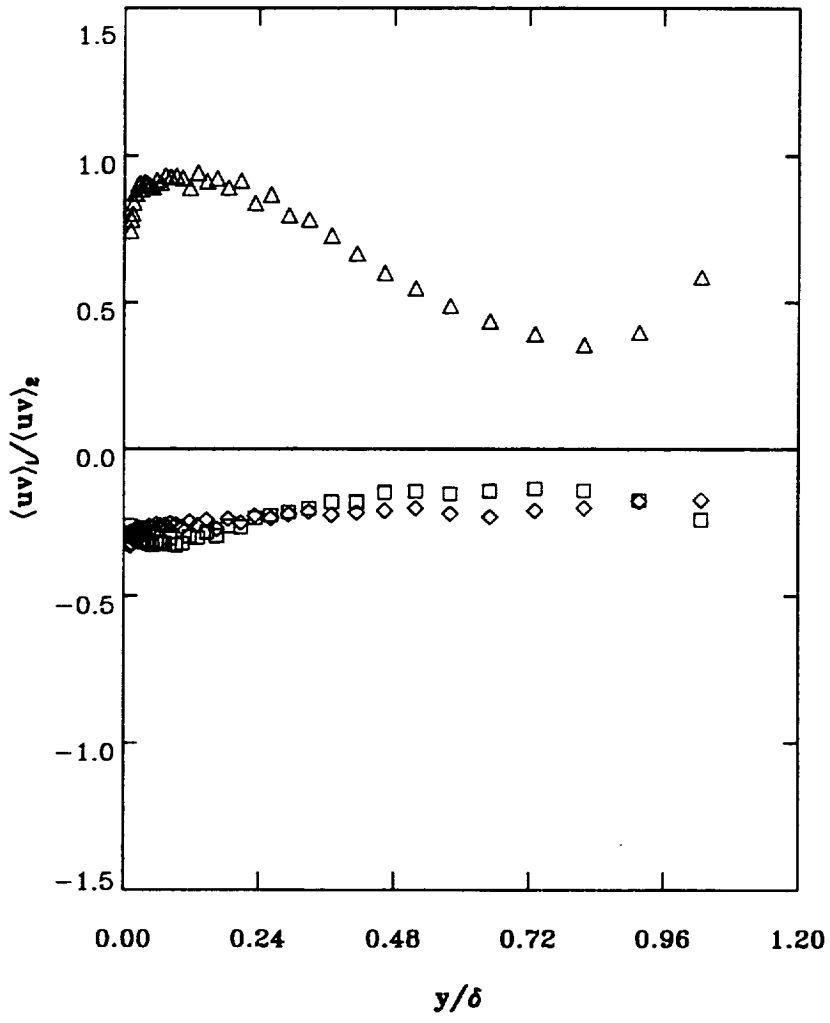

(c)

Figure 16. Concluded. (c) x = 38.55h. All symbols are same as in figure 15(a).

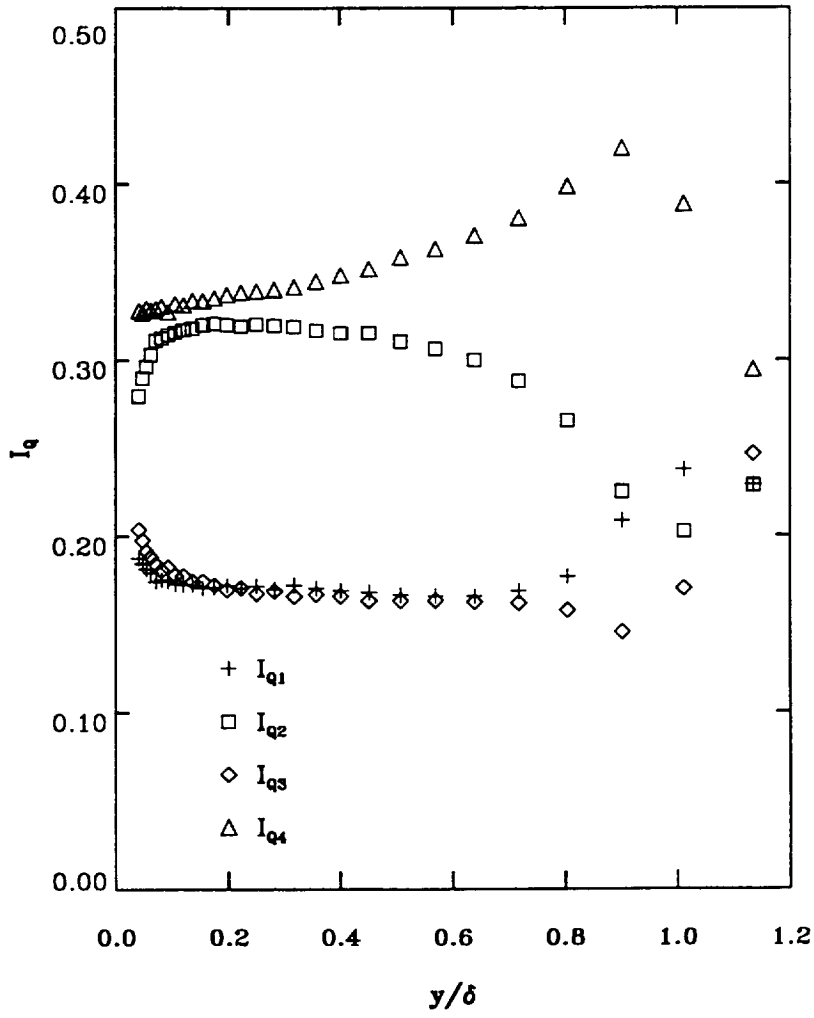

(a)

Figure 17. Development of the internal boundary layer; fraction of time spent by uv in each quadrant. (a) x = −1.05h.

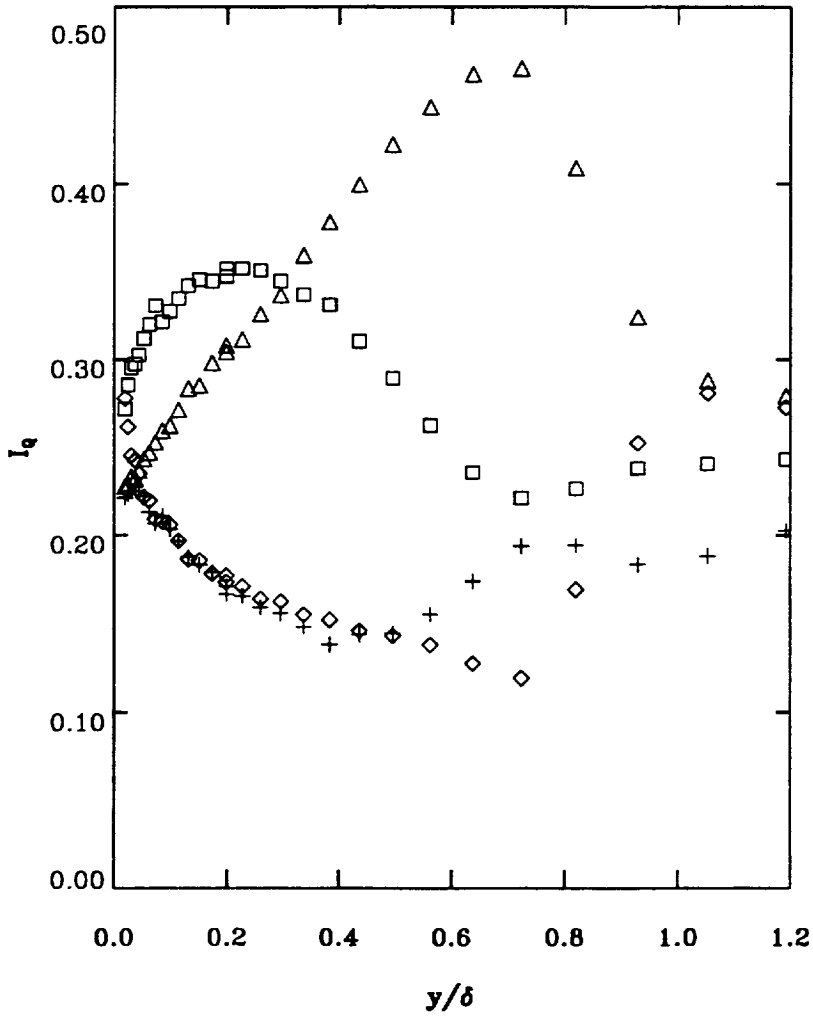

(b)

Figure 17. Continued. (b) x = 9.87h. All symbols are same as in figure 17(a).

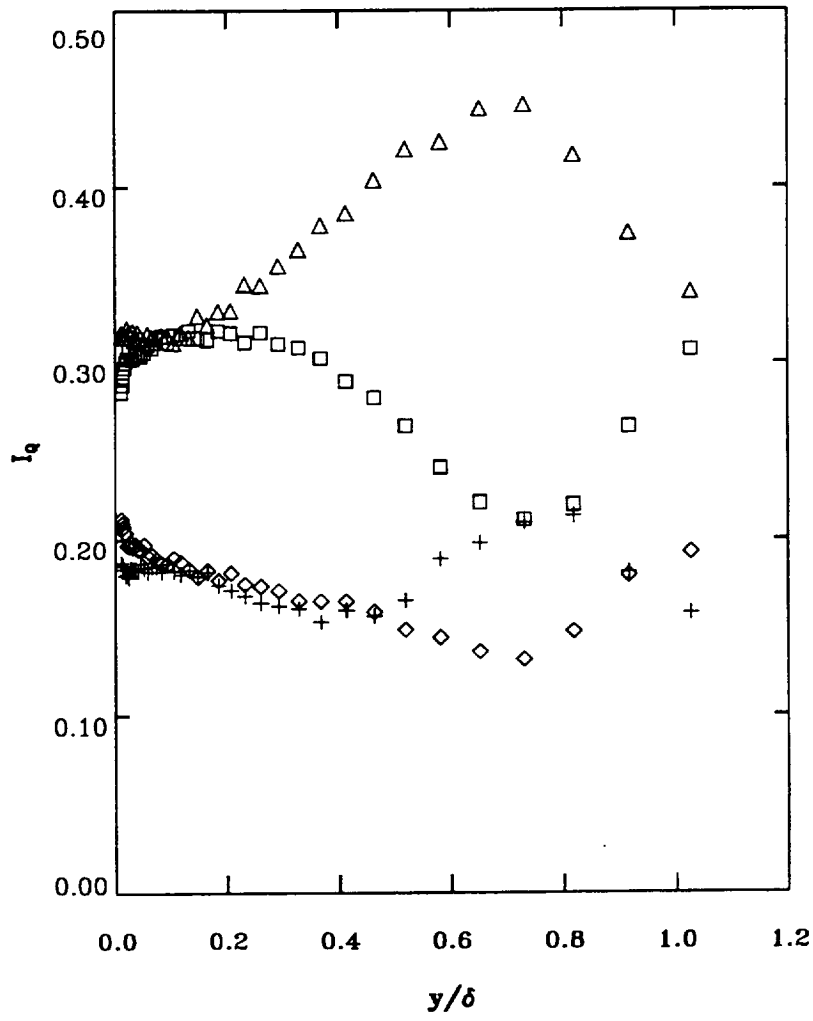

(c)

Figure 17. Concluded. (c) x = 38.55h. All symbols are same as in figure 17(a).

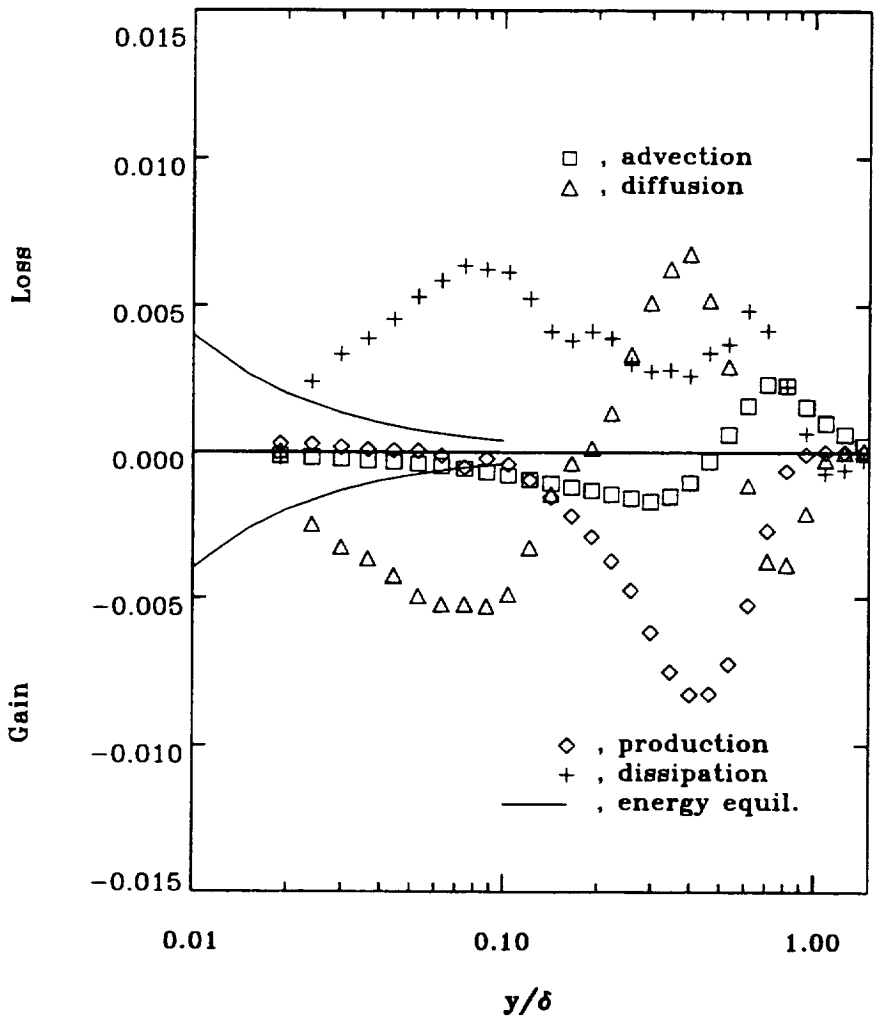

(a)

Figure 18. Development of the internal boundary layer: budgets of turbulent kinetic energy, normalized by U_e^3/δ, *with dissipation by difference. Lines denote local equilibrium, production = dissipation =* $U_\tau^3/\kappa y$. *(a) x = 9.87h.*

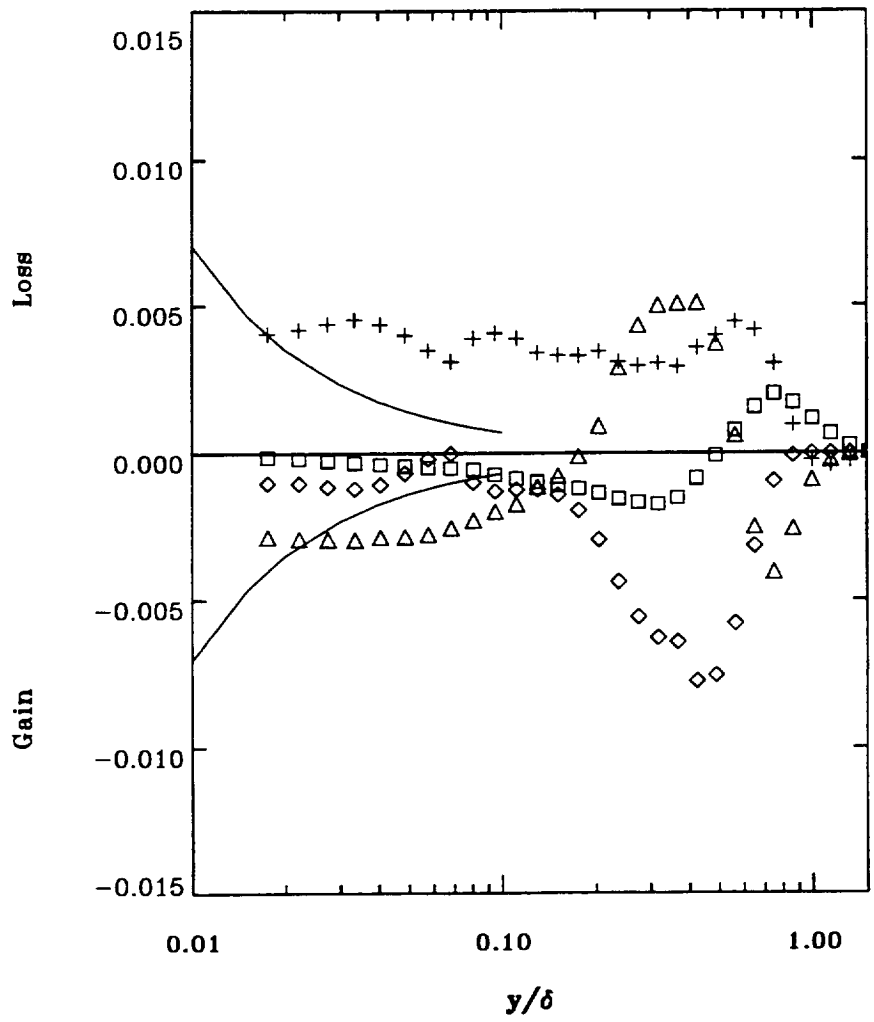

(b)

Figure 18. Continued. (b) x = 11.84h. All symbols are same as in figure 18(a).

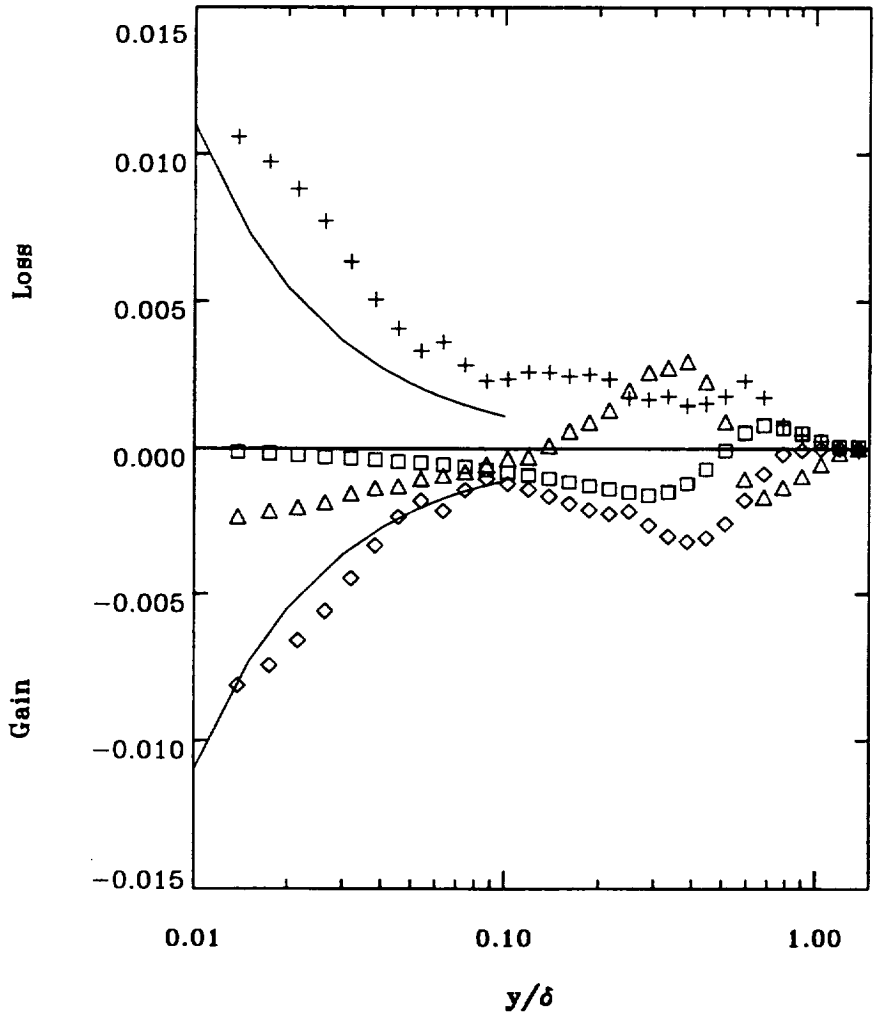

(c)

Figure 18. Continued. (c) x = 20.29h. All symbols are same as in figure 18(a).

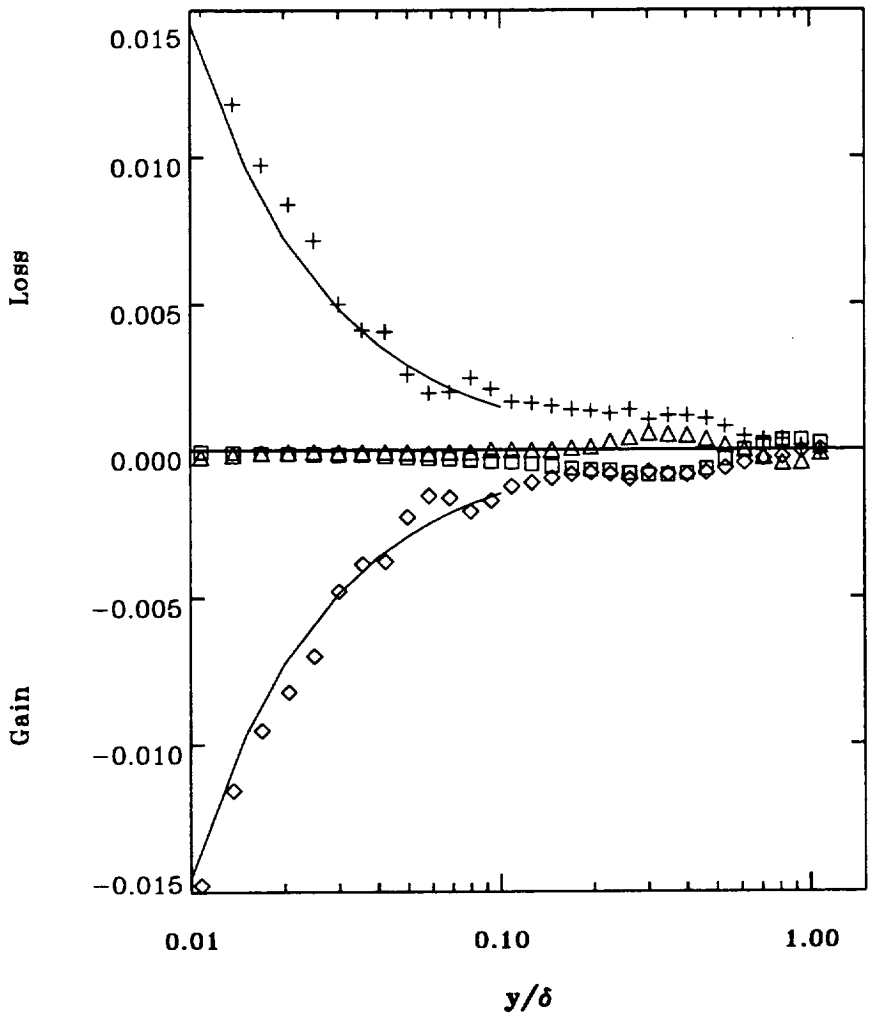

(d)

Figure 18. Concluded. (d) x = 38.55h. All symbols are same as in figure 18(a).

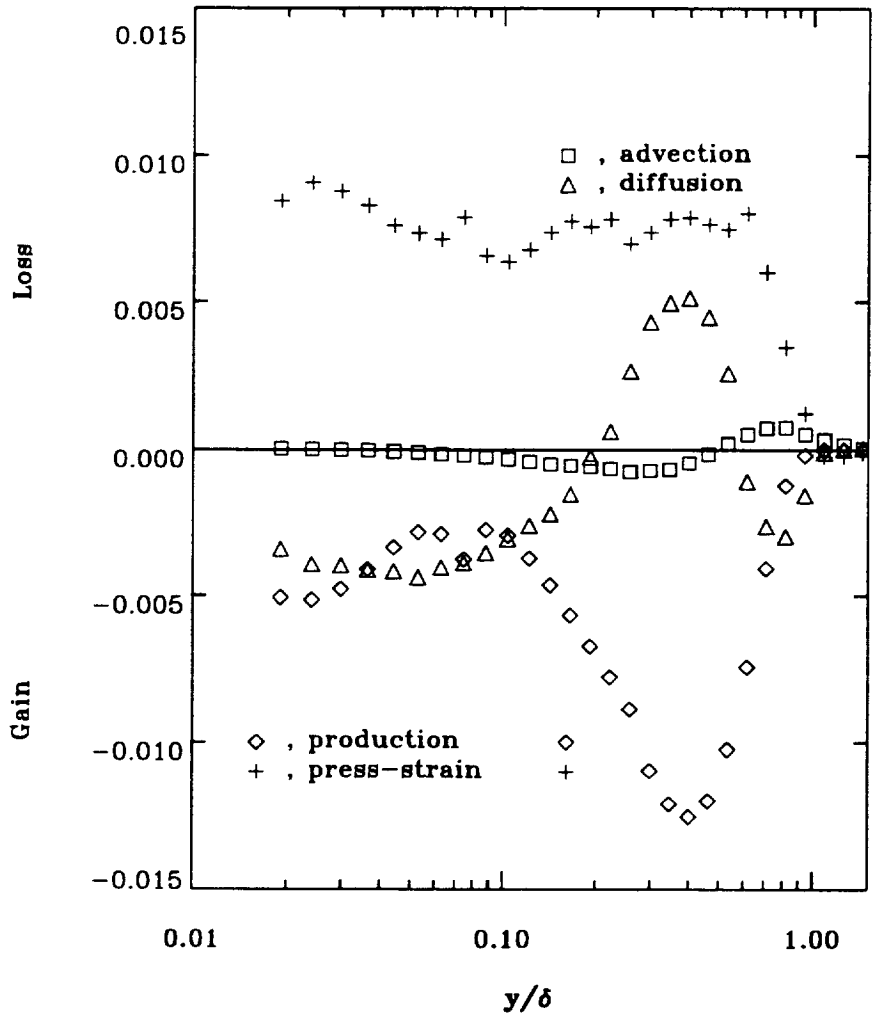

(a)

Figure 19. Development of the internal boundary layer: budgets of turbulent shear stress, normalized by U_e^3/δ, with pressure-strain "redistribution" by difference. (a) x = 9.87h.

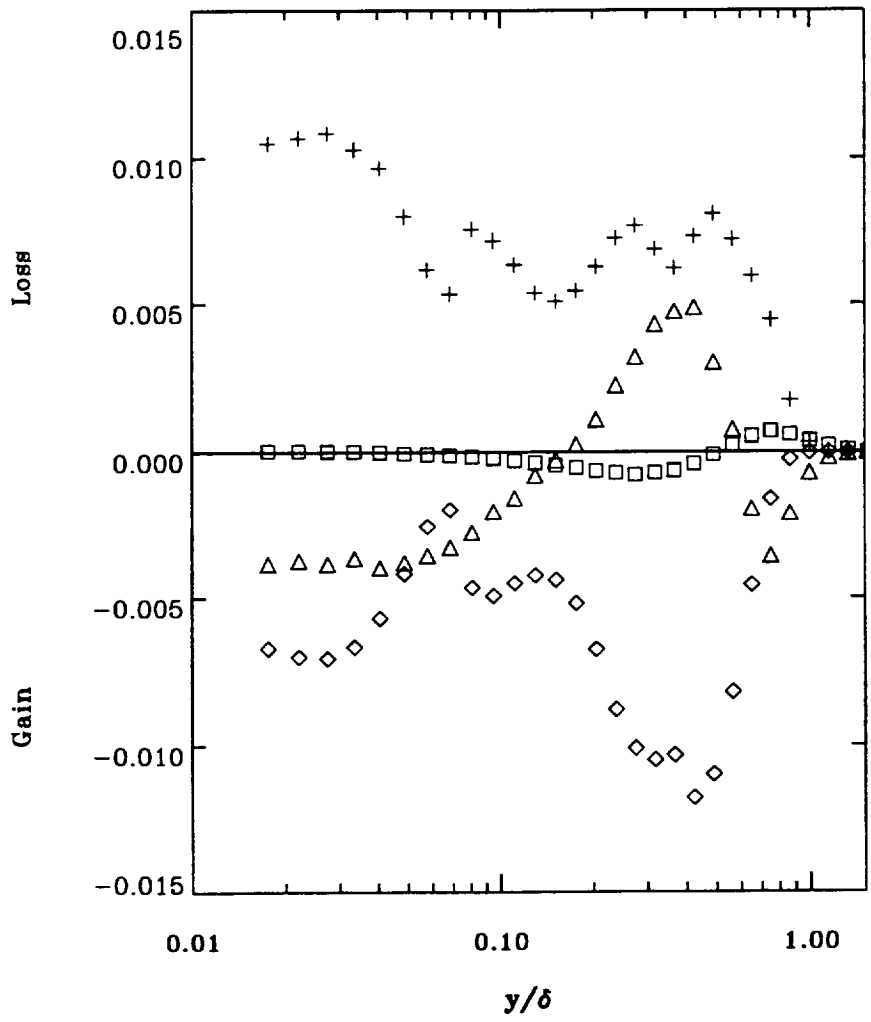

(b)

Figure 19. Continued. (b) x = 11.84h. All symbols are same as in figure 19(a).

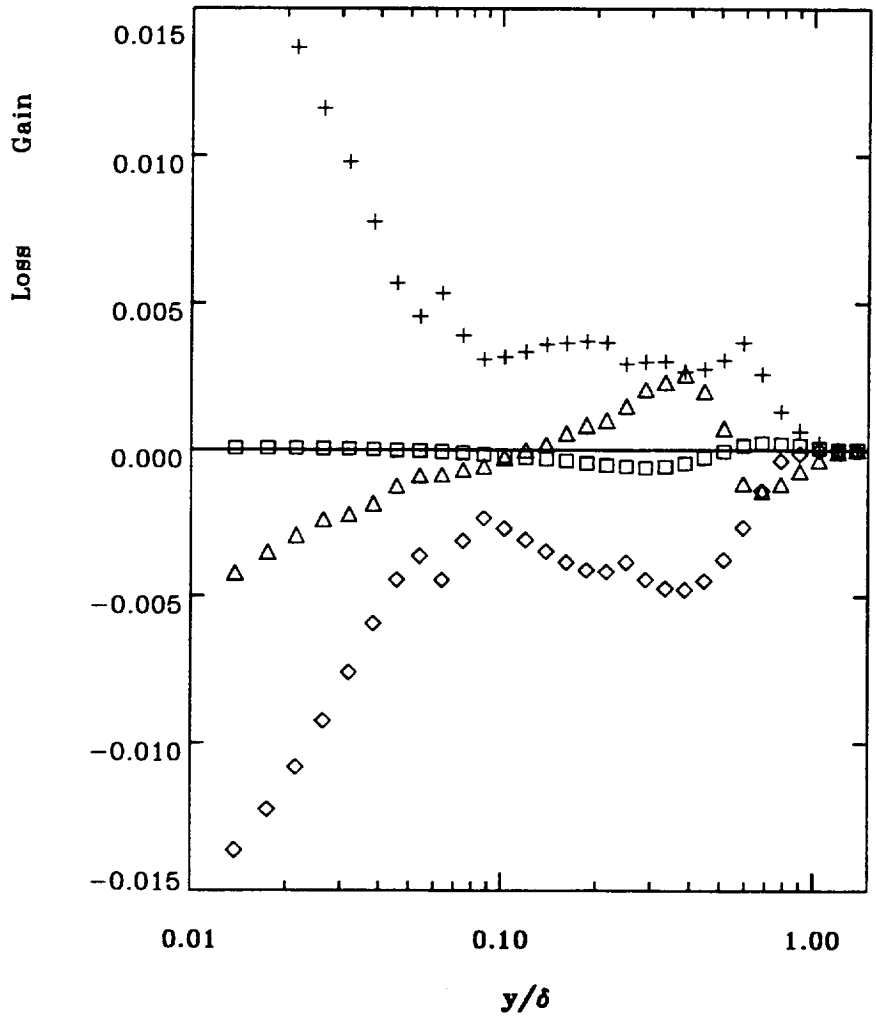

(c)

Figure 19. Continued. (c) x = 20.29h. All symbols are same as in figure 19(a).

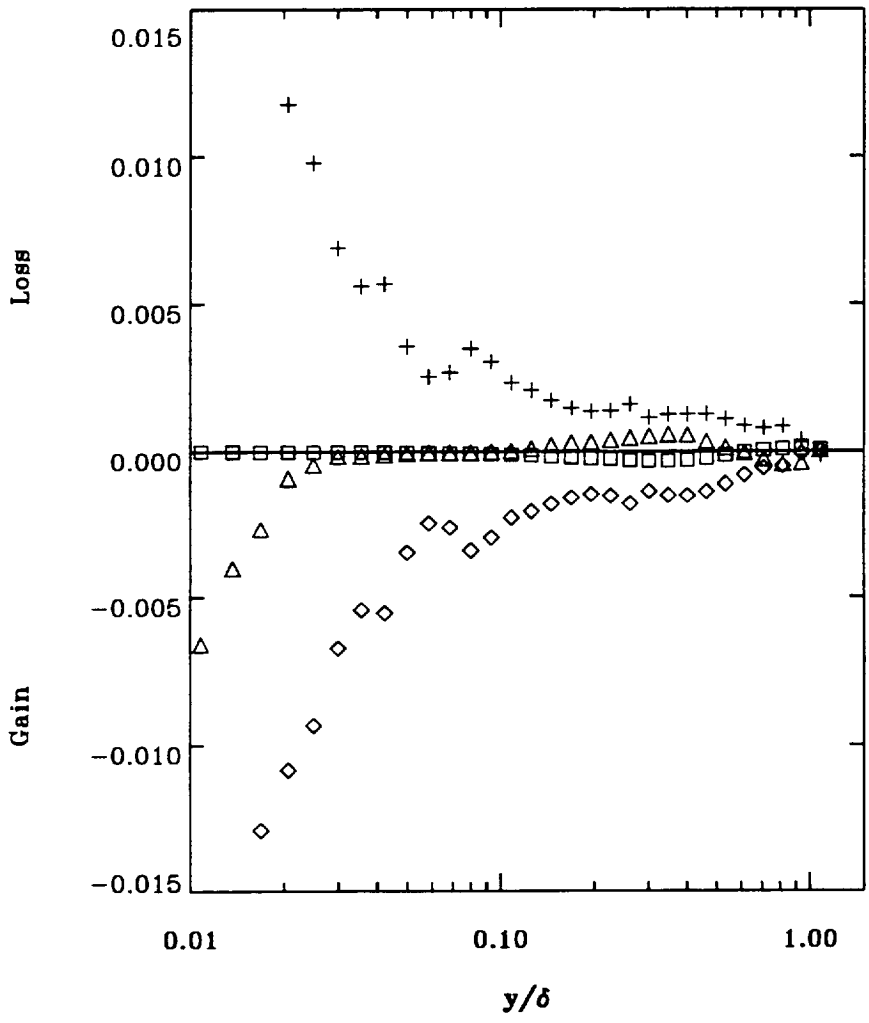

(d)

Figure 19. Concluded. (d) x = 38.55h. All symbols are same as in figure 19(a).

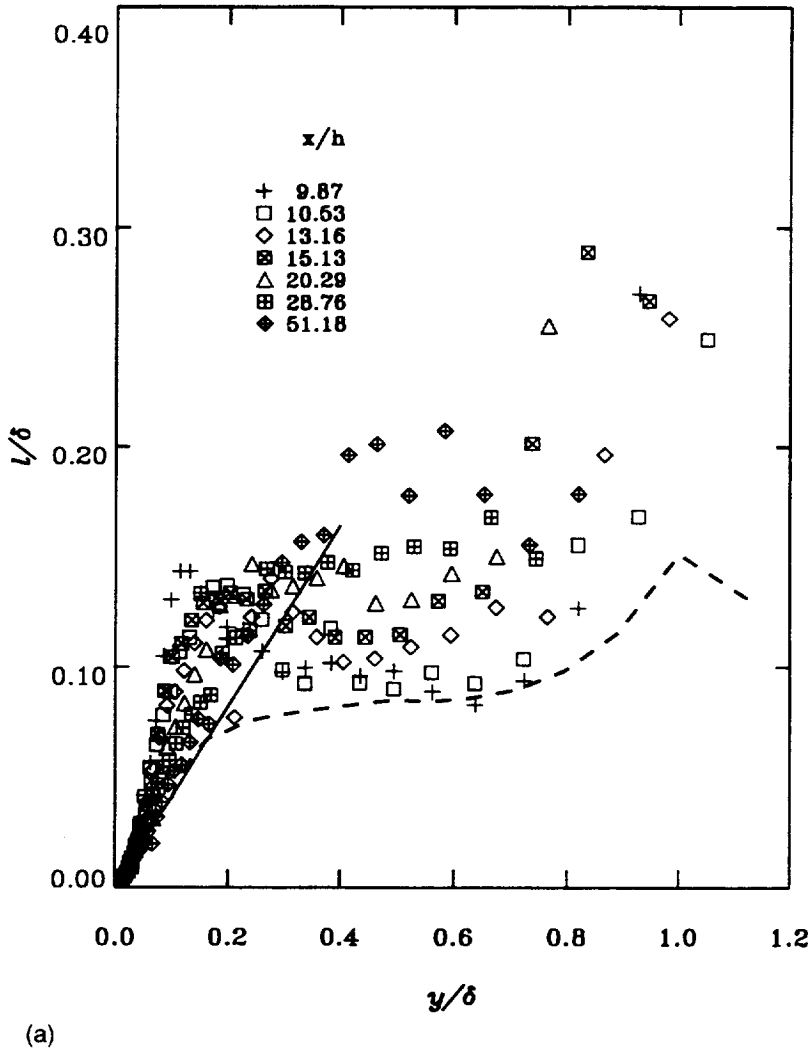

(a)

Figure 20. Development of the internal boundary layer: profiles of mixing length and eddy viscosity. Dash line represents upstream TBL. (a) Mixing length (sold line presents 0.41y).

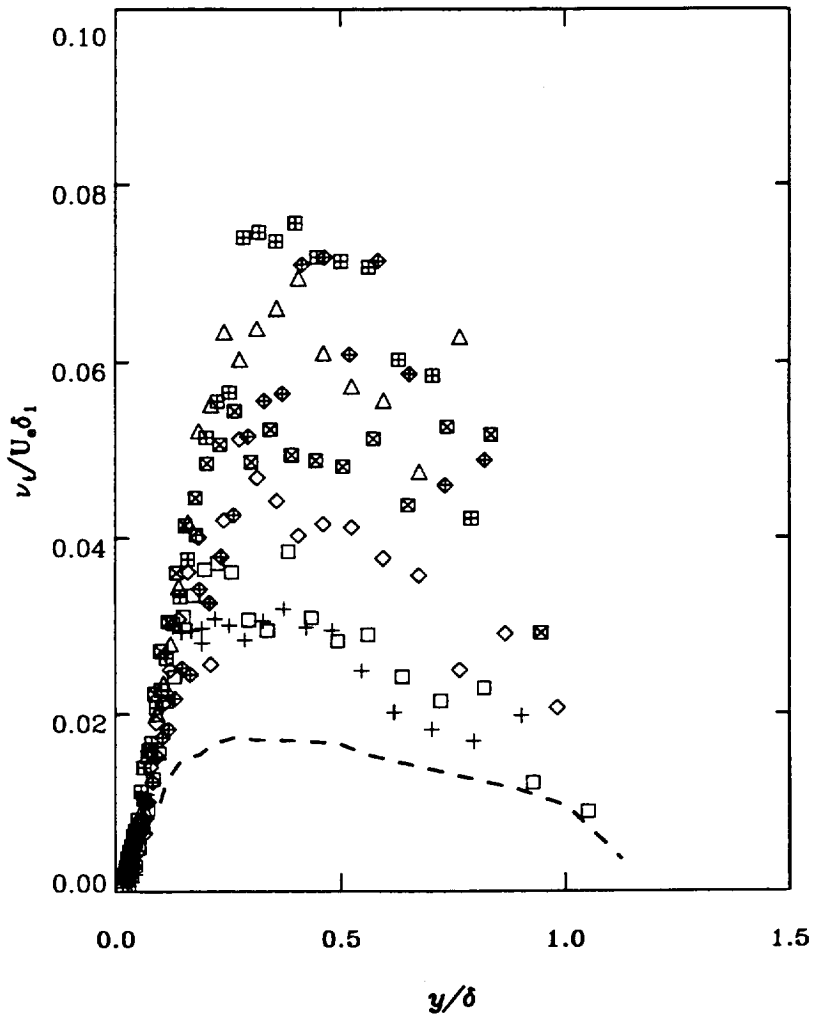

(b)

Figure 20. Concluded. (b) Eddy viscosity. All symbols are same as in figure 20(a).

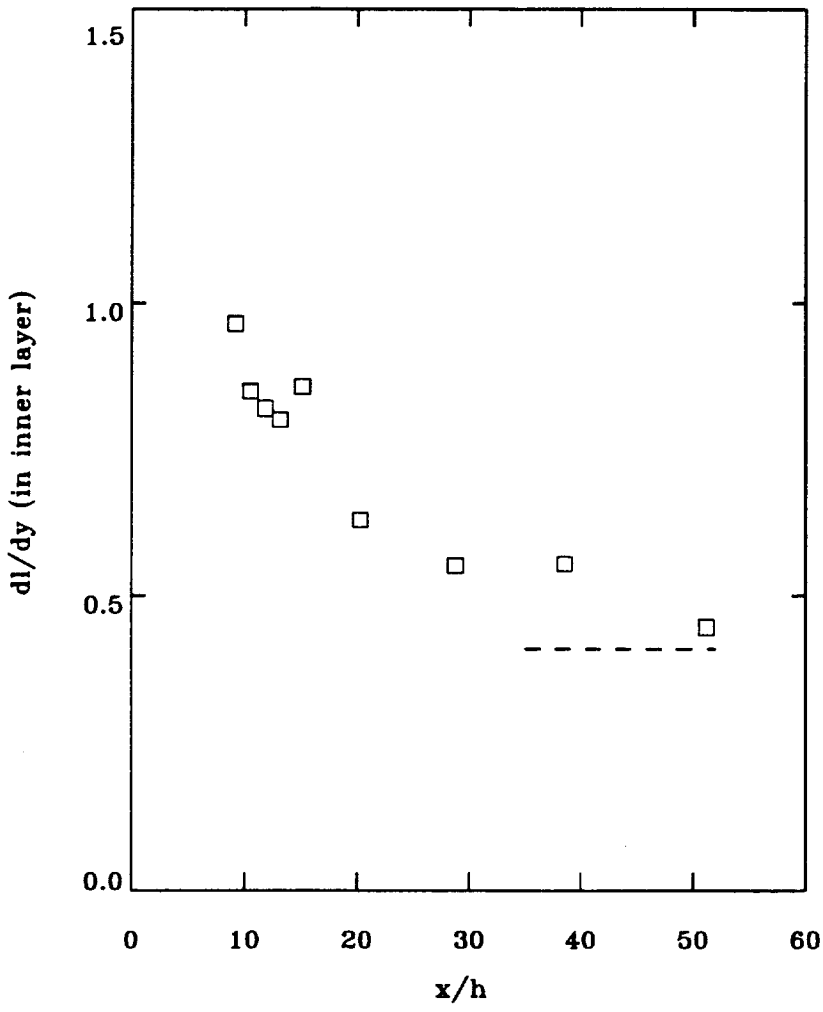

(a)

Figure 21. Development of the internal boundary layer: streamwise variation of mixing length slope and eddy maximum viscosity. (a) Slope of mixing length in inner layer (dash line denotes value of 0.41).

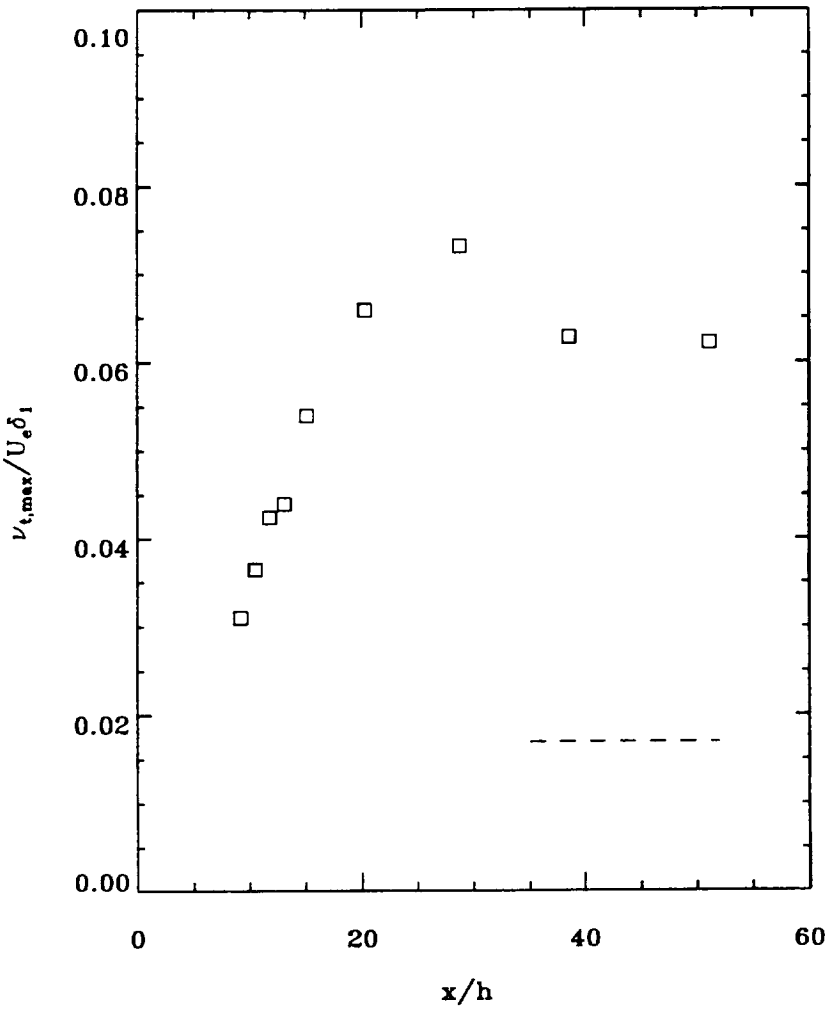

(b)

Figure 21. Concluded. (b) Maximum eddy viscosity (dash line denotes value of 0.0169).

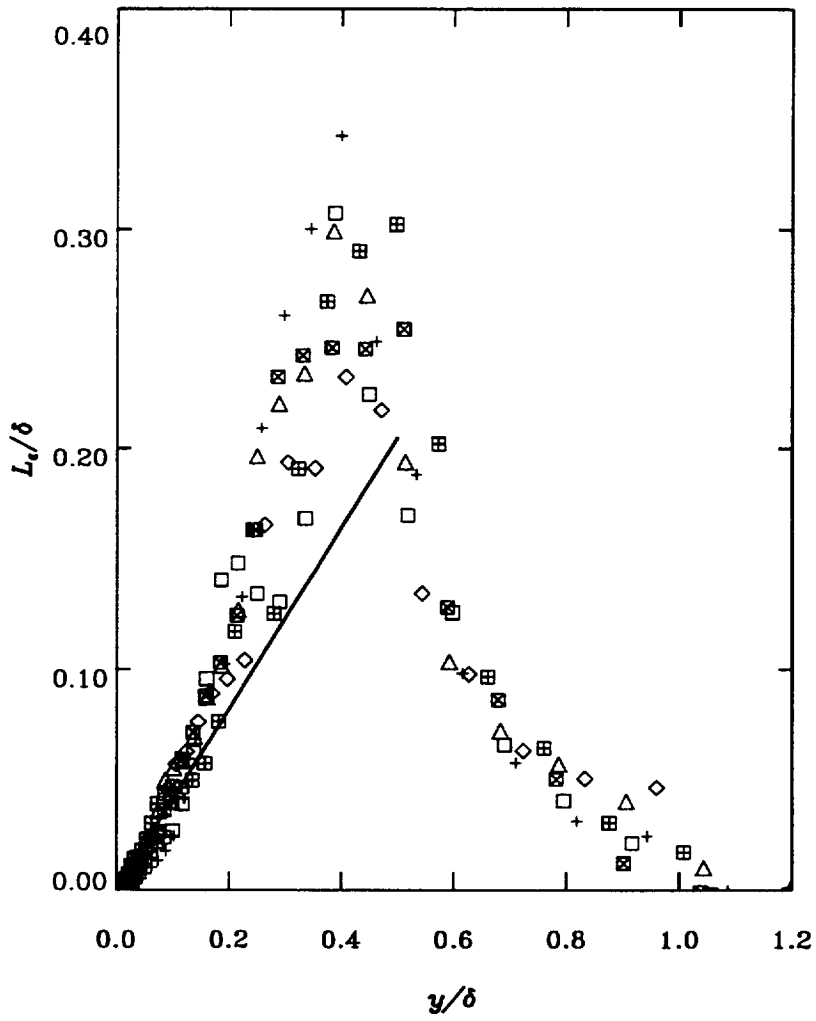

Figure 22. Development of the internal boundary layer: profiles of dissipation length parameter $L_\varepsilon = \left(-\overline{uv}\right)^{3/2}$. *All symbols are same as in figure 20(a).*

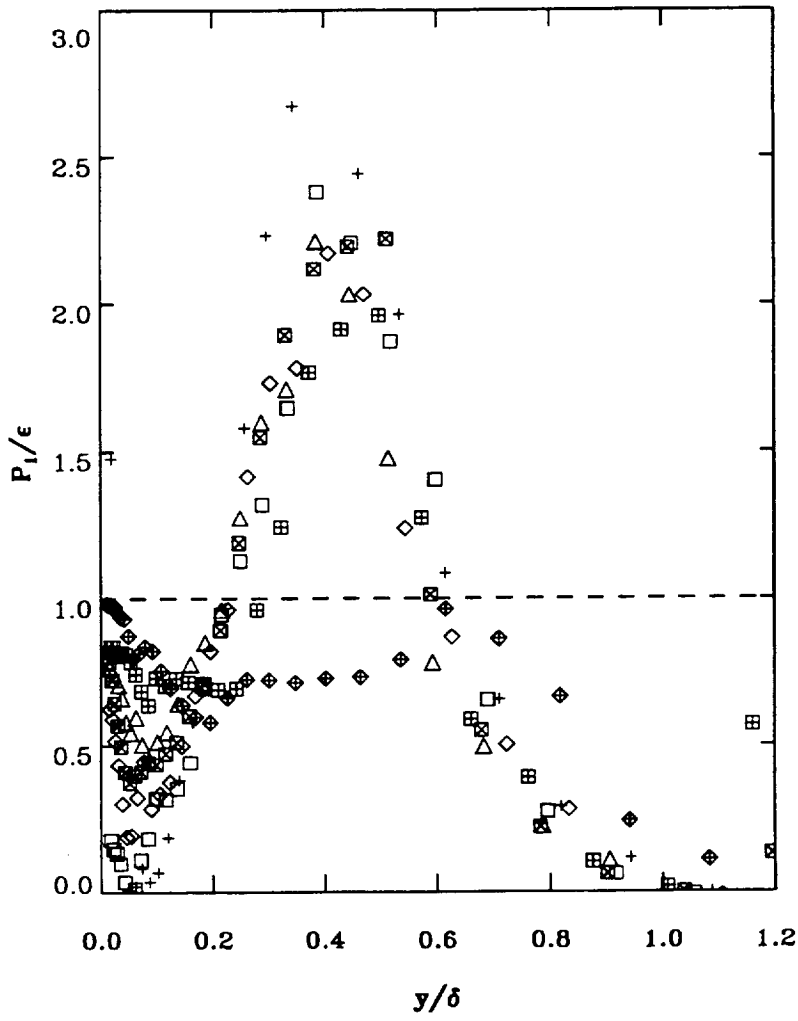

(a)

Figure 23. Development of the internal boundary layer: ratio of the turbulent kinetic energy production rate to dissipation rate. (a) P_1/ε. All symbols are same as in figure 20(a). Dash line represents equilibrium, production = rate of dissipation.

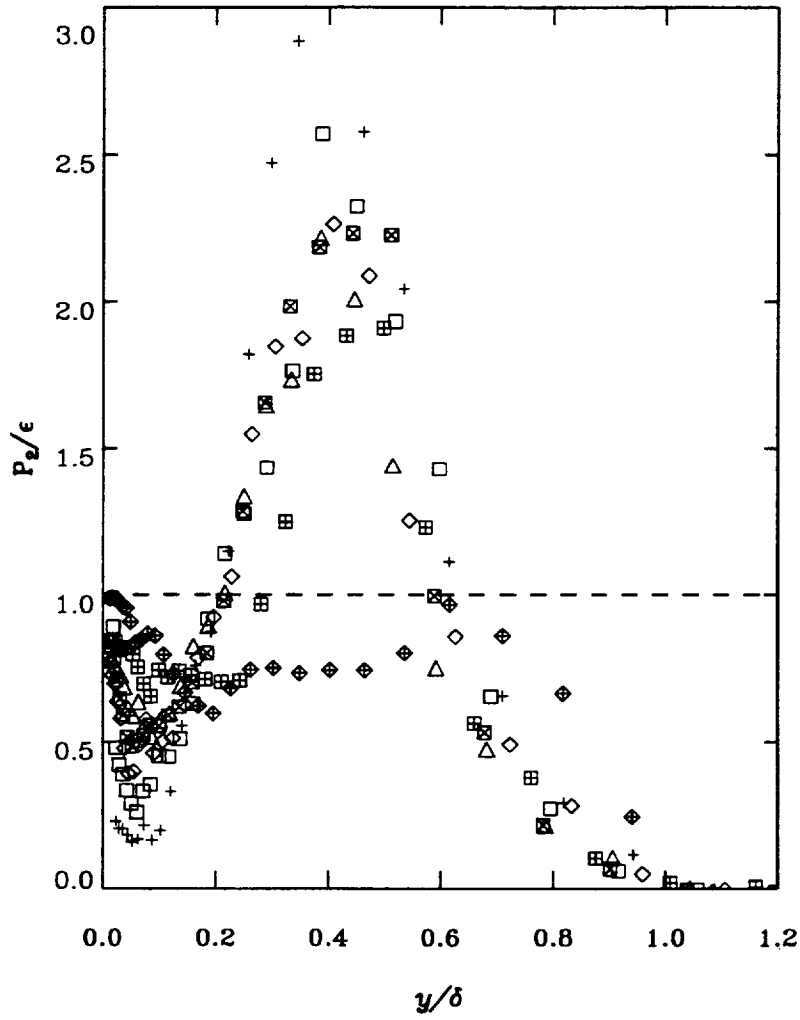

(b)

Figure 23. Continued. (b) P_2/ε. All symbols are same as in figure 20(a).

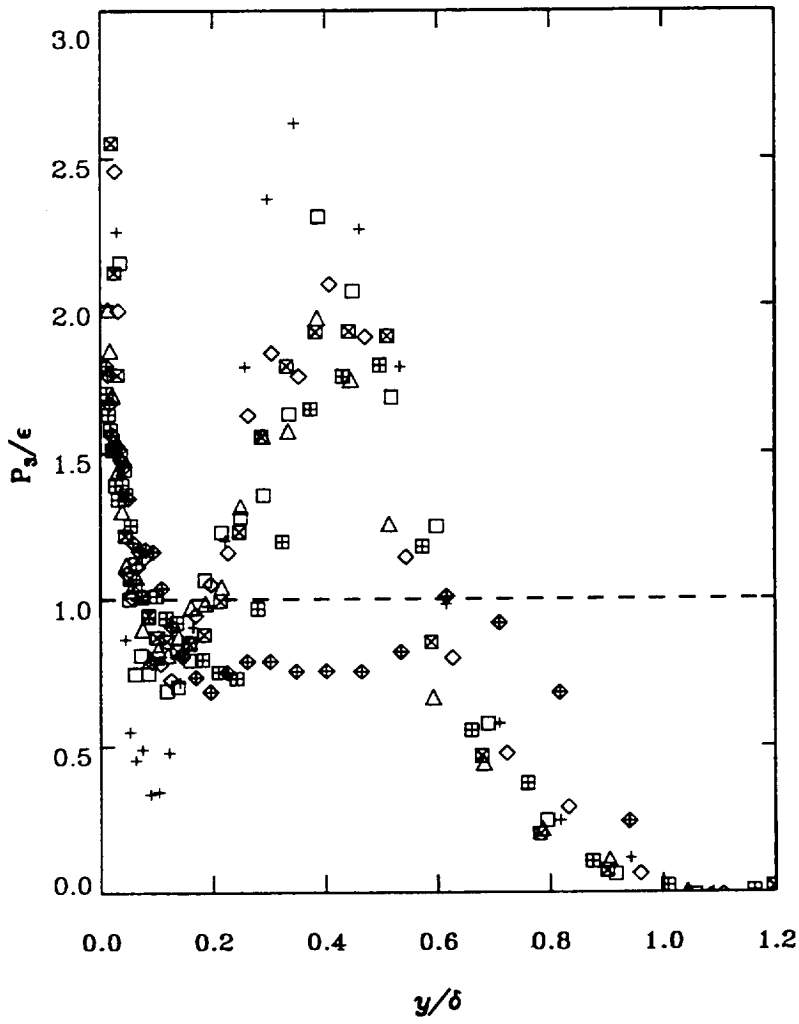

(c)

Figure 23. Concluded. (c) P_3/ε. All symbols are same as in figure 20(a).

REPORT DOCUMENTATION PAGE

Form Approved
OMB No. 0704-0188

1. AGENCY USE ONLY *(Leave blank)*	2. REPORT DATE	3. REPORT TYPE AND DATES COVERED
	April 1996	Technical Memorandum

4. TITLE AND SUBTITLE

An Experimental Study of a Separated/Reattached Flow Behind a Backward-Facing Step. $Re_h = 37{,}000$

5. FUNDING NUMBERS

505-59-50

6. AUTHOR(S)

Srba Jovic

7. PERFORMING ORGANIZATION NAME(S) AND ADDRESS(ES)

Eloret Institute
Ames Research Center
Moffett Field, CA 94035-1000

8. PERFORMING ORGANIZATION REPORT NUMBER

A-961198

9. SPONSORING/MONITORING AGENCY NAME(S) AND ADDRESS(ES)

National Aeronautics and Space Administration
Washington, DC 20546-0001

10. SPONSORING/MONITORING AGENCY REPORT NUMBER

NASA TM-110384

11. SUPPLEMENTARY NOTES

Point of Contact: Srba Jovic, Ames Research Center, MS 247-2, Moffett Field, CA 94035-1000
(415) 604-2116

12a. DISTRIBUTION/AVAILABILITY STATEMENT

Unclassified-Unlimited
Subject Category – 34

Available from the NASA Center for AeroSpace Information,
800 Elkridge Landing Road, Linthicum Heights, MD 21090; (301) 621-0390

12b. DISTRIBUTION CODE

13. ABSTRACT ***(Maximum 200 words)***

An experimental study was carried out to investigate turbulent structure of a two-dimensional incompressible separating/reattaching boundary layer behind a backward-facing step. Hot-wire measurement technique was used to measure three Reynolds stresses and higher-order mean products of velocity fluctuations. The Reynolds number, Re_h, based on the step height, h, and the reference velocity, U_0, was 37,000. The upstream oncoming flow was fully developed turbulent boundary layer with the $Re_\theta = 3600$.

All turbulent properties, such as Reynolds stresses, increase dramatically downstream of the step within an internally developing mixing layer. Distributions of dimensionless mean velocity, turbulent quantities and antisymmetric distribution of triple velocity products in the separated free shear layer suggest that the shear layer above the recirculating region strongly resembles free-shear mixing layer structure.

In the reattachment region close to the wall, turbulent diffusion term balances the rate of dissipation since advection and production terms appear to be negligibly small. Further downstream, production, and dissipation begin to dominate other transport processes near the wall indicating the growth of an internal turbulent boundary layer. In the outer region, however, the flow still have a memory of the upstream disturbance even at the last measuring station of 51 step-heights. The data show that the structure of the inner layer recovers at a much faster rate than the outer layer structure. The inner layer structure resembles the near-wall structure of a plane zero-pressure-gradient turbulent boundary layer (plane TBL) by $25h$ to $30h$, while the outer layer structure takes presumably over $100h$.

14. SUBJECT TERMS	15. NUMBER OF PAGES
Turbulence, Separated flow, Experiment, Hot-wire technique	94
	16. PRICE CODE: A05

17. SECURITY CLASSIFICATION OF REPORT	18. SECURITY CLASSIFICATION OF THIS PAGE	19. SECURITY CLASSIFICATION OF ABSTRACT	20. LIMITATION OF ABSTRACT
Unclassified	Unclassified		